Enhanced Plasmonic Upconversion in Coupled Metal-Semiconductor Nanoparticle Films

By

Nathan James Spear

Dissertation

Submitted to the Faculty of the

Graduate School of Vanderbilt University

in partial fulfillment of the requirements

for the degree of

DOCTOR OF PHILOSOPHY

In

Interdisciplinary

Materials Science

May 12, 2023

Nashville, Tennessee

Approved:

Janet Macdonald, Ph.D.

Richard Haglund, Ph.D.

Jason Valentine, Ph.D.

Joshua Caldwell, Ph.D.

David Cliffel, Ph.D.

This work is dedicated to the giants on whose shoulders we stand.

As armas e os Barões assinalados
Que da Ocidental praia Lusitana
Por mares nunca de antes navegados
Passaram ainda além da Taprobana,
Em perigos e guerras esforçados
Mais do que prometia a força humana,
E entre gente remota edificaram
Novo Reino, que tanto sublimaram.
-Os Lusíadas, Canto I

ACKNOWLEDGMENTS

There are, of course, many people without whom this work would not have been possible. I am now going to set about listing a few of them, roughly in chronological order. Chief among them, my parents. It is their patience, guidance, and wisdom that has produced much of the best of who I am. My brother, also, who is responsible for much of the rest. Messrs. Morgan, Modlin, and Brubaker, for leading the Riley High School Science Olympiad program, which was critical to developing my early interest in chemistry, optics, and materials science at whose intersection my dissertation lies. The brothers of ΦΚΣ ΑΞ chapter: *Stellis Aequus Durando*. Professors Martinez and Matson, who took a chance on me, and helped me grow as a budding researcher. My friends and fellow grad students at Vanderbilt, in particular Chris, Will, and Andrey for being as dear of friends as anybody could hope for. My colleagues in the Macdonald and Haglund labs, particularly Emil and Kent whose guidance in the first year of this project was invaluable. My advisors, Professors Janet Macdonald and Richard Haglund, whose brilliance, sincerity, passion, and (above all else) humanity serve as a shining example of the edifying and uplifting power of science. Yueming and Fabian, with whom I have collaborated this past year and who have both been thoughtful and engaging. Professor Jason Valentine, with whom I have worked this past year on a project not covered in this dissertation, but that I very much appreciate the opportunity to have engaged with; I have learned and grown so much during my time working on the STTR project. Professor Mahi R. Singh, who has collaborated with us to produce a wonderful analytic model of our nanoparticle system. To the current members of the Macdonald and Haglund labs: good luck, have fun. Finally, I would like to thank all the members of my committee not heretofore mentioned: Professors Joshua Caldwell, Jason Valentine, and David Cliffel; who have collaborated, challenged, and supported me during my time here.

The following were crucial sources of funding for work on this dissertation: Vanderbilt's Office of the Provost Interdisciplinary Discovery Grant, National Science Foundation (ECCS1509740), U.S. Department of Energy (DE-FG02-01ER45916), the VINSE graduate student fellowship, and the REU program that supported Joshua Queen and Amanda Wistuba the undergraduates with whom I have had the fortune to work with over the years (PHYS 1852158).

I must also bid farewell to the city of Nashville, TN, which has been my home for these past five years, a description regarding which I refer to the classic short story, "A Municipal Report":

"I stepped off the train at 8 P.M. Having searched the thesaurus in vain for adjectives, I must, as a substitution, hie me to comparison in the form of a recipe. Take a London fog 30 parts; malaria 10 parts; gas leaks 20 parts; dewdrops gathered in a brick yard at sunrise, 25 parts; odor of honeysuckle 15 parts. Mix. The mixture will give you an approximate conception of a Nashville drizzle. It is not so fragrant as a moth-ball nor as thick as pea-soup; but 'tis enough—'twill serve."

-O. Henry, 1904

TABLE OF CONTENTS

Page

LIST OF TABLES

LIST OF FIGURES

CHAPTER 1

Introduction

1.1 The Upconversion of Light

Upconversion of light denotes a set of processes by which the frequency of a light signal is increased when appropriate materials are exposed to sufficiently intense light fields. Two main classes of upconversion are salient to the materials system explored here: harmonic generation (HG) and multiple/multi-photon photoluminescence (**MPPL**).

Harmonic generation is the process by which a number of identical photons of incident light combine parametrically—that is, without energy transfer to or from the system— to produce a new photon of light with the energy of the input photons. This produces light with frequency that is integer multiples of the input signal (Equation 1).

$$\sum_1^n \omega = n\omega \tag{1}$$

Where n refers to the order of the upconversion process, the simplest of which is the case of second harmonic generation (SHG) in which two photons of frequency ω combine to form a new photon of energy 2ω. As no energy is lost to the system, the spectral width of the upconverted signal will depend on the width of the input signal, and not the properties of the upconversion media. However, there is some broadening of the linewidth with the preservation of the time-bandwidth product. With multiple photons of input light "consumed" to produce each photon of upconverted light, the quantity of upconverted light that is produced will depend nonlinearly on the intensity of the input signal. For even-order harmonics to be produced, the

upconverting material must not possess a center of inversion symmetry in the crystal structure. A general treatment of the role that crystalline symmetry plays in harmonic generation can be found in most optics texts, for a particular recommendation, I point the reader to chapter 11 section 3.2 of *Optical Properties of Solids* by Mark Fox[1].

The conventional approach of nonlinear optics texts [2] describes harmonic generation as operating through the generation of higher order polarization components ($P^{(n)}$) due to the intense input of electric fields (E) into the upconverting material, proportional to the nonlinear susceptibility χ^n.

$$P^{(2)} = \varepsilon_0 \chi^{(2)} E^2 \tag{2}$$

Where we consider an oscillating electric field of the form:

$$E(t) = \varepsilon_0 \chi^{(2)} E_0^2 sin^2(\omega t) \tag{3}$$

the nonlinear polarization induced by such a field is:

$$P^{(2)}(t) = \varepsilon_0 \chi^{(2)} E_0^2 sin^2(\omega t) = \frac{1}{2} \varepsilon_0 \chi^{(2)} E_0^2 [1 - cos(2\omega t)] \tag{4}$$

thus, if the second order nonlinear susceptibility is non-zero, and the material is driven at frequency ω, second order polarization will be induced—oscillating at 2ω—leading to the generation of second harmonic light.

The upshot of this view of harmonic generation is that optical stimulation of a material with intense electric fields induces dipole polarization components at harmonic frequencies. These dipoles can then emit light at that harmonic frequency, or as shall be examined here, they can interact with nearby resonators with which they spectrally overlap. Of particular importance among the potential interactions that these resonators can experience, is a recently described

phenomenon called cascaded third harmonic generation (**THG**). This process generates 3ω light via a two-step process of SHG followed by sum frequency generation (**SFG**) of the 2ω light generated by the SHG and another photon of the fundamental[3]. Each step in the cascaded process involved two-photons and thus is dependent on the second-order susceptibility; however, three input fundamental photons are required, thus producing a third-order dependence on input intensity. This contrasts with a direct mechanism of third harmonic generation—in which three photons of ω light combine in a single step to form 3ω light—which depends on the third-order susceptibility. These processes are difficult to disambiguate because both processes feature third-order dependence on the pump intensity. However, cascaded THG benefits from an intermediate harmonic resonance at 2ω to enhance the efficiency of the SFG step. Thus, proving the importance of this resonance to the observed enhancement of THG is an important indicator for a cascaded THG process.

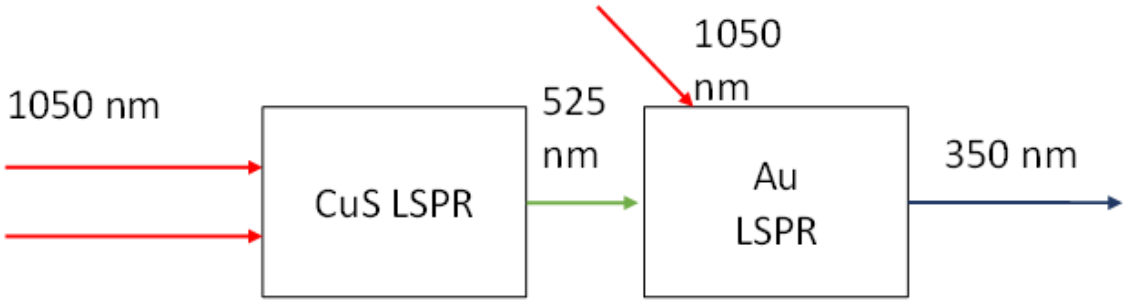

Figure 1.1 Diagram of cascaded THG in CuS/Au plasmonic nanoparticle system.

Multi/multiple photon photoluminescence are upconversion processes by which several photons act in concert to produce an excite electrons in a material. These excited electrons then decay and emits the energy as one photon, possessing greater energy than one of the individual inputs. Multiphoton photoluminescence is this process in which the absorption of the input photons occurs simultaneously, with no intermediate electronic excited state, and multiple

photon photoluminescence is this process in which the promotion of the electron occurs sequentially. These processes produce broadened output spectra, depending upon the lifetime of the exciton and relaxation of the excited electron within the conduction band. The response order of upconversion via MPPL varies widely, dependent upon the band gap energy of the material and the energy of the incident light. Additionally, due to the thermalization of the excited electrons before recombination, energy is transferred to the material during the MPPL process. Thus, high excitation intensities could lead to heating of the material, potentially lowering the optical damage threshold of the system.

1.2 Upconversion from plasmonic nanoparticles

Nanoparticulate materials are a class of acute interest for implementation in upconverting materials[4]–[6]. Three of the distinguishing properties that such materials possess are: high ratios of surface area to volume, localization and intensification of electric fields, and, for films of nanoparticles thinner than the wavelength of the light that is exciting them, lack of interference effects between the fundamental and upconverted fields.

The high surface area per unit mass (a result of square-cube law surface-to-volume scaling) of nanoparticulate materials is particularly advantageous for second-harmonic generation. The requirement of non-centrosymmetry for SHG generally disqualifies metallic materials from producing a significant 2ω signal. However, the crystalline symmetry of these materials is broken at the surface (due to the missing crystalline plane that would be above the material). Thus, for nanoparticulate materials, in which a significant fraction of the atoms are situated at surface sites, the non-centrosymmetric requirement is relaxed, and significant even-order harmonic generation can be measured[7]. This includes cascaded THG, which despite having a third-order dependence on input-field intensity, is dependent on the second-order susceptibility, and thus is sensitive to the non-centrosymmetry requirement.

Another important property of nanoparticulate materials is their propensity to localize and intensify electromagnetic fields. There are many examples of processes that lead to the localization of electric fields, such as the pseudo-random phenomena that stem from the interference of multiple light scattering paths in densely packed, disordered media such as substrates for Raman enhancement (SERS). These can boost the nonlinear conversion in localized hot spots[8]. Of particular interest for this dissertation, however, are resonant enhancement effects within and between plasmonic nanoparticles. Light at resonant frequencies can induce collective oscillations of surface charge carriers in sufficiently conductive nanoparticulate matter, known as localized surface plasmon resonances (LSPR). The coherent oscillation of these charges produces very strong local electric fields at the resonant frequency, which, following from Equation 1, induce higher-order polarization components. Thus, pumping plasmonic nanoparticles at their resonant frequency increases their efficiency in harmonic generation[9],[10].

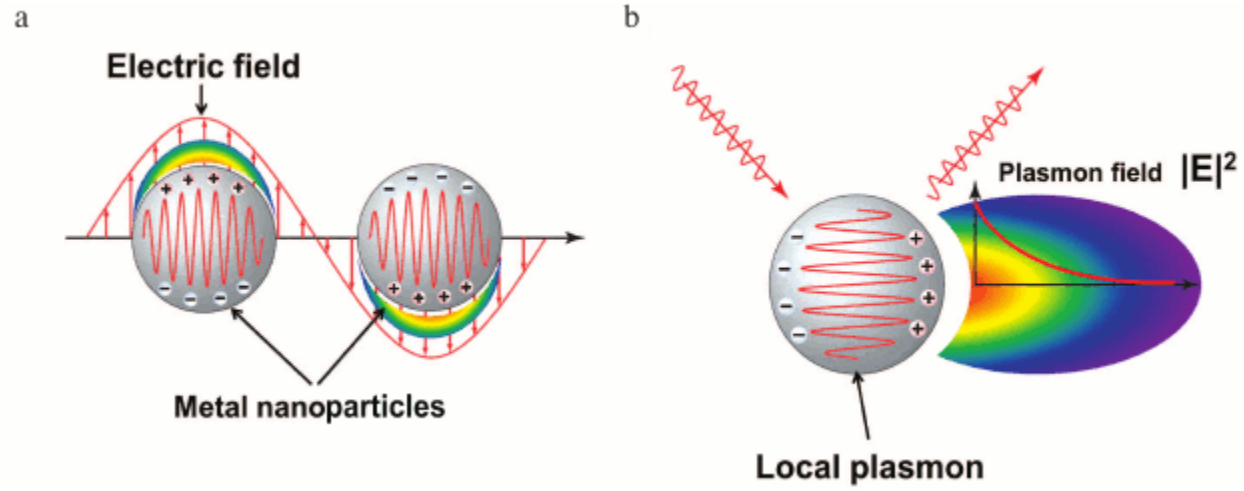

Figure 1.2 LSPR excitation by electric field (a) and field intensity distribution around a nanoparticle with excited plasmon (b). Copyright 2015 Springer Nature, reproduced with permission.

Finally, when nanoparticles are processed into thin films, they avoid one of the major design constraints of standard (macroscopic) nonlinear crystals: the requirement for phase matching. In macroscopic nonlinear crystals, there is a potential for interference to occur between the transmitted fundamental harmonic and the generated second-harmonic, which could lead to the negation (via destructive interference) of the 2ω signal. This is caused by a phase mismatch between the two frequencies that arises from the dispersion of the nonlinear medium. Conversely, appropriate phase matching can lead to the amplification of the generated second-harmonic signal. These nonlinear crystals must be thick to obtain a useful quantity of upconverted light due to their low efficiency of upconversion; however with appropriate crystal thickness and orientation, total conversion efficiencies of 10% are not abnormal. Plasmonic nanoparticles, on the other hand, feature high upconversion efficiencies due to resonant enhancement. These gains in efficiency allow for reduction of the path length that is required to produce an equivalent amount of upconverted light. Thus, nanoparticles can be processed into thin films which are not thick enough (with respect to the wavelength, $t<<\lambda$) to produce significant phase mismatch between the fundamental and harmonics. These thin-film nanoparticle material systems are relieved of the constraints on orientation and angle of incidence that weigh on standard nonlinear crystals. However, this comes at the cost of efficiency due to the lack of constructive interference to amplify the generated harmonic.

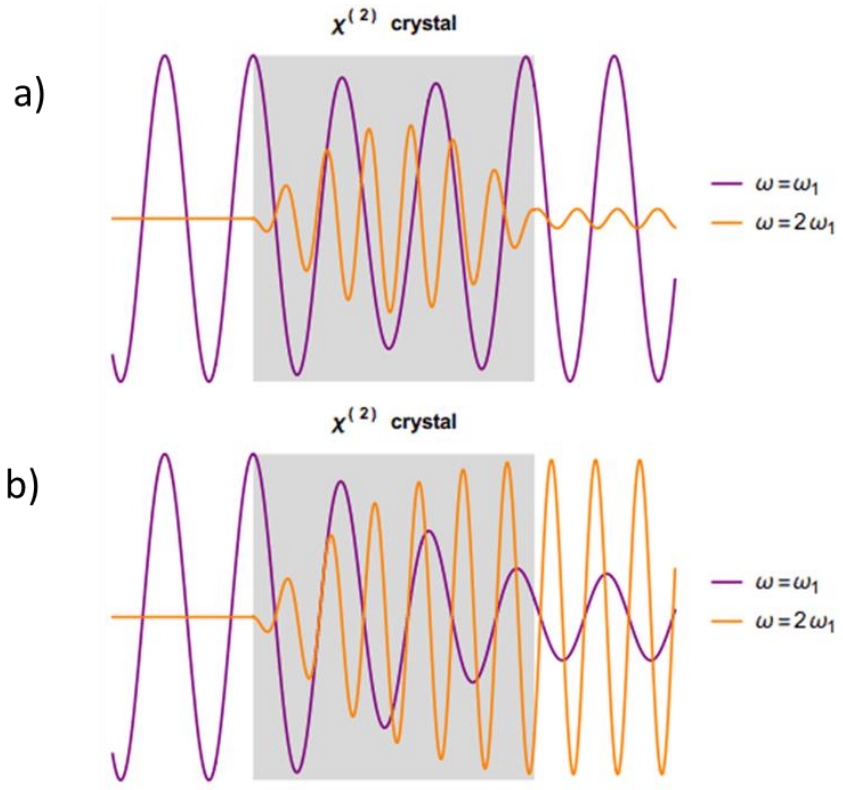

Figure 1.3 Schematic of SHG in a nonlinear crystal with (a) imperfect phase matching and (b) perfect phase matching. Reproduced with permission, Jacopo Bertolotti, 2018.

1.2.1 Metallic nanoparticles

The upconverting properties of a wide variety of metallic nanoparticles have been examined[9]. Those relevant to this dissertation are gold nanoparticles. Gold nanoparticles feature a surface plasmon resonance that is widely tunable through the visible range through tailoring of the particle size and aspect ratio. A wide variety of gold structures has been examined for upconversion, including gold nano-spirals by my forerunner in the Haglund group, Dr. Rod Davidson[11]. Generally, upconversion in Au nanoparticles requires carefully controlling the morphology of the Au structure to tune the LSPR of the structure[12], increase surface area, and create asymmetric elements. The Au nanoparticles can also be combined with other materials or structures to create coupled systems between the LSPR of the Au and an

optical feature of the coupled element[13]. To give just a brief sampling of the deep literature, the gold LSPR has been coupled to excitons in quantum dots[14], whispering gallery modes in nanorods[15], and the LSPR of other gold nanoparticles [16]. Importantly, Au nanoparticles will also exhibit MPPL when they are excited with light that is detuned from the LSPR, which arises from intraband transitions[17],[18].

In contrast to gold, aluminum nanoparticles have only a nascent literature, particularly in the subset of synthetically produced Al nanoparticles. That is, aluminum nanostructures derived from top-down methods such as e-beam lithography[19] have a relatively well-established literature, but synthetic routes to Al nanoparticle synthesis have only recently been reported [20], owing to the difficulty of managing the highly reactive (pyrophoric) aluminum reagents. Whereas gold, as a noble metal, will react to form metallic nanoparticles from its salts readily in a large variety of conditions (including, at its simplest, in water under ambient conditions with sodium citrate), aluminum is much more sensitive, and will oxidize to form Al_2O_3 unless great care is taken to ensure air-free reaction conditions. Yet, despite the difficulty, they exhibit promising surface plasmon resonances stretching throughout the UV-A band (320-400 nm) dependent upon the nanoparticle diameter.

1.2.2 Plasmonic Semiconducting nanoparticles

A subset of the semiconducting nanoparticles exhibits plasmonic resonances. These features arise from a high concentration of charge carriers, either from external dopants, or from intrinsic properties, as is the case for CuS. Some examples of self-doped plasmonic semiconductors include MoO_3, WO_{3-x} [21], $Cu_{2-x}S$, $Cu_{2-x}Se$, MoS_2, and NiO, [22]. The class of doped plasmonic semiconductors is much larger due to the number of combinations of semiconductor and dopant, a few of the more common examples include: Cs doped WO_3[23], $TiO_{2-x}H_x$ [24], In doped SnO_2[25], and Al doped ZnO[26]. In comparison to metallic

nanoparticles, this grouping of plasmonic semiconducting nanoparticles have a paucity of articles in the literature about their nonlinear optical properties. Of these materials, stoichiometric copper sulfide (CuS, Covellite) was selected for examination. The plasmonic resonance of CuS is broad and centered in the near IR [27], with a peak near 1064 nm, the wavelength of common Nd:YAG and Nd:glass lasers. This wavelength also places the plasmon resonance of appropriately sized gold nanoparticles at the second harmonic of the pump laser. This would permit for the examination of harmonic coupling between the LSPR of the CuS and gold. The spectral positioning of this LSPR combined with the synthetic expertise of the Macdonald group, especially in the phase control of metal chalcogenide nanoparticles (including copper sulfides), to make CuS the preeminent candidate for harmonic coupling with gold nanoparticles. Notably, the Tao group has examined the role of the surface plasmon resonance of CuS in two photon absorption[28], but harmonic generation from CuS was *terra incognita*.

1.3 Interaction between CuS and Au nanoparticles

One objective of this work will be to identify the mechanisms through which the gold and covellite nanoparticles interact. Coupling between plasmonic resonances is well described in the literature, via nonradiative mechanisms such as plasmon-induced resonant energy transfer (PIRET) [29]. Coupling between dipoles on the surface of two proximate nanoparticles, as in the case for plasmonic nanoparticles, features a characteristic dependence on the distance between the two particles to the inverse sixth power. Such direct coupling of surface dipoles also depends on the spectral overlap between the two resonances. However, in the CuS/Au system explored in this dissertation, there is no spectral overlap between the two LSPRs, nor between the gold LSPR and the CuS excitonic absorption. Rather, it is the second-harmonic components of the nonlinear polarization induced in the CuS nanoparticles by the pump laser

that couple to the LSPR of the gold. This coupling could serve to transfer second-harmonic energy from the CuS nanoparticles into the LSPR of the Au nanoparticles non-radiatively, which would then participate in a sum frequency generation process with another quantum of fundamental harmonic light from the pump laser, leading to the generation of third harmonic light in a cascaded process. This coupling would require spatial overlap between the local fields of the respective LSPR, thus, we expect that the enhancement effect should depend strongly on the separation between the two nanoparticle species. Supporting this hypothesis will rely on proving that the harmonic relationship between the two nanoparticles is critical to THG, that Au nanoparticles can efficiently generate the sum frequency of the fundamental and second harmonic signals (chapter 3), and that the two nanoparticles' interaction is spatially dependent and mediated by surface dipoles (chapter 4).

Understanding of the fundamental mechanisms that govern the interaction between harmonically coupled plasmonic nanoparticles will pave the way for development of these materials for nonlinear optical applications in thin films, in which applications standard upconverting crystals are poorly suited. Due to the short path length of these applications, the amplification by constructive interference between the fundamental and generated harmonic available in larger crystals cannot occur in thin films. Thus, the local field enhancement available from plasmonic nanomaterials is necessary for usable quantities of upconverted light to be produced. Combinations of nano-optic layers have been proposed for application in document verification[30] and currency anti-counterfeiting measures[11]. Furthermore, upconversion by harmonic generation does not exhibit the spectral broadening that occurs during upconversion from MPPL, nor is reliant on comparatively slow electronic transitions.

1.4 Scope of dissertation

This dissertation will examine the nonlinear optical properties of multilayer films

containing harmonically coupled plasmonic nanoparticles. In particular, the bulk of the text will concern a system comprising of layers of CuS and Au nanoparticles, with results from Al nanoparticles briefly discussed in a later chapter.

In the second chapter, the synthesis of CuS and Au plasmonic nanoparticles, their fabrication into bilayer films via a simple, scalable bath method, and the multiple sources of upconversion that these films exhibit will be described. The nonlinear order of the upconversion signals will be analyzed and the efficiency of harmonic generation from the bilayer films will be compared to standard nonlinear crystals such as β-barium borate (BBO). The enhancement of harmonic generation from the combination of CuS and Au nanoparticles into a bilayer film will be demonstrated.

In the third chapter, the critical role of the harmonic relationship between the LSPR of the two types of plasmonic nanoparticles will be explored and the mechanism of harmonic generation enhancement through a cascaded SFG process will be discussed. The bilayer films exhibit SFG between a fundamental and second harmonic pump beams. An analytic model of third harmonic generation from the CuS and Au nanoparticles will be presented that explains the observed THG enhancement as occurring due to incoherent surface dipole interactions between the two nanoparticle layers.

In the fourth chapter, the hypothesis of the analytic model that the interaction between the harmonic nanoparticles occurs via surface dipole interactions will be supported by experiments that add an Al_2O_3 layer of varying thickness between the nanoparticles. The final section will deal with the results from a preliminary exploration of the nonlinear optical properties of synthetically produced aluminum nanoparticles.

In the fifth and final chapter, the dissertation will be concluded, with a summary of the work

contained in the preceding chapters and an outlook on the future research prospects for nonlinear multiply-plasmonic nanoparticle films.

CHAPTER 2

Synthesis and nonlinear optical properties of Au and CuS nanoparticles and fabrication into bilayer films

2.1 Introduction

The second-order nonlinear response of metal nanostructures is a well-known example of the effects of both the broken symmetry at surfaces and the resonant enhancement generated through localized surface plasmon resonances (LSPRs). Plasmonic resonances of coupled metal nanostructures can enhance the non-linear properties of materials through near-field dipole-dipole coupling[31],[32] and also enhance the non-linear response of metallic materials themselves[12],[33]. In the specific case of second harmonic generation (SHG), further enhancements can be achieved by designing nanostructures with additional resonances at the fundamental, second harmonic, or both. Examples include arrays of split-ring resonators[34], of gold nanofeatures that support Fano resonances[35], and of LSPR active gold nanoparticles that couple into optical whispering gallery modes[36]. Enhancement of SHG via two-plasmon coupling has also been demonstrated using arrays of differently sized or shaped plasmonic features in specific geometric arrangements[37]–[40], or by combining metals with differing plasmon energies (e.g. bi-plasmonic heterobimetallic Au/Ag nanorods[41]).

The complexity of the structures for multiplasmonic enhancement of second harmonic generation have driven near-total reliance on lithography to obtain precise control over composition, shape, and arrangement of the individual nanostructures. However, lithography imposes significant limitations on device geometry and scalability. Alternatively, colloidal nanoparticles can provide similar control over composition and shape of the nanostructures and yet are also amenable to solution processing and conformal deposition.

The synthesis of metal nanoparticles with prominent LSPR absorption of varying composition and shape, typically of Au, Ag and their alloys, is a maturing field. The narrow-band LSPRs of these nanomaterials are tunable from the UV through the visible and NIR[42],

and have been widely employed for plasmon-enhanced second-harmonic generation. However, plasmon resonances in metal nanoparticles tend to be relatively spectrally narrow – and thus this strategy for designer coupled plasmonic SHG structures tend to be useful primarily for a single input/output frequency pair.

Heterostructures that couple the *plasmon* of a metal with the *exciton* of a semiconductor have been shown to enhance the generation of second harmonic light[43],[44]. In this case, second-harmonic generation from the semiconductor nanocrystal is enhanced by the local field effects of the metal plasmon resonance[45]. These studies showed that separation of the semiconductor and the metal components was important, as direct contact between them allows inter-facial charge transfer that damps the SHG[46].

Many semiconductors, including the large family of copper chalcogenides have NIR plasmon resonances that can be tuned by changing composition, doping, or morphology[47]. These materials have untapped potential in *plasmon-plasmon* coupled heterostructured nanomaterials for second-harmonic generation. Moreover, these semiconductor plasmon resonances turn out to be relatively broad[48]. Therefore, a large spectral bandwidth can be covered through many potential combinations of semiconductor nanocrystals with an LSPR at a fundamental frequency, which couple resonantly to a metal nanoparticle with an LSPR at the second-harmonic frequency. These combinations of resonantly coupled plasmonic nanocrystals are a promising strategy for broadly tunable emission of upconverted light, with the added benefit that the nanoparticle constituents are synthesizable by standard solvothermal techniques and solution processable into films.

Here we demonstrate for first time that *plasmonic semiconductors* can be used in conjunction with metallic nanoparticles to enhance second harmonic generation or other multiphoton upconversion mechanisms. We specifically study a heterostructure comprising a bilayer of nanoparticle films. The first contains CuS (covellite) nanoparticles which feature a broad LSPR in the near infrared (NIR) ($\lambda_{LSPR,CuS}$ = 900-1600) nm and the second layer contains gold nanoparticles which feature a visible spectrum LSPR ($\lambda_{LSPR,\ Au}$ = 510-610 nm), when excited by a femtosecond Nd:glass laser (1050 nm).

Covellite exhibits electronic properties typical of a heavily doped semiconductor due to an intrinsically high concentration of holes (h^+). These holes act as positive charge carriers, giving covellite a *p*-type character and a plasmon resonance that absorbs strongly from 900 to 1600 nm[27]. Plasmonic states in covellite function as intermediate virtual states in two-photon absorption, and in coupled plasmon-exciton complexes for two-photon photoluminescence. In CuS, the second harmonic of the bluest edge of the plasmon resonance overlaps with the onset of excitonic absorption (2.5 eV, 496 nm, just below the conduction-band edge). A three-fold enhancement of two-photon photoluminescence in covellite was demonstrated at an excitation wavelength of 855 nm, where this plasmon-exciton energy matching condition occurs[28]. Excitations at lower photon energies, such as the 1050 nm light used here, are insufficient to produce an excitonic state via two-photon absorption.

However, in the Au-CuS heterostructure, enhanced SHG exceeding the incoherent sum of the individual components was still observed for laser excitation at 1050 nm. Upconverted light produced by SHG was separated from that produced by multiphoton photoluminescence (MPPL) by using appropriate filters; in addition, the full spectrum of upconverted light was also measured. Both the MPPL and SHG signals were enhanced by the heterostructure; at high pump laser intensities the enhancement of the MPPL was small compared to the SHG. The discovery and exploitation of this SHG enhancement with colloidal nanocrystals could lead to the development of efficient non-linear materials on planar or non-planar surfaces through solution processing, and with further development of the colloidal chemistry, to non-bleaching, non-blinking, free-standing, upconversion nanocrystal hybrid systems as biological imaging probes and contrast agents.

2.2 Synthesis and facile bath method of Au and CuS nanoparticles

Au and CuS nanoparticles were synthesized using standard solvothermal techniques (Figure 2.1 a and b). The nanoparticles were then assembled into heterostructured films using a facile bath method[49],[50] as diagramed in Figure 2.1c. Descriptions of Au & CuS nanoparticle synthesis[27],[51], optical characterization methods, and heterostructure characterization are available in Section 3.7.

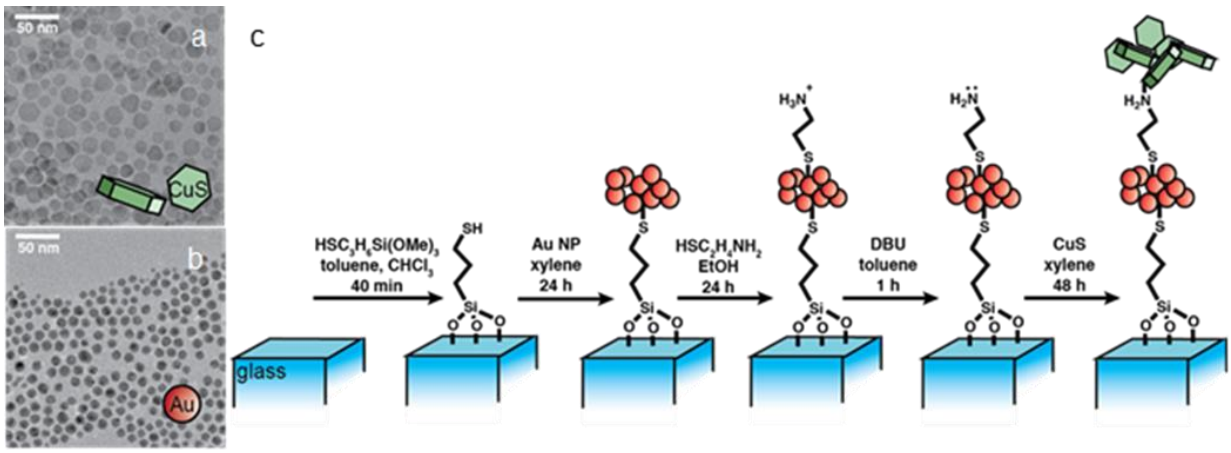

Figure 2.1 (a)TEM and schematics of CuS nanoparticles. (b) TEM and schematic of Au nanoparticles. (c) Schematic of the film deposition process.

Additionally, a laser-induced annealing effect on the film was observed upon repeated exposure of the sample to the laser. Initial decreases in signal leveled off after several exposures to the laser permitting stable measurement conditions, as shown in Appendix A.1. These two factors were compensated by controlling the focal-spot placement on the sample and ensuring pre-measurement exposure for approximately 15 minutes to the laser.

The anisotropic geometry of CuS nanoparticles allows excitation of both transverse and longitudinal plasmon modes; however, CuS exhibit only a single broad, intense extinction band due to overlap of the two allowed modes. For Au nanoparticles, the isotropic shape facilitates the dominance of a single plasmon resonance centered at 560 nm (Figure 2.2a). The presence of Au nanoparticles on the functionalized glass slide was confirmed by both the Au plasmon resonance peak (λ_{LSPR}, Au = 560 nm) in UV-vis-NIR spectroscopy as shown in Figure 2.2a and SEM micrographs (Appendix A.2), which show an even coverage of Au nanoparticles on the glass surface. Profilometry indicated the film was multilayered, as the ~30 nm thickness of a film layer from the bath method is greater than the diameter of the Au nanoparticles (~7 nm) (Appendix A.3**)**. Profilometry also demonstrated that CuS films were approximately twice as thick as than those of Au. This ensured sufficient upconverted signal from films containing only

CuS nanoparticles, despite their relatively low nonlinear susceptibility.

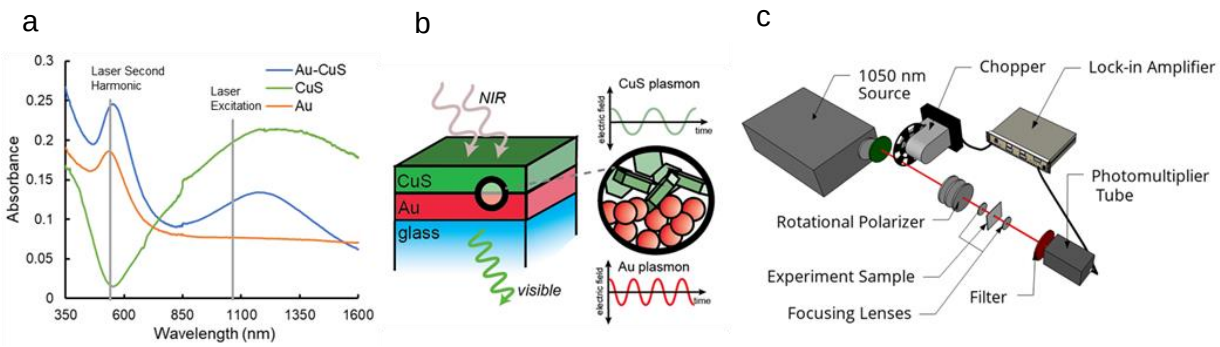

Figure 2.2 (a) UV-vis-NIR spectrophotometry of typical nanoparticle films deposited on glass microscope slides. The fundamental wavelength of the pump laser and the second harmonic are denoted by gray lines. (b) Illustration of SHG enhancement by plasmonic resonance in Au-CuS hybrid film. (c) The nonlinear optical properties experimental configuration.

Deposition of CuS onto the sample was confirmed by the broad CuS plasmon extinction peak (λ_{LSPR}, CuS = 1300 nm) in UV-Vis-NIR spectroscopy. Comparison of the plasmon extinction between films containing only Au or CuS nanoparticles and nanoparticle heterostructures shows that there is no shift in the linear plasmonic response of either Au or CuS (Figure 2.2a). Thus, enhanced nonlinear activity in either species due to shifts in the dielectric environment[52] is unlikely.

2.3 Upconversion in Au, CuS, and hybrid nanoparticle films produced by the bath method

The nanoparticle films were exposed to 150 fs pulses from a mode-locked Nd:glass laser operating at 1050 nm wavelength, at a pulse repetition frequency of 100 MHz that induced the generation of visible upconverted light as illustrated in Figure 2.2c. The beam was attenuated with crossed polarizing filters, and the intensity of the visible light monitored with a photomultiplier tube (PMT). The PMT was not sensitive in the IR region, with a cutoff around 700 nm.

A short-pass optical filter (edge at 720 nm), together with the sensitivity drop of the PMT in that spectral region, reduced the NIR signal from the laser fundamental below the detection

limit. Spectroscopy of a SHG material (BBO), as shown in Appendix A.4, supports this conclusion by demonstrating complete attenuation of the fundamental beam and the presence of a peak at 525 nm. All nanoparticle films— CuS, Au and the hybrid Au/CuS— demonstrated a supralinear intensity response. In addition to SHG at double the frequency of the pump-laser fundamental, the LSPR of gold nanostructures, especially gold nanorods and dimers, enhances a broad photoluminescence spectrum due to multiple-photon absorption[18]. Multiple-photon photoluminescence (MPPL) has been identified as requiring two-, four-, and six-photon absorptions although few experiments have been able to separate the influence of two-photon SHG from the MPPL components[53]. In contrast to the sharp SHG signal (set by the bandwidth of the laser), the MPPL feature is a broad emission feature ranging from ~400-650 nm. Short-pass and notch filters were used to capture the SHG signal and the MPPL, respectively.

Films containing only gold nanoparticles produced a strong nonlinear response consistent with many literature reports (Figure 2.3a). Second harmonic generation has been demonstrated in gold nano-particle arrays, hemispherical gold caps on silica nanospheres, gold dimer nano-antennas and gold nanorods[33],[54]. However, for the Au nanoparticle films, filtering of the upconverted light to capture SHG or MPPL signal demonstrated that only a small contribution of the upconverted light was from the second harmonic (Figure 2.3b); instead, most of the output was from the MPPL contribution (Figure 2.3c). This is likely because SHG from the interior of the gold nanoparticles is improbably due to its inversion symmetry.

The nonlinear response of the CuS-only films was modest, roughly a factor of 15 less than that of the gold films at the strongest laser intensity employed. This is consistent with their centrosymmetric structure, which prevents SHG from the bulk, but allows weak surface SHG enhanced by its NIR plasmon resonance. Additionally, at 1050 nm laser excitation, two-photon absorption is not sufficient to excite valence band electrons of CuS into the conduction band. Thus, two-photon absorption followed by SH emission can only proceed via surface or trap states in the band gap[55]. Correspondingly, the MPPL contribution from films containing only CuS (Figure 2.3c) was much smaller than the SHG contribution (Figure 2.3b).

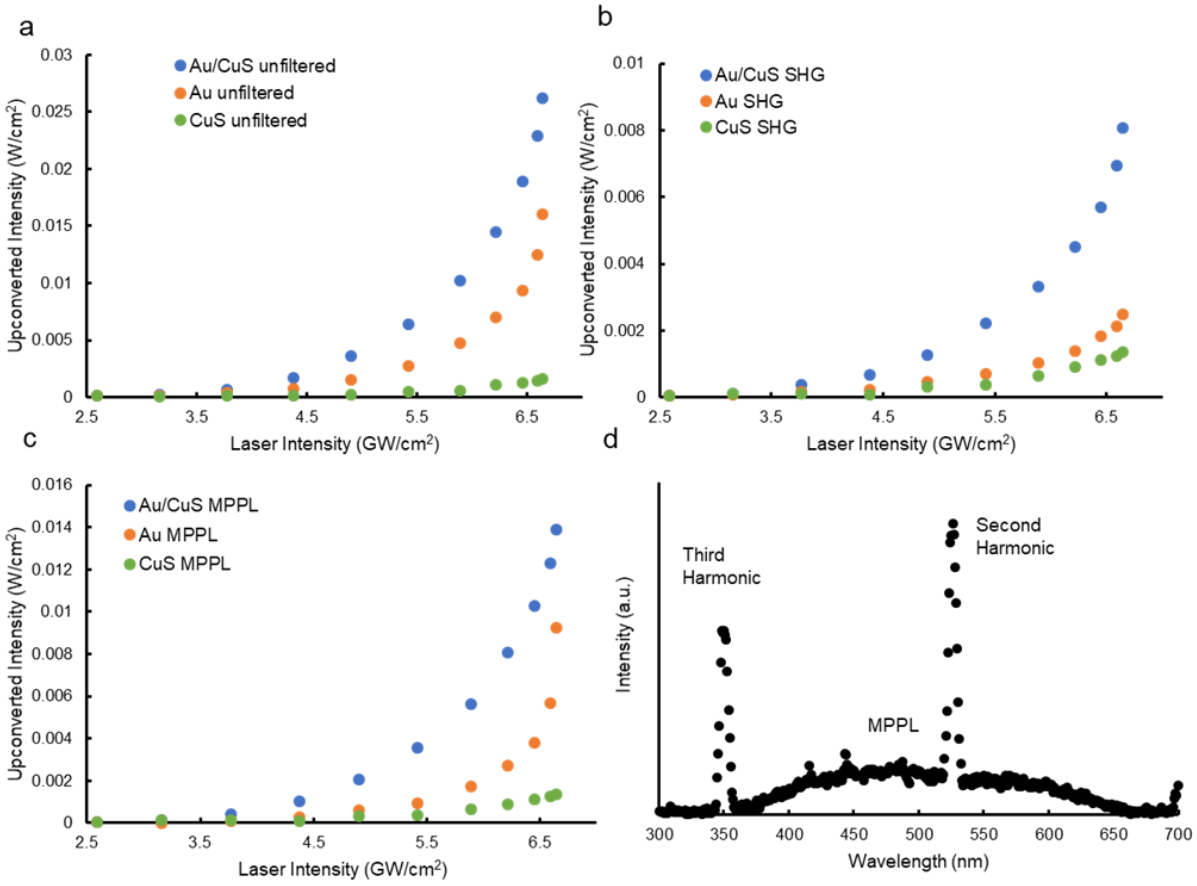

Figure 2.3 (a) Intensity of the unfiltered visible light generated versus the input laser intensity for each film type: Au only (orange), CuS only (green) and heterostructure (blue). (b) Intensity of light generated by the films at the second harmonic of the pump laser. (c) Intensity of visible light produced by the films not at the second harmonic. This light corresponds to upconversion by MPPL. (d) Spectrum of output light produced by nanoparticle heterostructure demonstrating upconversion by both higher harmonic generation and multiple photon photoluminescence mechanisms.

At pump intensities above about 4 GW/cm^2, the heterostructure films produced a strong nonlinear response. Importantly, the emission from the hybrid films was still greater than the incoherent sum of the two components. To quantify the enhancement due to coupling between the nanoparticles, the visible light contribution of the nanoparticle components was measured as a fraction of the upconverted light produced by the hybrid films.

$$\chi_j = \frac{(I_{Au,j} + I_{CuS,j})}{I_{hybrid,j}} \quad j = SHG, MPPL, Unfiltered \tag{1}$$

Thus, higher values of χj correspond to larger SHG enhancement due to hybridization, because less of the hybrid film output is attributable to its nanoparticle components.

Figure 2.4c plots the values of χ_j for SHG and MPPL across the pump laser range of 3.5-7 GW/cm^2. The SHG and MPPL signals are enhanced similarly at lower pump intensities, such that the values of χ_{SHG} and χ_{MPPL} are similar. However, at intensities above 6 GW/cm^2, the high-order dependence of MPPL from the Au nanoparticles reflects the increase of upconverted signal attributable directly to the Au nanoparticles; this, in turn, drives a decrease in χ_{MPPL}. The SHG signal does not exhibit a similar change in the order of response as the MPPL signal, and thus the magnitude of χ_{SHG}, remains constant across the full range of laser intensities.

To further quantify the enhancement that film hybridization pro-vides, a modification of the analytical enhancement factor (AEF) defined by Jais et. al. was used[43].

$$AEF = \frac{I_{Au-CuS}/\rho_{Au-CuS}}{I_{Au}/\rho_{Au}} \tag{2}$$

Where I is the SHG intensity and ρ is the optical density of Au nanoparticles at 525 nm. The enhancement effect strengthens as the input intensity increases for the SHG signal. At the maximum pump-laser intensity (6.64 GW/cm^2), the AEF for the SHG signal was 3.3,

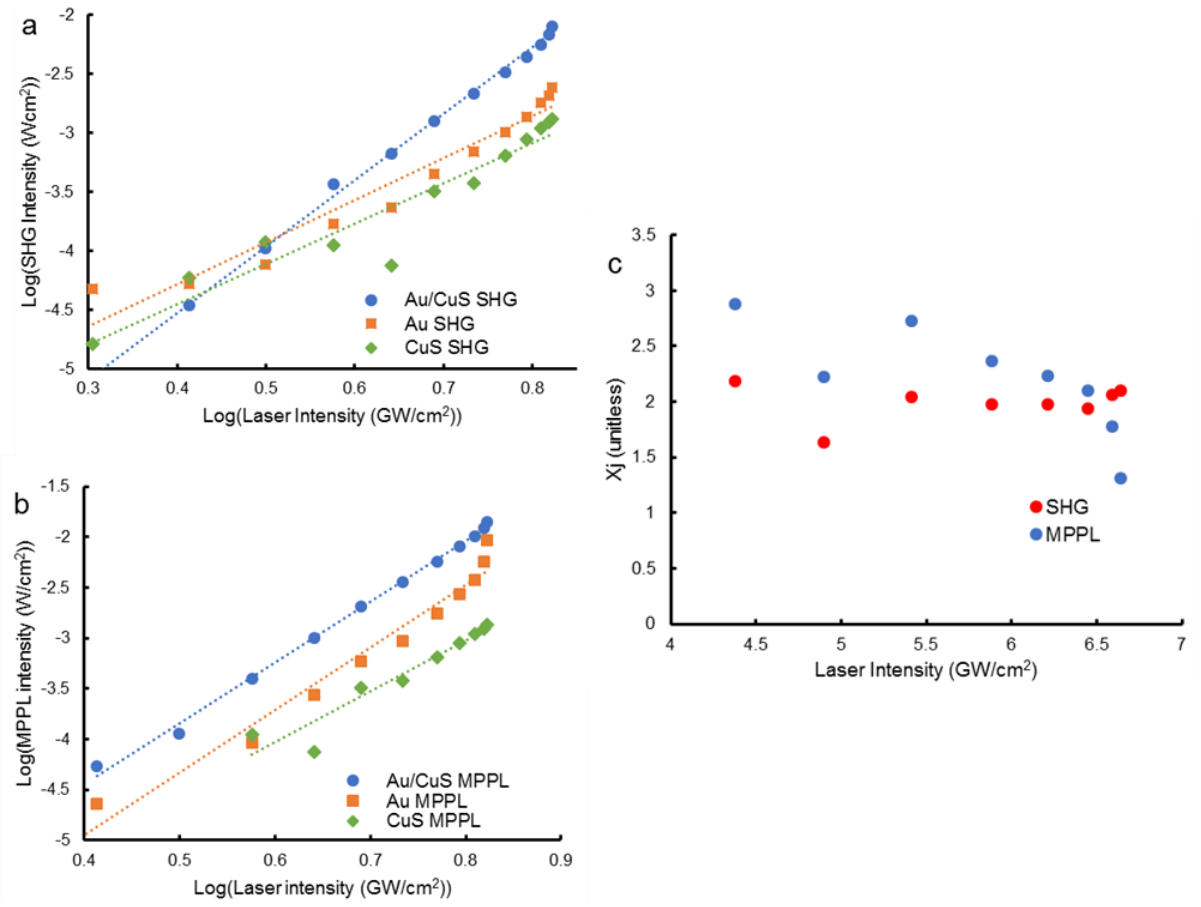

Figure 2.4 Double-logarithmic plots of the upconverted light intensity as a function of pump-laser intensity. (a) Fit for the SHG signal (515-560 nm). (b) Fit for the MPPL signal (560-720 nm). (c) The fraction of upconverted signal in hybrid samples that is directly attributable to the nanoparticle constituents (χ_j, Equation 1) for the SHG and MPPL components as a function of pump laser intensity.

while the AEF for the MPPL signal was 1.7. The measured visible light intensity as a function of pump-laser intensity was used to construct a double-logarithmic plot of the data whose slope yields the order of the nonlinearity that produces upconversion, the values for the order coefficients for the MPPL filtered and SHG filtered data are shown in Table 1 & 2 respectively. The variances in the fit coefficients are the ± one standard deviation limits.

2.4 Multivalent upconversion response order

Inspection of the log-log plots for the Au films suggests that at the highest pump-laser intensities, the order of the nonlinearity increases. This is indicated by the increasing slope of

the orange line in Figure 2.4a and b, in the fit to those data above 6 GW/cm^2 (Au high). Although the Au slope increase occurs in both the MPPL and SHG regimes, it is far more prominent in the MPPL regime. This suggests that any observed order increase in the 515-560 nm spectrum is due to contribution from MPPL overlapping with the SHG signal. This also explains why the order in the SHG regime is greater than two, as would be expected from an SHG signal.

Spectral overlapping of the MPPL and SHG signals caused the response in that part of the spectrum to take on the response characteristics (n>2) of MPPL. This conclusion is supported by the spectrum of the upconverted output (Figure 2.3d) which features convolution of the SHG and MPPL peaks in the 520-540 nm spectrum.

Table 2.1 Values of log-log fitting coefficients for MPPL filtered data (400-502 nm, 562-700 nm)

	Au film (low)	Au film (high)	Au:CuS	CuS film
a	-7.42±0.31	-12.3±2.0	-6.84±0.078	-7.05±0.44
b	6.17±0.44	12.3±2.5	5.99±0.11	5.03±0.59
R^2	0.96	0.89	0.99	0.91

Table 2.2 Values of log-log fitting coefficients for SHG filtered data (522-552 nm)

	Au Film	Au:CuS	CuS film
a	-5.72±0.18	-6.79±0.051	-5.82±0.23
b	3.57±0.27	5.65±0.075	3.43±0.34
R^2	0.95	0.99	0.91

The mechanism of the enhancement awaits further investigation, in particular using time-resolved techniques to elucidate the dynamics of the harmonics and the broadband MPPL emission. However, we can draw some conclusions. The MPPL mechanism is effective especially in gold, as a result of intraband transitions in the *sp* band that occur concurrently with interband *d*-to-*sp* transitions to create a *d*-band hole that serves as the final state for an *sp*-to-*d* interband transition[18]. The SHG and THG signals, on the other hand, arise from virtual transitions originating in the d band in gold, where they are quite efficient; a similar mechanism must be operative in the CuS, but to judge from the relative yields in Fig. 3(a)-(c), must be much less efficient, even though the hole-rich valence band in CuS might seem to enable virtual multi- or multiple-photon transitions.

The enhancement mechanism may be modeled by thinking of the planar components of the heterostructure as resonant, coupled cavities in close but not intimate contact, with the CuS nanodisks resonant near the fundamental frequency of the laser, the gold nanoparticles at the second harmonic. The coupling is weak; with a coupling constant on the order of 10-12 if it scales with the relative upconversion intensities in Figs. 3(b)-(c). Moreover, this is evidently not the entire story, because the largest broadband MPPL signal arises from the heterostructure, and this is not explainable either by the combination of intraband and interband transitions seen in gold, or by excitonic transitions – which cannot be accessed at these pump-photon energies. In particular, the broadband MPPL signal does not extend into the ultraviolet where the THG signal is observed.

It is interesting to compare the efficiency of SHG from the hybrid nanoparticle films to that of SHG from β-barium borate (BBO), perhaps the most widely used nonlinear harmonic-generating crystal. For laser intensities below the SHG enhancement threshold (4 GW/cm^2), normalized to the thickness of the sample and laser power squared, the BBO and hybrid nanoparticle films have nearly equivalent (2.2::1 Au/CuS:BBO) SHG per unit thickness. On the other hand, at the highest measured pump intensity (6.64 GW/cm^2), when the intensity of SHG is normalized to sample thickness and the square of the pump-laser intensity, the hybrid

nanoparticle film has almost an order of magnitude greater yield per unit thickness than BBO (9.2::1). This is about twice the volume-normalized yield from lithographically fabricated gold Archimedean nanospirals[11]. Since the second-harmonic yield is also proportional to the effective second-order susceptibility deff, this implies that the hybrid bi-layer has deff~13 pm/V.

Nanoparticle films containing only Au and CuS nanoparticles were also evaluated. For films with the same optical density of nanoparticles as the hybrid sample, normalized by length and laser power squared, the nanoparticle films produced modestly more second harmonic light than BBO (2.8::1), and the CuS nanoparticle films produced less visible light than BBO (0.2::1). This further highlights the relatively low nonlinear response of CuS nanoparticles when excited at 1050 nm without the presence of the Au nanoparticles. Optimization of the films and nanocrystal orientation, density, and interlayer spacing is expected to further improve this material property.

2.5 Conclusion

In summary, Au nanospheres have a plasmon resonance at the second harmonic of the fundamental plasmonic resonance of CuS nanoparticles. Hybrid CuS/Au nanoparticle heterostructures exhibited an analytic enhancement factor for the second harmonic signal of 3.3, exhibiting greater second harmonic yield than the sum of either nanoparticle film alone. This suggests that there is a coupling effect between the plasmon resonance of the CuS nanoparticles and the Au nanoparticles. The presence of Au nanoparticles attenuates the bleach of the CuS nonlinear absorption in hybrid films. The hybrid films exhibit greater upconversion efficiency per unit thickness than BBO, a high-performance nonlinear crystal.

This work demonstrates that a thin film heterostructure that places semiconducting and metallic nanoparticles in close proximity can enhance nonlinear optical properties by coupling of plasmons. Such a material system has important advantages for nonlinear optical materials, in that plasmon-plasmon processes are ultrafast compared to excitonic processes and the ease

with which the nanoparticle films can be fabricated via solution processing. Many plasmonic metal and semiconducting combinations can be envisioned with plasmon bands ranging from the NIR to the UV, making this design highly tunable. In this particular system, the plasmon resonance at the fundamental is centered on the favored wavelength for dispersionless propagation in the telecommunications band. In these nanoparticle films, phase matching is not required. This development in nanocrystal-based nonlinear optical materials will allow reduced size of optical components, reaching toward the domain of planar nano-optical devices. Further exploration of the dependence of SHG yield on the interaction distance between coupled plasmonic elements, the effect of coupling between plasmonic elements on the third-harmonic generation, and of alternative material systems will allow increased understanding of the fundamental mechanisms that govern coupling between plasmonic nanoparticles.

CHAPTER 3

The dependence of THG upon plasmonic harmonicity

3.1 Introduction

Metal nanostructures have been widely employed to enhance nonlinear optical processes, such as second harmonic generation (SHG),[38],[56],[57] third harmonic generation (THG), [10],[58],[59] and multiphoton photoluminescence (MPPL) [17],[18],[60]. Metal nanoparticles with their high electron polarizabilities, intense optical resonances and high surface-to-volume ratio, become effective substrates for optical phenomena that occur on surfaces. As examples, when excited with an intense light field, the localized surface plasmonic resonances (LSPR) generates gigantic local electric fields, enhancing Raman signals of nearby molecules, or yielding high upconversion efficiency. Plasmonic properties can be varied by material and structural factors,[61],[62] in addition to bimetallic alloys [63],[64].

Increasingly complex coupled systems have been prepared that demonstrate strong nonlinear response enhancement, especially for coupled semiconductor and metallic nanoparticle systems [43],[52],[65]. In such systems, for example, the metal nanoparticles modify the nonlinear response of the semiconductor nanoparticle via coupling between the plasmonic resonance and excitons in the semiconductor [45]. Our complementary approach has been to examine the enhancement of the harmonic generation of a heterostructured film comprising of plasmonic semiconductor and plasmonic metallic nanoparticles separated by a thin layer of insulating ligands. In contrast to plasmon-exciton approaches, dually resonant systems feature additional local electric field enhancement from both nanoparticles, further increasing harmonic generation efficiency [66],[67].

An emerging class of these biplasmonic structures feature plasmonic resonances that harmonically couple to each other, that is, such that one resonance is energetically located at a

excitation fundamental and the other resonance located at a harmonic of the excitation energy [68]–[70]. These systems have promise as platforms for efficient and thin-film harmonic generators. A CuS nanostructured thin film with uniform distribution has been prepared with a simple and cost-effective chemical bath deposition method (CBDM) show high quality of optical and electric properties [71]. The LSPR peak of CuS can be tuned by electrochemical reduction [72]. Besides CBMD, many deposition methods have been reported [73],[74].

CuS belongs to a class of heavily doped colloidal nanocrystals of metal chalcogenides that exhibit both semiconductor and plasmonic behavior. Their plasmonic behavior originates from the collective oscillation of excess free carriers associated with constitutional vacancies, leading to a NIR plasmon resonance. Moreover, the LSPR features of metal chalcogenide nanoparticles are controlled by their geometric parameters, such as size, shape and in addition to the constitutional free carrier density determined by the particular stoichiometric composition and crystal structure [47],[75],[76]. Covellite CuS possesses semi-metallic character due to a large concentration of delocalized holes in the valance band from stoichiometric constitutional S2- vacancies. The extinction band of CuS results from the convolution contributions of a weak out-of-plane and a dominant in-plane dipolar LSPR mode[77],[78]. These modes can be separated by a change to the crystal orientation or the incident light polarization [27].

The LSPR of metallic gold are from the collective oscillation of Fermi-edge electrons. The resonant energy is tunable from the UV through to the near-infrared predominantly by changing geometry: shells, aspect ratio, shape, and alloying with other elements. Particle size can also tune the LSPR, as red-shifted quadrupolar resonances become increasingly important for large particles [79]–[81]. The size of the nanoparticle also effects the dephasing time of the collective resonance, with spherical particles larger than 50 nm producing long dephasing times, on the order of tens of fs. Very small nanoparticles, with diameter less than 3 nm, are not large enough to feature near field effects. Instead, excitation decays into hot electrons within 1 fs. Intermediate sizes, such as the 15 nm particles predominantly examined here, feature dipolar LSPR with medium dephasing times that decay into hot electrons [82].

Resonant excitation of LSPR can enhance SHG [83]. Such enhancement has been

demonstrated in various structural designs of gold nanoparticles: split-ring-resonators,[34] arrays of gold nanorods,[84],[85] a single dimer of gold nanospheres,[86] and hybrid plasmon-fiber cavity systems [87]. However, few studies have been reported on the enhancement of harmonic generation from Au nanoparticles in conjunction with harmonically resonant plasmonic semiconductor nanoparticles such as the hybrid Au/CuS nanoparticle films that we explore herein. This combination has the potential for dual plasmonic structures in which the resonances are spectrally located such that a harmonic relationship exists between the excitation energies of their respective LSPR.

Previously, we observed that Au/CuS bilayer nanoparticle films enhanced the yield of second-harmonic light by a factor of 3.3 compared with the sum of constituent nanoparticles on their own [88]. Additionally, these films exhibited signals from several upconversion pathways, including SHG, THG and MPPL peaks. It was expected, that, as a third order process, THG would be far less intense the second order SHG; yet, in these initial studies, it was noted that the third harmonic signal was similar in intensity as the second harmonic signal. This observation suggested that the plasmonic interactions between Au and CuS nanoparticles were serving to enhance THG as much or more than the enhancement of SHG. Which is consistent with other plasmonic nanoscale systems, due to their large third order polarizability and centrosymmetry[9] . Additionally, a THG process derived from plasmonic interactions has the advantage of occurring within the context of ultrafast processes, which means that there is no delay due to the thermalization and recombination steps as occurs plasmon-exciton coupled systems. The peak excitation frequency of Au/CuS bilayer heterostructures is also centered near the telecom O- and E-bands, meaning that it can be integrated into thin-film optical modulators for fiber telecommunications making for exciting applications of such structures in ultrafast communication technologies.

Herein, we demonstrate that the dominance of THG or MPPL upconversion mechanisms can be switched by the detuning of CuS or Au plasmon resonance from the harmonic condition. Additionally, to separate THG from possible degenerate sum frequency generation (SFG), a dual beam setup with both fundamental (frequency ω) and second harmonic (frequency

2ω) beams was constructed [89],[90]. By changing the ratio of ω:2ω intensity, we observed for the first-time simultaneous excitation of the LSPR of both nanoparticles in the Au/CuS nanoparticle films. This simultaneous excitation increased the efficiency of THG, lowering the detection onset threshold (the lowest power at which signal could be measured above the background). Finally, a dipole-dipole interaction analytic model for the enhancement of THG from Au/CuS bilayer heterostructured films is presented. The behavior predicted by the model closely matches experimentally measured data, suggesting that interactions of surface dipoles between nanoparticles is an effective approach to understanding the upconversion properties of Au/CuS films.

3.2 CuS orientation effects on upconversion mechanism

Au nanoparticles of were synthesized following literature precedent in several sizes: 3nm,[91] 15 nm,[51] and 100 nm [92]. The gold nanoparticles of 3 and 100 nm diameters, which were synthesized in water, needed to be transferred to an organic solvent for film deposition. This was accomplished following a transfer ligand-based approach to give surface capping of octadecylamine [93]. Likewise, CuS nanoparticles were synthesized using well established approaches. These disk-shaped nanoparticles had an average diameter of 15 nm and were capped with oleylamine. Nanoparticles were deposited sequentially onto glass slides using spin coating to form bilayer films. The structure of the films and optical properties were confirmed through Scanning Electron Microscopy in secondary electron and backscatter detection modes (Appendix B.1) and UV-vis-NIR spectrophotometry, respectively. The thickness of the films was 120 nm as measured using profilometry (Appendix B.2). These methods confirmed the bilayer structure of the nanoparticles on the glass, as well as the presence of the thick, encapsulating layer of oleylamine ligand surrounding the nanoparticles. The ligand layer is critical to preventing the nanoparticle layers from coming in direct contact; were this to occur, then the nanoparticles will quench each other's LSPRs,[94] preventing harmonic coupling. In the bilayer films reported on here, the oleylamine layer separates each nanoparticle from its neighbors by a few (3-10) nanometers, forming a somewhat diffuse layer

of nanoparticles whose density is dependent upon the number of oleylamine molecules that intercalate between the nanoparticles. While there is considerable variation in the spacing of the nanoparticles from one to the next, over the length of the spot size of the laser (10 μm) there is an averaging effect which homogenizes the upconversion response at various sampling points across the film.

The processing conditions under which CuS nanoparticles were deposited had a large impact on upconversion properties. If nanoparticles were drop-cast onto a substrate (with Au nanoparticles already situated thereupon) and allowed to dry into a layer, the LSPR was blue shifted compared to the colloidal measurement. SEM and in-plane XRD indicated that the CuS disks would orient face-to-face and lie in stacks on their edges. The particle stacking had the effect, causing the blue-shifted, out of plane (axial) mode of the plasmon resonance to become the predominant resonance (Figure 3.1a) [27]. This blue shift caused the LSPR of CuS to no longer align with the excitation frequency of the laser. Thus, this change in processing effectively detuned the surface plasmon from the resonant condition. Upon stimulation by a 1050 nm laser, the detuned sample exhibited the broad emission peak characteristic of MPPL (Figure 3.1b). Without the resonant enhancement from the surface plasmon at the fundamental frequency, harmonic generation was not efficient enough to be detected at the excitation intensities available in our experiment (6.7 GW/cm^2).

In contrast, when CuS nanoparticles were added to the films through spin-coating, SEM (Figure 3.1c,d) indicated the particles were mostly aligned with basal planes parallel to the surface. The LSPR centered at 1300 nm indicated that the in-plane (transverse) mode dominated the profile of the LSPR. With laser excitation at 1050 nm, a signal centered on 3ω was measured, although it was not possible with only this experiment to determine of this signal resulted from THG or SFG. While THG and SFG typically have a narrow line width dictated by the laser's characteristics, in these experiments wide slit setting was used on the monochromator to measure these data to maximize the signal-to-noise ratio, resulting in an artificially broadened peak. In short, the tuning and detuning of the CuS plasmon resonance indicates that coincidence with the laser fundamental is a necessary component in bi-plasmonic

systems to observe the strong 3ω signal indicative of harmonic generation, instead of only MPPL.

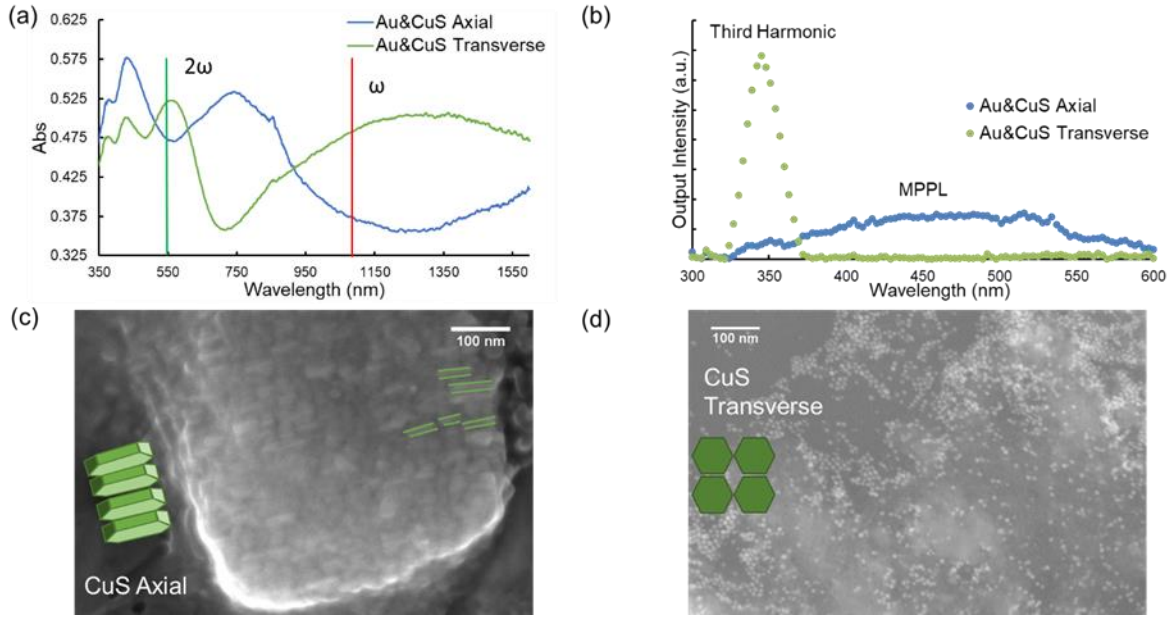

Figure 3.1 (a) UV-vis-NIR spectrophotometry of two heterostructure films deposited on glass microscope slides: Au with CuS in axial orientation (blue), Au with CuS in transverse orientation (green). (b) Spectra of output light produced by the two nanoparticle heterostructures. (c) SEM images of CuS nanoparticles with axial orientation produced by drop casting. The green lines highlight the edges of select nanodisks as a guide to the eye. (d) SEM images of CuS nanoparticles with transverse orientation produced by spin coating.

3.3 Au nanoparticle size effects on THG enhancement

The tuning of the plasmon resonance of Au nanoparticles was also integral to the efficiency of harmonic generation. Spin coated films were prepared with Au nanoparticles of 3, 15, and 100 nm diameters. The amount of third harmonic light produced by these films was measured, then identical layers of CuS were coated on top of the Au nanoparticle layers. This allowed for comparison of the extent to which the LSPR of the Au nanoparticles of differing sizes interact with the LSPR of CuS. The selected sizes of Au nanoparticles were chosen because of their have significant differences in their collective plasmon oscillations (Figure 3.2a). The 15 nm Au nanoparticles exhibited narrow, dipolar LSPR with its peak centered at λ=550 nm. This resonance corresponds most closely to the second harmonic of the stimulating laser (and thus the second harmonic of the plasmon resonance of the CuS nanoparticles). The 100 nm Au

nanoparticles had a broader resonance than the 15 nm particles, and the peak absorption wavelength was shifted towards the red in addition to longer dephasing times (tens of fs) and broadband scattering. Conversely, 3 nm diameter Au nanoparticles have a very low absorbance cross section and have very short dephasing times (1 fs) such that the excitation quickly decays into hot electrons, precluding an LSPR absorbance peak [95],[96].

The efficiency of the generation of 3ω light (350 nm) from heterostructured films containing 3, 15, and 100 nm diameter Au nanoparticles varied widely. Films containing 15 nm Au nanoparticles and CuS nanoparticles demonstrated the strongest signal at the third harmonic, with a 20x factor of enhancement over the sum of the light produced by Au and CuS on their own (Figure 3.2b). The LSPR of the 15 nm Au nanoparticles closely aligns with the harmonic condition (Au LSPR at 2ω) that produces enhancement of harmonic generation.

In stark contrast, films with 100 nm diameter Au particles produced a much more modest amount of third harmonic light. Indeed, there appeared to be no enhancement effect, as films with 100 nm Au and CuS nanoparticles produced only as much third harmonic signal as the sum of their parts. The LSPR of the 100 nm Au nanoparticles is detuned from the harmonic condition, and this appears to inhibit harmonic coupling of the CuS and Au plasmonic resonances (Figure 3.2c) which is needed for efficient production of 3ω light. Similarly, films containing 3 nm Au and CuS nanoparticles also only generated as much third harmonic light as the sum of each nanoparticle layer on their own, once again suggesting that there is no enhancement by bringing nanoparticles into proximity unless they also satisfy the harmonic condition. The 3 nm particles feature very low LSPR absorbance, and so again, the harmonic condition between the CuS (LSPR at laser fundamental ω) and Au (at 2ω) seems to be necessary for enhancement of the signal at 3ω. Notably, third order dependence was measured for samples at all sizes of Au nanoparticles (Appendix B.3). On their own, the 100 nm Au nanoparticles generated less 3ω light than 15 nm Au particles on their own by a factor of five at the highest excitation intensity. 3 nm diameter Au nanoparticles also produced a lesser quantity of upconverted light than 15 nm diameter particles by a factor of 1.5. Taken together, these results strongly suggest that

enhancement of 3ω signal only occurs when the plasmon resonance of the Au is energetically situated at the second harmonic of the laser. The enhancement of harmonic generation, then, is a resonant effect mediated by the LSPR and thus is size dependent, rather than having its origins in crystallographic or macroscale material properties.

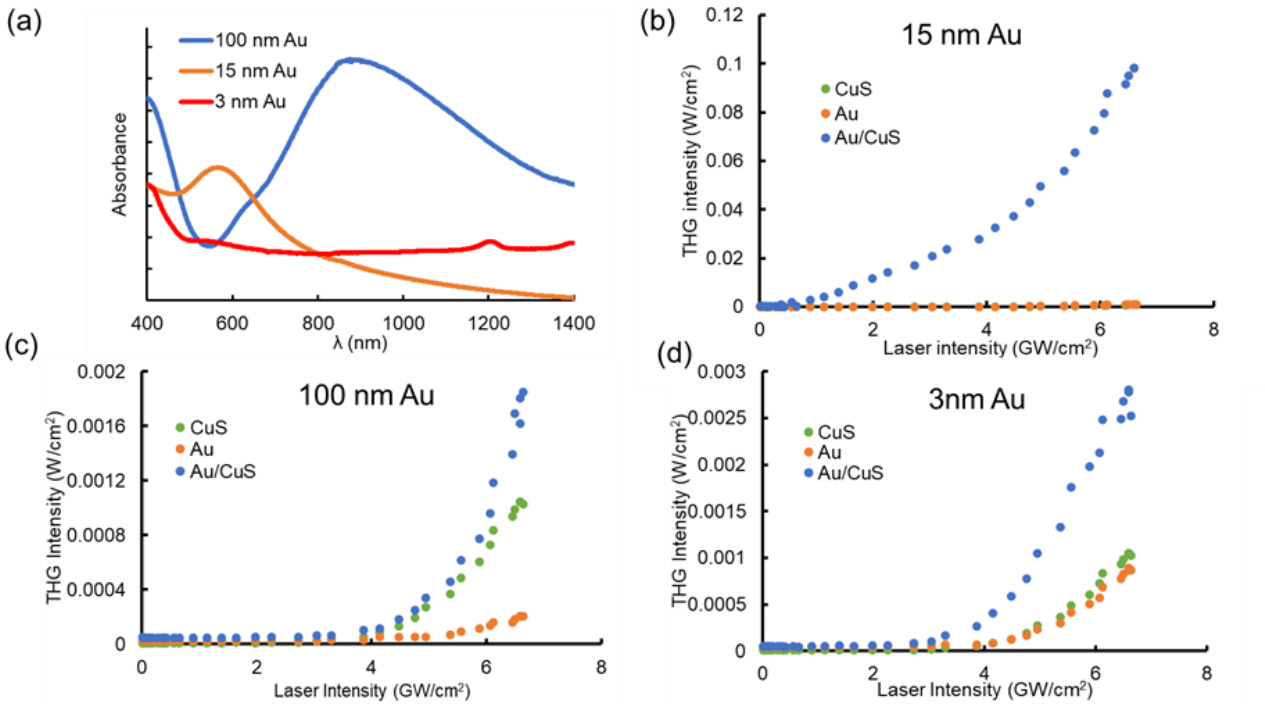

Figure 3.2 (a) UV-vis-NIR spectrophotometry of three size Au films deposited on glass microscope slides. Intensity of the THG signal generated by 1050 nm excitation as a function of the input laser intensity for films with different Au nanoparticle diameters and CuS in the transverse orientation (b) dAu=15nm (c) dAu=100nm (d) dAu=3nm

3.4 Dual simultaneous excitation of Au and CuS nanoparticles in a hybrid film

With the integral role of the harmonic positioning of the LSPR in Au and CuS nanoparticles confirmed, the question remained of how the upconversion of the light to the third harmonic was occurring in the bilayer films, as two separate mechanisms were likely. Ambiguity existed between a direct THG process (ω + ω + ω = 3ω) and a degenerate cascaded process (ω + ω=2ω then ω + 2ω = 3ω); a cascaded THG process would explain why the third harmonic signal was similar in intensity compared to the second harmonic in our previous

study due to the second order nature of the SHG and SFG steps [88]. Both the cascaded and direct THG possess an order of 3, thus further experimentation was required to disambiguate between the two processes by testing the possibility of SFG in the nanoparticle bilayer films directly using separate ω and 2ω beams[3].

The films were contemporaneously stimulated with both 1050 nm (ω) and 525 nm (2ω) light by the use of a beam splitter and a high-efficiency frequency doubling crystal, β-barium borate (BBO), in an approach similar to the demonstration of SFG in other nanostructured materials (Figure 3.3a) [89]. This approach decouples the SHG and SFG steps in the cascaded THG process, allowing for direct testing for the capability of the nanoparticle films to perform the second (SFG) step in cascaded THG. Simultaneous excitation at 1050 nm and 525 nm directly induces surface plasmon resonances in the CuS and Au, respectively. With both plasmon resonances actively stimulated, the yield of light at the third harmonic increased greatly with respect to single beam stimulation at the same intensity, from the addition of the SFG signal (Figure 3.3b).

Excitation at 2ω in addition to the ω stimulation enhanced generation of 3ω light in these bi-plasmonic systems across varied intensities of w and 2w. These experiments were performed by decreasing the reflectance: transmittance ratio in the beam splitter, which in effect lowers the relative amount of 1050 nm light and increases the quantity of 525 nm light, causing an increase in the light yield at 3ω. Indeed, even comparing dual beam excitation with different mixes of components, the mix with more 2ω excitation produced a greater quantity light at 3ω (50:50 BS curve is above 70:30 and 100:0 at the same laser intensity).

The use of the 50:50 split in the excitation beam stands out, as this mixture has overall low power as a result of losses in the beam splitter and during the upconversion process. A mixture of linear and nonlinear components produced an overall order of 1.68 with respect to the ω intensity (Figure 3.3c). This mixture is composed of SFG (first order with respect to ω) and MPPL (6^{th} order, see chapter 2) mechanisms producing 350 nm light under this excitation condition. The presence of the MPPL signal is demonstrated in Appendix B.4.

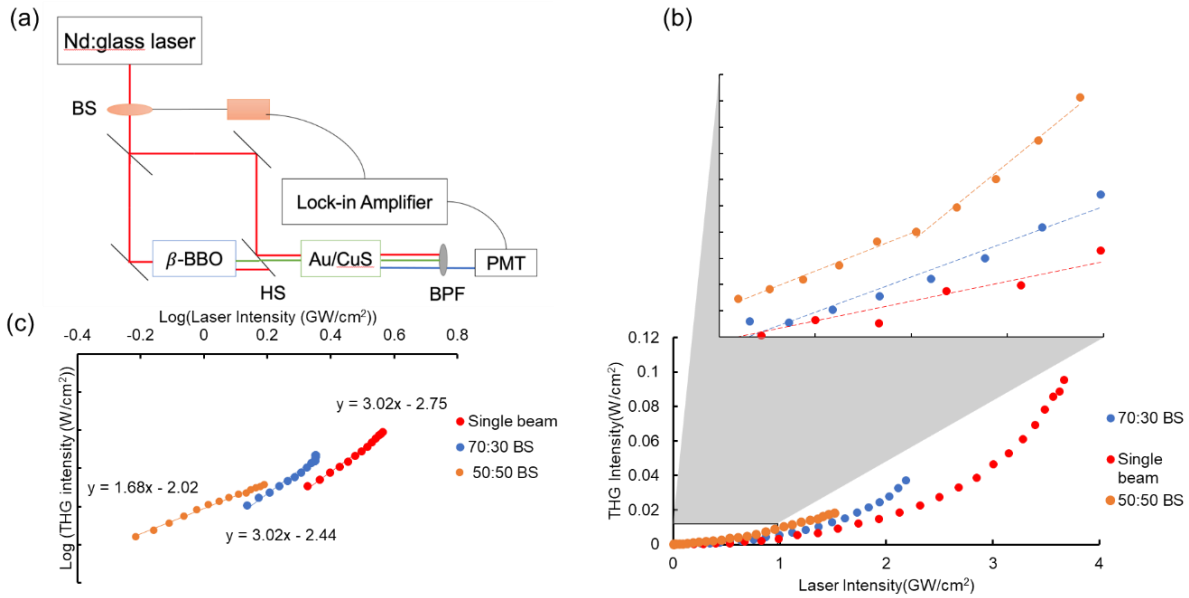

Figure 3.3 (a) A simplified diagram of the experimental dual-beam setup. BS= Beam splitter, HS= Harmonic separator, BPF=350 nm Bandpass filter. Red line is 1050 nm fundamental beam, green is 525 nm (2ω) beam, and blue 350 nm (3ω) beam. (b) Intensity of THG output generated by hybrid films as a function of fundamental beam intensity after beam splitter for different R:T ratio beam splitter: 100:0 (red—power of 2ω 0 μW), 70:30 (blue—power of 2ω beam 185 μW), 50:50 (orange—power of 2ω 300 μW). (c) Double-logarithmic plots of THG intensity as a function of pump laser intensity.

With the feasibility of SFG in CuS-Au nanoparticle bilayer films established, the observed enhancement of THG due to the presence of a harmonic plasmon resonance suggests that a cascaded mechanism of SFG seeded by SHG is responsible, rather than enhancement of a direct THG process. To examine the validity of this explanation, we built a dipole-dipole interaction analytic model and observed its correspondence with experimental measurements. To set about building an analytic description of the harmonic generating properties Au-CuS nanoparticle bilayer films, we considered the effect of the electric field of each nanoparticle upon the other nanoparticle. In an approach akin to that taken for similar heterogenous nanoparticle ensembles [65],[97], coherence between the LSPR fields was not considered because the dephasing time of the plasmons are much shorter than the duration of the pump pulse, meaning that the resonances very quickly lose coherence and thermalize—due to electron-electron collisions—once the pump pulse ends.

3.5 Analytic model of THG enhancement from harmonic relationship between

plasmonic nanoparticles

To examine the validity of this explanation, we built a dipole-dipole interaction analytic model and observed its correspondence with experimental measurements. To set about building an analytic description of the harmonic generating properties Au-CuS nanoparticle bilayer films, we considered the effect of the electric field of each nanoparticle upon the other nanoparticle. In an approach akin to that taken for similar heterogenous nanoparticle ensembles [65],[97], coherence between the LSPR fields was not considered because the dephasing time of the plasmons are much shorter than the duration of the pump pulse, meaning that the resonances very quickly lose coherence and thermalize—due to electron-electron collisions—once the pump pulse ends.

The full derivation and model details are available in Supporting Section S2. In brief, the far-field intensity of the third harmonic (I_{THG}) output by the bilayer system will be the sum of the 3ω signal originating from each component.

$$I_{THG}^{hybrid} = I_{THG}^{Au} + I_{THG}^{CuS} \quad (1)$$

Each component in turn, will be dependent upon the intensity of the electric fields around them. For example, the CuS nanoparticles will have terms for fields from the laser pump beam (I_p^3) and the LSPR field of the Au nanoparticles (I_{Au}^3), but also the cross terms between the Au LSPR and the pump beam ($I_p^2 I_{Au}$ and $I_p I_{Au}^2$). Scaling factors $\Pi_{Au/CuS}$ are needed to account for the extinction coefficients of the particles at the pump frequency (we expect Π_{Au} to be much smaller than Π_{CuS} at w and vice versa at 2w judging from their absorbance spectra). Thus, the general statement for THG from the Au-CuS nanoparticle system is:

$$I_{THG}^{hybrid} = \left[\alpha_{cst}^{Au}\Lambda_{au}^6\left|F_{ppp}^{Au}\right|^2\left\{{I_p}^3 + 9{\Pi_{CuS}}^2{I_p}^2 I_{CuS} + 9{\Pi_{CuS}}^4{I_{CuS}}^2 I_p + {\Pi_{CuS}}^6{I_{CuS}}^3\right\} + \right.$$

$$\left.\alpha_{cst}^{CuS}\Lambda_{CuS}^6\left|F_{ppp}^{CuS}\right|^2\left\{{I_p}^3 + 9{\Pi_{Au}}^2{I_p}^2 I_{Au} + 9{\Pi_{Au}}^4{I_{Au}}^2 I_p + {\Pi_{Au}}^6{I_{Au}}^3\right\}\right] \quad (2)$$

$$E_{spp}^{Au} = \Pi_{Au}E_P \qquad \Pi_{au} = \frac{V_{Au}g_l}{4\pi r^3}\zeta_{Au} \quad (3)$$

$$E_{spp}^{CuS} = \Pi_{CuS}E_P \qquad \Pi_{cus} = \frac{V_{CuS}g_l}{4\pi r^3}\zeta_{CuS} \quad (4)$$

α_{cst}, Λ, and F_{ppp} are constants relating the charge carrier density and mobility of Au and CuS as

well as nanoparticle size and spacing to the nonlinear susceptibility of these materials Equation 5.

$$\chi_{ppp}^{Au} = \frac{2\mu_{21}^3 p_{Au}}{V_{Au}\in_0 \hbar^3}\left(\Lambda_{Au}^3 F_{ppp}^{Au}\right) \quad (5)$$

Equation 2 implies a bilateral relationship between the two nanoparticles, with each nanoparticle enhancing the local electric fields for the other nanoparticle. Thus, we see that Equation 2 is composed of two components, one of which represents THG from the Au nanoparticles—with intensity terms from the pump beam and the local field of the CuS LSPR—and the other of which represents THG from CuS nanoparticles, again with intensity terms from the pump beam and the Au LSPR.

Under single beam excitation at 1050 nm (ω), the absorbance of the Au plasmon is negligible, equation 2 Simplifies to:

$$I_{THG}^{hybrid} = \left[\alpha_{cst}^{Au}\Lambda_{au}^6\left|F_{ppp}^{Au}\right|^2\left\{{I_p}^3 + 9{\Pi_{CuS}}^2{I_p}^2 I_{CuS} + 9{\Pi_{CuS}}^4 {I_{CuS}}^2 I_p + {\Pi_{CuS}}^6 {I_{CuS}}^3\right\} + \alpha_{cst}^{CuS}\Lambda_{CuS}^6\left|F_{ppp}^{CuS}\right|^2\left\{{I_p}^3\right\}\right] \quad (6)$$

because the Π_{Au} terms are near zero due to how far off 1050 nm stimulation is from the Au resonance. Under dual-beam excitation all of the terms of Equation 2 are nonzero, and it is the additional terms containing Π_{Au} which account for the increase in measured THG in the dual-beam mode.

The importance of the harmonic condition between the LSPR of Au and CuS nanoparticles is explicable with the simple model of the superposition of two waves (with the same group velocity) and different frequencies,[98] f_1 and f_2. This approach models near-field coupling between the respective LSPR of the nanoparticles as opposed to the treatment provided in Appendix B.5, which considers the LSPR as acting incoherently upon each other. This resulting superimposed wave has greater amplitude than the input waves (Equation 7), in which the amplitude term (E_m) has doubled.

$$E(x,t) = E_m\cos(k_1x - \omega_1 t) + E_m\cos(k_2x - \omega_2 t) = 2E_m\cos\left[\frac{k_1-k_2}{2}x - \frac{\omega_1-\omega_2}{2}t\right]\cos\left[\frac{k_1+k_2}{2}x - \frac{\omega_1+\omega_2}{2}t\right] \quad (7)$$

In the resulting expression, the amplitude envelope of the resulting oscillation is controlled with the first cosine term. This means that the amplitude profile (beat frequency) is largely controlled by the difference in frequency, which is consistent with the rotating wave approximation in nonlinear optics, invoked above (Equation 8) [99].

$$f_{beat} = (f_1 - f_2) \tag{8}$$

Thus, when the resonant frequencies of the two oscillations are in a harmonic relationship ($f_1 = 2f_2$) the beat frequency is the same as the frequency of the fundamental oscillation ($f_{beat} = f_2$). Due to the increase in amplitude of the superimposed wave, this has the effect of enhancing the electric field intensity. Notably, if the resonances are tuned away from the harmonic condition, then the beat frequency will not match the fundamental frequency and would not enhance the excitation intensity as effectively, as there lacks coherence between the resonant mode and the excitation pulse. If we apply this approach to the plasmonic resonances of Au and CuS nanoparticles in a bilayer film, treating the LSPR as dipolar oscillations (as above) each of which are actively being pumped at their respective resonant frequencies— as is the case for the simultaneous dual beam excitation condition, but not in the 1050 nm only excitation— then the beat frequency is the same as the resonant frequency of the CuS nanoparticle (f_{beat}= 285.5 THz, 1050 nm). Thus, the amplitude of the electric field at ω is enhanced by the presence of the Au LSPR, which concomitantly increases the quantity of THG from the CuS.

The upconverting properties of the Au/CuS bilayer heterostructure are accurately predicted by the model. In particular, the third harmonic enhancement effect in samples containing 15 nm Au nanoparticles (as measured experimentally) were reproduced by plotting Equation 2 with Π_{Au} and Π_{CuS} as fitting parameters (Figure 3.4a). The validity of the obtained values these coupling constants was confirmed by separate calculation from the known values of the physical constants (Appendix B.5). We see that the simple addition of signal from films containing Au and CuS separate from each other, without the I_{au} & I_{CuS} terms that come from the local field of one nanoparticle's plasmonic resonance acting on another nanoparticle, is lower than the combined film, in which the nanoparticles interact. Indeed, the relative quantity

of enhancement closely matches experimentally measured increase from having both nanoparticles. The spectral width of the output THG signal is also agrees with experimentally measured values (Figure 3.4c). Using the spectral profile of the pump laser and plugging the arbitrary intensity thereof at a variety of wavelengths into Equation 1, then plotting the THG output intensity for these wavelengths, the spectral width of the experimental results was closely matched.

3.6 Conclusion

Thin bilayer films containing Au and CuS nanoparticles, with surface plasmon resonances at the frequency of a pump laser (CuS) and at the second harmonic (Au), respectively, exhibited enhanced THG over the individual films as a result of dipole-dipole, incoherent interactions between the nanoparticles. Using the dipole approximation, an analytic model that accounts for both the action of the Au LSPR on harmonic generation in CuS and the action of the CuS LSPR on harmonic generation in Au accurately predicts the upconversion properties of these bilayer nanoparticle films. Additionally, the process-property relationships between the deposition-controlled orientation of the CuS nanoparticles and the output spectrum were explored. It was found that CuS nanoparticles, stacked face-to-face (with their edge facing out), showed a blue-shifted LSPR compared to face-up nanoparticles. This difference in excitation energy corresponded to the disappearance of the 3ω signal in the output spectrum, indicating that the LSPR of the nanoparticles was critical to the upconversion mechanism. Similarly, shifting the Au plasmon resonance by changing the nanoparticle diameter in different bilayer films shows that the enhancement effect due to the Au nanoparticle can be eliminated if the resonance of the particles is not resonant with second harmonic of the pump beam. This also supports the assertion that the interactions between the Au and CuS nanoparticles in these films are mediated by their LSPRs. Moreover, direct excitation of the Au LSPR at 2ω with simultaneous excitation at the CuS plasmon resonance at ω demonstrated efficient sum frequency generation This suggests that the plasmon resonance of Au enhances the generation of 3ω light in a cascaded THG process.

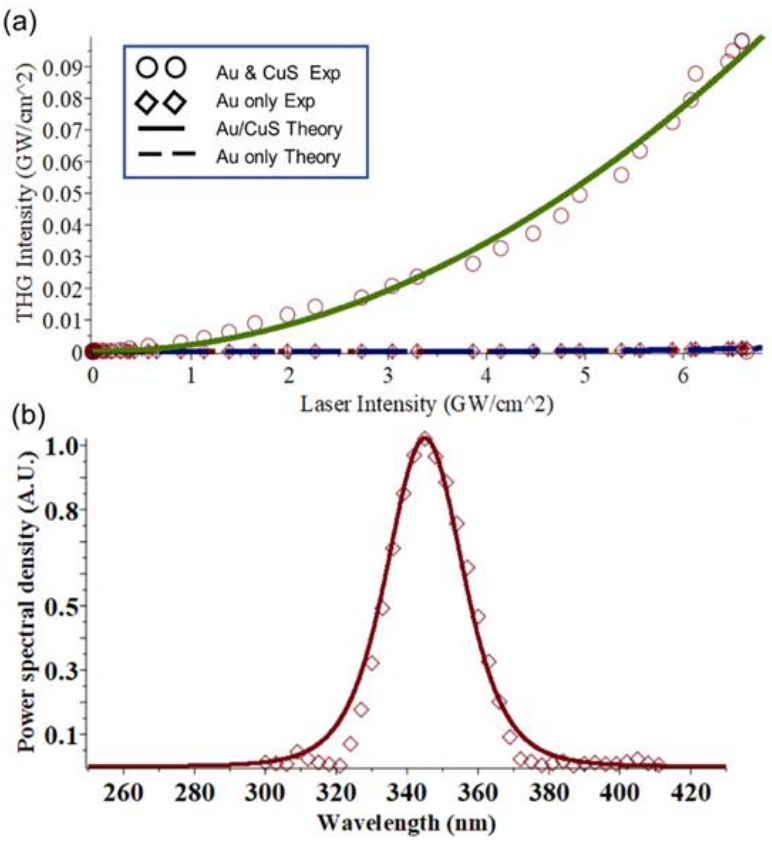

Figure 3.4 Correlation between experimental results and predicted values from dipole-dipole analytic model. (a) THG signal as a function of input intensity from predicted from analytic model for: 15 nm diameter Au & CuS nanoparticle hybrid film (solid green) and Au nanoparticle only (dashed purple). Experimental data from bilayer films are plotted as circles and data from single species films with diamonds. (b) The predicted output intensity of upconverted light at various wavelengths, diamonds are experimental data. Line theoretical fit centered on 3ω with a fitting full width at half max of 25 nm.

To further explore the fundamental mechanisms that govern interactions between harmonically resonant plasmonic nanoparticles, the effect of the properties of the gap between the two nanoparticle layers should be investigated. Directly probing the nanoparticle interface with localized measurement techniques such as near-field spectro-microscopy will potentially yield insights into the coupling mechanism that governs the enhanced harmonic generation. Off-resonant excitation from an optical parametric amplifier (OPA) would allow us to explore the various upconversion mechanisms that these films, and possibly demonstrate switching between generation of harmonics and MPPL. Finally, the concept of harmonic interactions between plasmonic nanoparticles for upconversion can be extended to three-plasmon systems

or engineered multilayers to increase higher-order harmonic generation and overall efficiency of these systems.

3.7 Experimental methods

Nanoparticle Synthesis & Film Deposition

Nanoparticles of CuS and Au were synthesized as described in previous reports[88],[91],[92] (Equations 9 and 10). For the 3 and 100 nm Au nanoparticles, which were synthesized in H_2O, an additional ligand exchange step was necessary to prepare them for film deposition.

$$AuCl_3 + \text{1,2-hexadecandiol} + \text{1-Octadecene} + \text{Oleylamine} + \text{Oleic acid} \xrightarrow{130\ ^{o}C} Au \quad (9)$$

$$CuCl + \text{1-Octadecene} + \text{Oleylamine} + \text{Oleic Acid} \xrightarrow[180\ ^{o}C]{\text{S:OLAM}} CuS \quad (10)$$

In this procedure, 400 mg of octadecylamine (Sigma-Aldrich, 90%) was dissolved 10 mL of $CHCl_3$ with 1 mL of Dodecanethiol (Sigma-Aldrich, 98%) and placed in a separation funnel. To this solution, 20 mL of as synthesized aqueous colloidal Au was added and vigorously mixed. The layers separated after 3 minutes, and the nonpolar layer (now containing the Au nanoparticles) was extracted. This colloidal suspension was then cleaned by a centrifugation procedure in which 35 mL of ethanol were added and then centrifuged at 8000 rpm for 5 minutes. The supernatant was decanted, and the pellet of nanoparticles was redissolved in a small amount of toluene. This procedure was performed twice. Deposition of nanoparticles was performed with a Ni-Lo scientific Ni-Lo 5 spin coater. To prepare the nanoparticle suspension for deposition, excess solvent was removed with a rotary evaporator until the liquid was reduced to a dark ink. The concentrated nanoparticle suspension was then pipetted onto a glass slide until the substrate was completely covered, (1 mL for a 2 X 2 cm section) and spun at 600 RPM for 30 seconds or until dry. The nanoparticle loading on the slide was controlled during the concentration step, with lesser nanoparticle concentrations producing fewer nanoparticles in film. For the deposition of CuS, it was found that the addition of a small amount of oleylamine (3%vol) prior to concentration and deposition improved the quality of the final film and

prevented cleaning of the already deposited Au nanoparticles off the substrate.

Alternatively, nanoparticles could be deposited by the bath method (employed in chapter 2). In this method, Fischer Scientific glass microscope slides (3 cm x 1 cm x 1 mm) were sectioned into four parts with a diamond tipped scribe. The glass sections were cleaned by placing them in a petri dish with 30 mL of piranha solution (1:4 H2O2:H2SO4) for 10 min on each side.29 The glass sections were then rinsed with deionized water and dried in an oven for 10 min at 107°C. Cleaned glass sections were exposed on both sides for 40 min to a toluene/chloroform (70/30%v) bath into which 40 μL of (3-mercaptopropyl)trimethoxysilane was added immediately after the glass slides were placed in the bath.30 The sections were rinsed with toluene and dried with a stream N2 and placed in an oven for 7 min. The functionalized glass sections were then held vertically (to ex-pose both sides of the glass) in a gold nanoparticle deposition bath with 30 mL of xylene and 44.2 μmol of Au nanoparticles (aliquot re-dispersed in toluene from synthesis assuming 100% yield) for 24h. The slides, faintly pink in color as is typical of Au nano-spheres in air, were rinsed with toluene and dried with a stream of N2. For samples containing only Au nanoparticles the process was stopped at this point. For hybrid samples, the slides were held vertically in a bath containing 2-aminoethanethiol saturated in 30 mL of ethanol for 24 h. In order to prevent surface charging, the slides were then placed in a 1% (volume) solution of the base diazobicy-cloundec-7-ene (DBU) in toluene for 1 h. Finally, the slides were placed in a bath of 250 μmol of CuS nanoparticles dispersed in 30 mL of xylene for 48 h. For samples containing only CuS nanoparticles, the Au nanoparticle and 2-aminoethanethiol deposition steps were skipped, proceeding instead straight from (3-mercaptopropyl)trimethoxysilane deposition to the deposition of CuS nanoparticles. Regardless of which method was employed, the structure of the nanoparticle films was confirmed with scanning electron microscopy (SEM) (Zeiss Merlin SEM) at 1.10 kV with the InLens secondary electron detector and at 5 kV with the NTS-BSD backscatter detector. Powder X-ray diffraction (XRD) patterns were acquired both in and out of the plane of the film in a Rigaku SmartLab X-ray diffractometer with a CuKα source and a D/teX Ultra 250 detector (out of plane) and an SC-70 detector (in plane). The operating voltage

was 40 kV and current were 44 mA. Samples were prepared by drop casting concentrated nanoparticle colloids onto glass microscope slides.

Optical measurements

Extinction spectra of the nanoparticle film samples were acquired in a Jasco V-670 UV-vis-NIR spectrophotometer with an integrating sphere from 350 to 1800nm. Optical measurements were conducted using the nonlinear microscope depicted in Figure 3.3a. A femtosecond mode-locked Nd:glass laser (Time-Bandwidth GLX-200 oscillator) provides pulses of center wavelength 1050 nm at an average power of 230 mW and 177 fs duration with a repetition rate of 100 MHz and an energy per pulse of 3 nJ. The laser beam was mechanically chopped at a frequency of 265 Hz, with a duty cycle of 20%, thus, each exposure of the sample lasts roughly 750 μs. Repeated exposures produce an annealing effect on the film [46], but a steady state is reached, permitting stable measurement condition. Images of the laser exposure site after annealing are available in appendix B.10. The beam is split into a path that proceeds directly to the sample, and one that is upconverted to 2ω by beam splitters with various R:T ratios (Thorlabs BST11 70:30 (R:T) and BSW11 50:50 (R:T) UV Fused silica plate beam splitters). The transmission beam is upconverted with a 0.5 mm thickness β-Barium Borate (BBO) crystal, and then the unconverted fundamental frequency was removed by a harmonic separator (Optosigma YHS-25.4C05-1064). The two beams are then focused onto the sample with a beam waist of 10 μm, ensuring via the construction of the beam path that the length through which they traveled was the same. To determine the order of the dependence of THG on fundamental pump intensity, we placed a rotational polarizer on the ω beam. Using this, the laser power was adjusted by varying the angle between the output polarization of the pump laser and the rotational polarizer. The pump power was measured in a Thorlabs S130C power meter with a PM100D readout. Measurements of the THG signal were carried out with a band pass filter (Optosigma VPF-25C-10-25-350). Our detector was a solid-state photomultiplier tube (PMT, Hamamatsu, R9875U, NMA0340) operating at 1.1 kV for ultraviolet light detection. A Newport ¼ m 74100 Monochromator and the PMT detector were used to collect the output spectrum of the nanoparticle heterostructures.

CHAPTER 4

Distance dependence of plasmonic interactions between harmonic nanoparticles

4.1 Interstitial Al_2O_3 separating the Au and CuS layers

Following the investigations of chapters 2 and 3, a question yet remained—by what mechanism do the Au and CuS nanoparticles interact with each other? The effect of distance between the two nanoparticles was explored to elucidate how exactly the presence of the CuS nanoparticles induces greater nonlinear polarization in the Au nanoparticles (and vice versa). The work of Summer L. Arrowood had already established that direct interfacing between the Au and CuS nanoparticles led to the extinction of their respective surface plasmon resonances[94]; a thin insulating layer was required to prevent direct electronic transfer between the two layers. However, the bath method of deposition did not provide enough control over the amount of ligand that coordinated between the Au and CuS nanoparticles to reliably tune separation over the nanometer scale. Attempts to change the separation distance between the nanoparticle layers by changing the length of the ligand (from 2-aminoethanethiol to 11-aminoundecanethiol) between them failed, likely due to the presence of multiple intercalated layers of ligand, rather than a single monolayer.

Thus, an alternative approach to layer separation was employed requiring sputter deposition of Al_2O_3 layers of varying thickness on top of the Au nanoparticle layer and then depositing the CuS nanoparticles atop the alumina layer. The alumina layer was deposited in the Angstrom Amod multimode deposition chamber (Figure 4.1a). The deposition rate was characterized on blank glass slides via spectroscopic ellipsometry. This extrapolated deposition rate was then used to fabricate films of defined thickness on top of the Au nanoparticle layer.

The thickness remains to be confirmed via atomic force microscopy (AFM) as part of ongoing investigations of this system. Several samples were prepared with Al_2O_3 layer thicknesses ranging from 10-50 nm.

Similar quantities of CuS in the transverse orientation were deposited on the alumina layer via spin coating as confirmed by the optical density measured by UV-vis-NIR absorption (Figure 4.1b). The capability of these films to generate second- and third-harmonics were then compared to each other under single beam excitation with the Nd:glass laser. A plot of the quantity of 3ω light generated at peak excitation laser intensity for each Al_2O_3 layer thickness revealed a sharp inflection in behavior around 15 nm in thickness (Figure 4.1c). For layers thicker than 15 nm, the bilayer films produced a relatively low quantity of 3ω light. Moreover, THG efficiency did not vary with layer thickness in this range, as the nanoparticles essentially acted as independent layers; the intense local electric fields from their plasmon resonances were effectively shielded from each other by the insulating alumina. As the alumina layer thinned to less than 15 nm, the nanoparticles start to be able to influence each other, and a rapid rise in the yield of 3ω light is evident.

Table 4.1 Peak intensity of THG signal for Au/CuS bilayer films as a function of separation between the layers.

Separation Distance(nm)	Peak THG Intensity (W/cm^2)
10	0.216
12	0.084
15	0.028
30	0.014
50	0.012
60	0.018

This curve fits neatly to a t^{-6} dependence, which is a hallmark of nonradiative surface dipole interactions, such as PIRET. This further supports the central claim that the interaction that enhances harmonic generation between Au and CuS nanoparticles is mediated by their plasmon resonances, despite the fact that there is no spectral overlap between the surface plasmon resonances of the two nanoparticle species. The resonance instead occurs between the second-order polarization components in the CuS nanoparticle and the LSPR of the Au, which possess spectral alignment. Evidence for nonradiative energy transfer mechanisms, might seem contrary to the observed SFG in CuS/Au bilayer films between coincident ω and 2ω beams, which would seem to imply a radiative intermediate (Chapter 3).

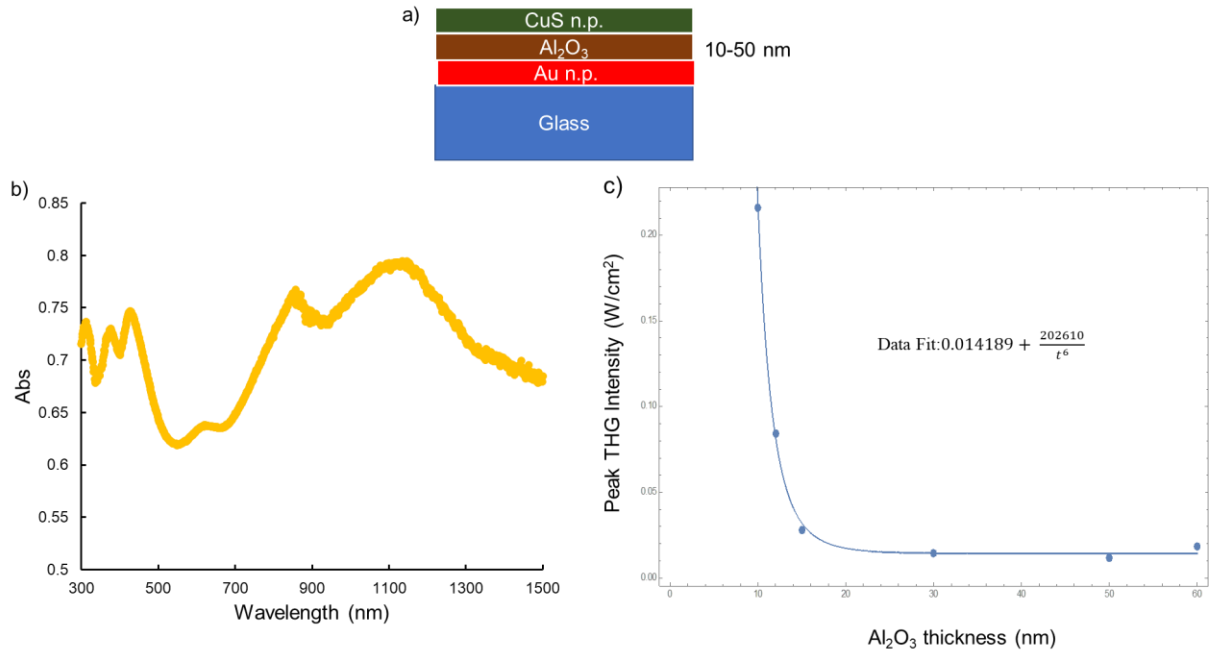

Figure 4.1 (a) Schematic of film structure of Al_2O_3 separation layer experiments. The CuS and Au nanoparticles layers have a combined thickness of 120 nm (Appendix B.2) (b) UV-Vis-NIR spectrophotometry of Au/CuS film with 50 nm Al_2O_3 interlayer (exemplary of all samples with Al_2O_3 layer). (c) peak THG intensity as a function of interlayer thickness with fitting parameters.

However, when the Au LSPR was detuned from the harmonic condition the observed THG signal dramatically decreased, which means that the Au plasmon resonating at 2ω is critical to the cascaded SFG process. Whether this resonance is pumped directly by an incident 2ω beam,

or induced non-radiatively by a resonant energy transfer, the second step (ω+2ω= 3ω) of the cascaded process occurs as the result of a coherent buildup of the fundamental and second harmonics[3].

The distance dependence data of Figure 4.1c satisfies both the distance dependence of the interaction between the two nanoparticles and the relative magnitude of the enhancement effect. Despite gigantic increases in the local electric field due to the LSPR, which provides HG enhancement of several orders of magnitude when pumped directly, a 20x increase (between the thickest to the thinnest Al_2O_3 layered samples) in THG was observed in our CuS/Au system. This difference is due to the inefficiency of coupling through the second order components of the polarization of the CuS, which are naturally less because they are proportional to the susceptibility tensor $\chi^{(2)}$. However, with the coherent buildup occurring in the cascaded THG mechanism, we none the less see 3ω signals on the order of the 2ω signal, due to the consumption of the 2ω light coherently into the cascaded mechanism. A full treatment of this proposed mechanism will require modelling of *E* field enhancement due to coupling between the two nanoparticles species that takes into account the conversion between the first- and second-order polarization in the CuS nanoparticles before coupling to the Au LSPR. However, this substantial task lies beyond the scope of this dissertation and will be one of the central challenges of succeeding work.

4.2 Synthesis and upconverting properties of Al nanoparticles

Thus far, we have examined systems in which two nanoparticle elements resonate at the fundamental and second harmonic of the pump frequency. A significant increase in the efficiency of THG form these structures has been demonstrated, which directly invites conceptual extension to structures with resonant elements at higher harmonics. That is, resonance at ω and 2ω led to enhancement of SHG and THG, thus a structure with resonance at ω, 2ω, and 3ω would lead to enhancement of SHG, THG, and fifth harmonic generation (FHG).

Recently developed [20], colloidally produced Al nanoparticles are a suitable material,

with a size-dependent LSPR band extending across the near UV. Synthesis of the Al nanoparticles generally followed the literature procedure, with the notable alteration of utilizing neat titanium isopropoxide rather than a solution diluted in toluene.

$$(CH_3)_2C_2H_5NAlH_3 + \text{Oleic Acid} \xrightarrow[\text{THF/1,4-dioxane}]{Ti(O^iPr)_4} Al + H_2 + (CH_3)_2C_2H_5N \qquad (1)$$

Injecting neat titanium isopropoxide rather than a solution in toluene eased the air-free requirements on the reagent preparation—which will form TiO_2 if exposed to air or water—allowing the synthesis to be performed on a Schlenk line. In aluminum nanoparticle reactions, the titanium serves as a catalyst for the aluminum reduction; TiO_2 cannot serve this purpose, thus the formation of TiO_2 must be avoided. The reaction proceeded as described, and cleanup provided a drab grey suspension possessing a strong piscine odor (due to the presence of unremoved dimethylethylamine). A 5% vol. solution of acetic acid was used to clean the reaction glassware after removing the nanoparticle product, this acidic solution protonated the byproduct amine, allow for solubility in water. This limited the impact of the stench compounds on unsuspecting coworkers. XRD confirmed that the product was pure aluminum without any titanium alloying or side products (Figure 4.2a). Size and optical properties of the nanoparticles were confirmed with TEM and UV-vis-NIR spectrophotometry respectively (Figure 4.2b and c), showing 100 nm diameter particles with an LSPR peak at 370 nm, slightly red shifted from the third harmonic of the pump laser (350 nm). The nanoparticles were processed into films by spin coating following the procedure outlined in section 3.1 by adding 100 μL of oleic acid per dram of nanoparticle suspension to prevent aggregation during the deposition process. Testing of the Al nanoparticle nonlinear optical properties initiated with single-beam excitation of Al nanoparticles on their own.

As with other nanoparticle species that we have examined, THG and MPPL components were produced by the sample (Figure 4.2d). The MPPL signal was less intense than that measured from Au nanoparticles for similar particle loading at the same excitation intensity.

With the baseline performance of Al nanoparticles established, future experiments will feature films that will be prepared containing the combinations of CuS, Au, and Al nanoparticles. With the addition of a resonant state at 3ω, we hypothesize that the generation of 4th harmonic light (at λ = 262 nm) will be enhanced in a doubly cascaded process similar to the observed enhancement of THG. That is, we hypothesize that there will be a three-step process of SHG (ω+ω=2ω), SFG (2ω+ω=3ω), and SFG again (3ω+ω=4ω). The baseline 4th and 5th HG efficiency of Au and CuS nanoparticles without Al was established using filtering and a new PMT sensitive in the UV range to select for these harmonics. No fourth harmonic signal was measured from these samples, probably due to the centrosymmetry of the constituent nanoparticles and lack of plasmon resonance at the 3rd harmonic frequency to enhance a cascaded mechanism. A 5th harmonic signal—with low intensity—was measured from the Au/CuS samples (Figure 4.2e). The creation of trilayer films and a full exploration of their upconverting properties lies beyond the scope of this dissertation and is entrusted to my colleague, Yueming Yan.

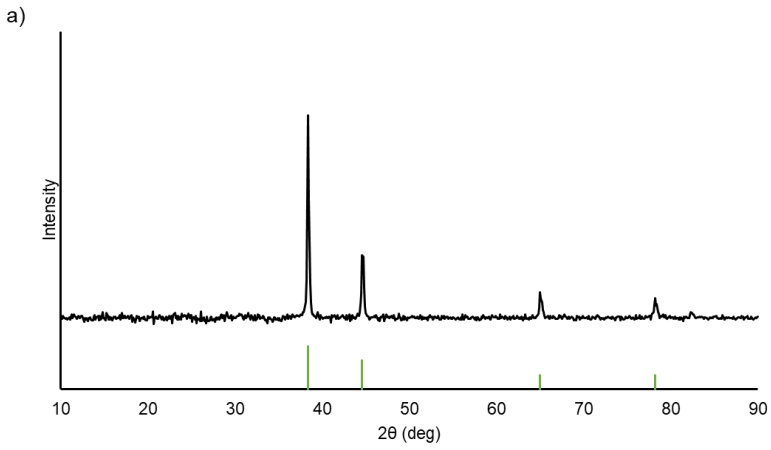

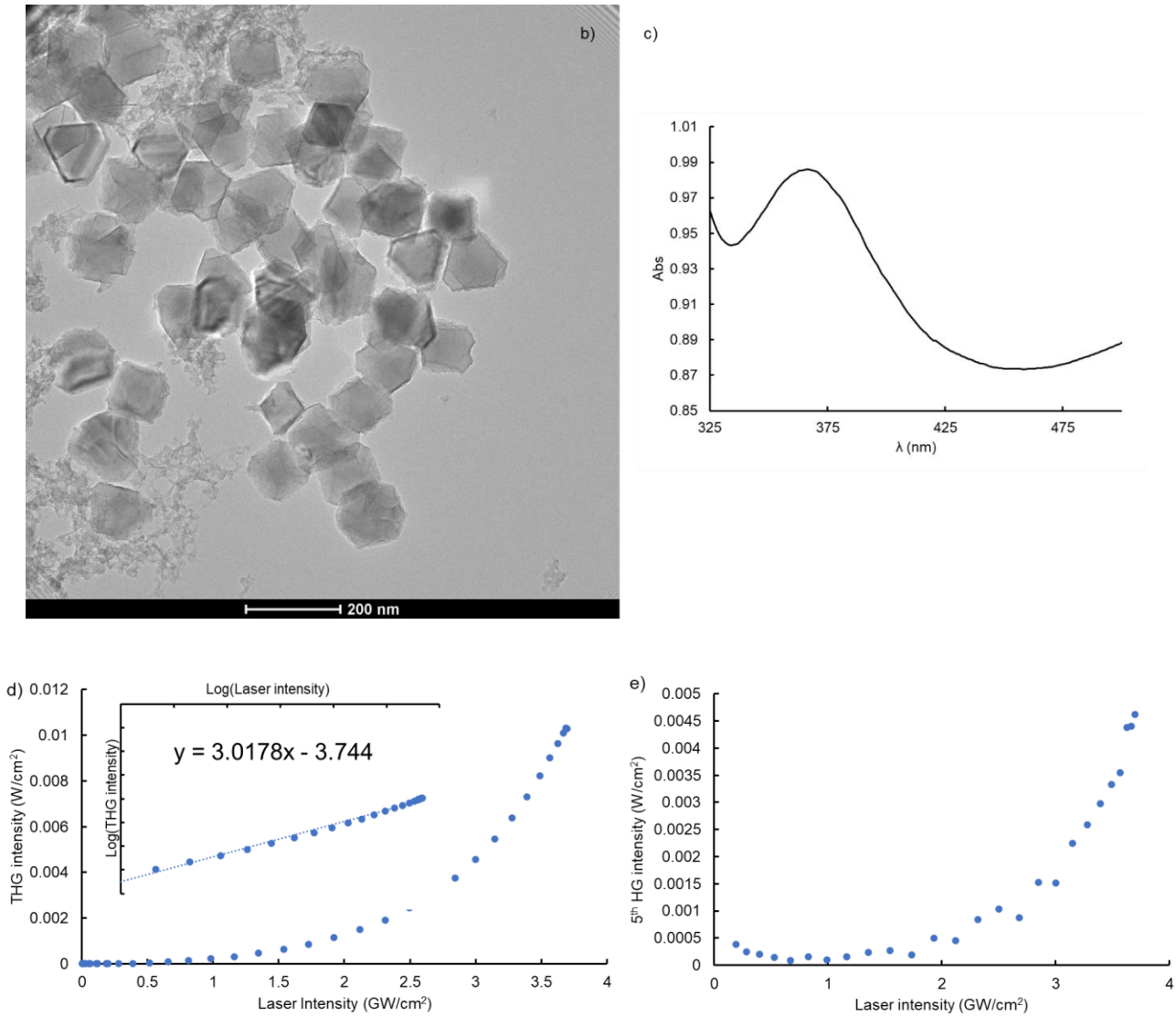

Figure 4.2 Summary of Al nanoparticle results. (a) XRD of synthesized Al nanoparticles. (b) TEM of representative Al nanoparticles. (c) UV-Vis-NIR of Al nanoparticles suspended in THF. (d) THG output of Al nanoparticle film with (inset) log-log plot demonstrating 3rd order dependence. (e) FHG signal from Au/CuS nanoparticle film.

4.3 Conclusion

In this chapter, the latest, and still ongoing, explorations of harmonic generation from multi-plasmonic nanoparticle thin films was discussed. First, the effect of nanoparticle distance on the observed enhancement of THG produced by the Au/CuS film was examined by adding an interstitial layer of alumina between the nanoparticle layers. The amount of third-harmonic light

that the films were able to produce varied with the inverse sixth power of the alumina layer thickness. With thick (t > 30 nm) alumina layers, the CuS and Au nanoparticles acted independently as separate nanoparticle films and no THG enhancement was observed. Preliminary interpretation of this result suggests that the interaction between the nanoparticles species is mediated by surface dipole interactions, with relatively short ranges, that decay rapidly. This is consistent with the hypothesis that harmonically coupled plasmonic nanoparticles will exhibit mechanisms such as PIRET between them, despite not possessing direct spectral overlap. Future directions in this project will involve utilizing alumina deposition techniques that allow for very thin layers, such as atomic layer deposition (ALD), to achieve insulating interlayers of thickness less than 10 nm. Further characterization of the Alumina layer uniformity is also called for via a high-resolution method such as AFM.

Second, recent efforts to synthesize and characterize aluminum nanoparticles to add onto CuS and Au nanoparticle structures was reported. Literature syntheses were adapted to produce and deposit Al nanoparticles, which then demonstrated THG with similar efficiency as Au nanoparticles. Future work on this project will require tuning the Al nanoparticle synthesis to produce nanoparticles whose LSPR is perfectly coincident with the third harmonic of the pump laser. Attempts to follow the literature approach of varying the THF/1,4-dioxane ratio to control nanoparticle diameter failed, possibly due to premature addition of capping ligand, which quenches the reaction[100], or due to the use of neat Ti(O^iPr) rather than dilute catalyst. Once harmonically coincident Al nanoparticles have been achieved, films containing CuS, Au, and Al nanoparticles can be fabricated and the efficiency of second, third, and (particularly) fifth harmonic generation can be examined.

CHAPTER 5

Conclusion

5.1 Dissertation Summary

A large class of nonlinear materials show enhanced harmonic generation by exciting the localized surface plasmonic resonance (LSPR) of metallic or semiconducting nanoparticles. Moreover, material systems containing coupled plasmonic elements have been shown to increase performance beyond that of a single LSPR. In this work we have described a novel bilayer nanoparticle system in which plasmonic coupling occurs between the LSPRs of a metallic nanoparticle component (Au) and the second harmonic of the LSPR of a semiconducting nanoparticle component (CuS), under laser excitation at 1050 nm, the resonance fundamental of the CuS. These nanoparticles were solvothermally synthesized and then processed into thin bilayer films whose upconversion order, absorption efficiency, and spectral profile were characterized. Multiple sources of upconverted light were detected, including second, third, and fifth harmonic, as well as a broadband MPPL signal. The effect of plasmonic interactions between CuS and Au nanoparticles on upconversion occurring via the mechanisms of second- and third- harmonic generation and multiple photon photoluminescence was also explored, with the finding that the THG signal featured the greatest enhancement. The critical importance of a harmonic relationship between the resonant frequencies of the two nanoparticles was demonstrated for both the fundamental and second harmonic resonance, showing that detuning either LSPR from the resonant condition led to a quenching of the enhancement effect. Dual beam stimulation of the films with fundamental and second harmonic light demonstrated sum frequency generation as a viable source of 3ω light, suggesting that a cascaded mechanism of SHG followed by SFG (between the fundamental and second harmonic signals) may be the mechanism for the observed enhancement of THG. An analytical model is also presented that

describes the interactions between the CuS and Au as occurring between surface dipoles and predicts the observed upconversion enhancement reasonably well. The dependence of upconversion on the distance between the nanoparticles was also explored by adding interstitial layers of Al_2O_3 between the Au and CuS nanoparticle layers. The enhancement of harmonic generation was found to be proportional to the inverse sixth power of the interstitial layer thickness, consistent with the treatment of the coupling as occurring via nonradiative resonant energy transfer between surface dipoles. Finally, upconversion from Al nanoparticles, whose LSPR occurs at the third harmonic of the fundamental excitation wavelength is examined.

5.2 Field outlook

Understanding the processes that govern the interaction between harmonically aligned plasmonic nanoparticles will open a pathway to developing ultrafast, usable efficiency upconversion thin-film devices by clarifying the conditions that efficiently generate harmonics without background multiphoton photoluminescence. While further investigation in the sub-10 nm regime of Al_2O_3 interlayer thickness will help confirm the observed t^{-6} trend, a complete treatment of importance of interparticle spacing will require a simulation component. Finite difference time domain (FDTD) simulations via Lumerical could be used to model, a series of geometries that may exist in the films, whose behavior is an aggregate of various spacings and orientations. Because the plasmon resonances of CuS and Au do not overlap, these simulations would not show any coupling occurring between them if we simply used the actual values of their complex permittivity. Thus, one approach would be to construct a material whose resonance overlaps with Au, and whose optical density is equal to the efficiency of the generation of second order polarization components in the CuS (when pumped at 1050 nm), thus, in effect, modelling the coupling occurring between the Au and the second order components of the CuS LSPR.

A series of fundamental experimental investigations also remain. These include the completion of the trilayer CuS/Au/Al structure, which will show if the concept of cascaded harmonic generation can be extended beyond the third harmonic. Furthermore, the nonlinear properties of harmonically resonant nanoparticle films when pumped off their fundamental

resonance remains unexplored. Utilizing a tunable optical parametric amplification (OPA) setup will allow for pumping of these systems across a wide range of frequencies, and for the examinations of a broader range of materials, including various combinations of plasmonic semiconductors and metallic nanoparticles. The materials systems explored in this dissertation only featured interactions between plasmonic resonances, but with the appropriate plasmonic semiconductor, there is the possibility of harmonic plasmonic-excitonic-plasmonic systems $CuS_{2-x}Se_x$/Al for example. Many variations on the positioning of these absorbance features could be constructed. Additionally, pump-probe experiments could be utilized to get detailed information on the dynamics involved in the interaction between the plasmon resonances. Such an approach was recently reported on Au/CuS Janus particles in solution[101].

The approach in synthesis and fabrication discussed in this dissertation has major engineering advantages over top-down methods that many investigators use to explore multi-plasmonic systems. Foremost among the advantages is the scalability of solvothermal synthesis as a method of producing nanoparticles and the bath method of depositing them. Other advantages include low cost, conformal (substrate geometry independent) coatings, and thin layer sizes. However, a major weakness of this approach is control. Control over spacing, density, and orientation are far superior in top-down methods such as e-beam lithography. Thus, it may be worth including some top-down elements for the purposes of scientific exploration, such templating the substrate surface, or directly growing the nanoparticles on the substrate. While these approaches have been employed to explore bi-plasmonic systems composed of metal structures, multi-plasmonic systems incorporating both semiconducting and metallic resonances are less prevalent.

Although this dissertation has established the baseline properties of such systems, much work remains before biplasmonic nanoparticle films could be integrated into thin, conformal optical components.

Appendix A

Supplemental Figures for Chapter 2

A.1 Annealing effect in nanoparticle films. Peak lock-in amplifier (LIA) signal of (a) the same sample spot for consecutive laser exposures. Each exposure had a duration of 10 minutes. (b) Peak LIA voltage after the annealing effect is no longer observable in a different sample from (a)

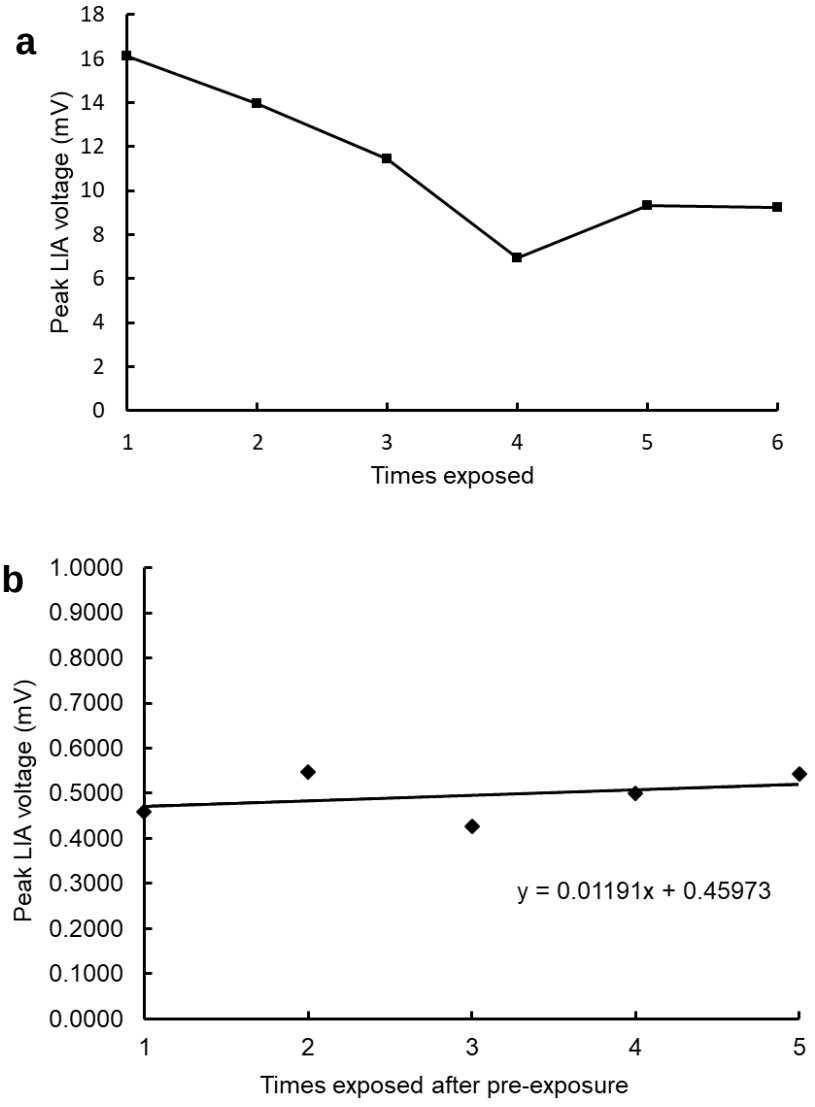

A.2 SEM images and profilometry trace of the fabrication process of hybrid nanoparticle films. (a) Bare, unfunctionalized glass microscope slide after cleaning. (b) Sample surface with Au nanoparticle layer. (c) Hybrid film deposited without DBU treatment leading to aggregation and deposition of CuS islands. (d) Bilayer film containing both Au and CuS nanoparticles connected by linker molecule 2-aminoethanethiol.

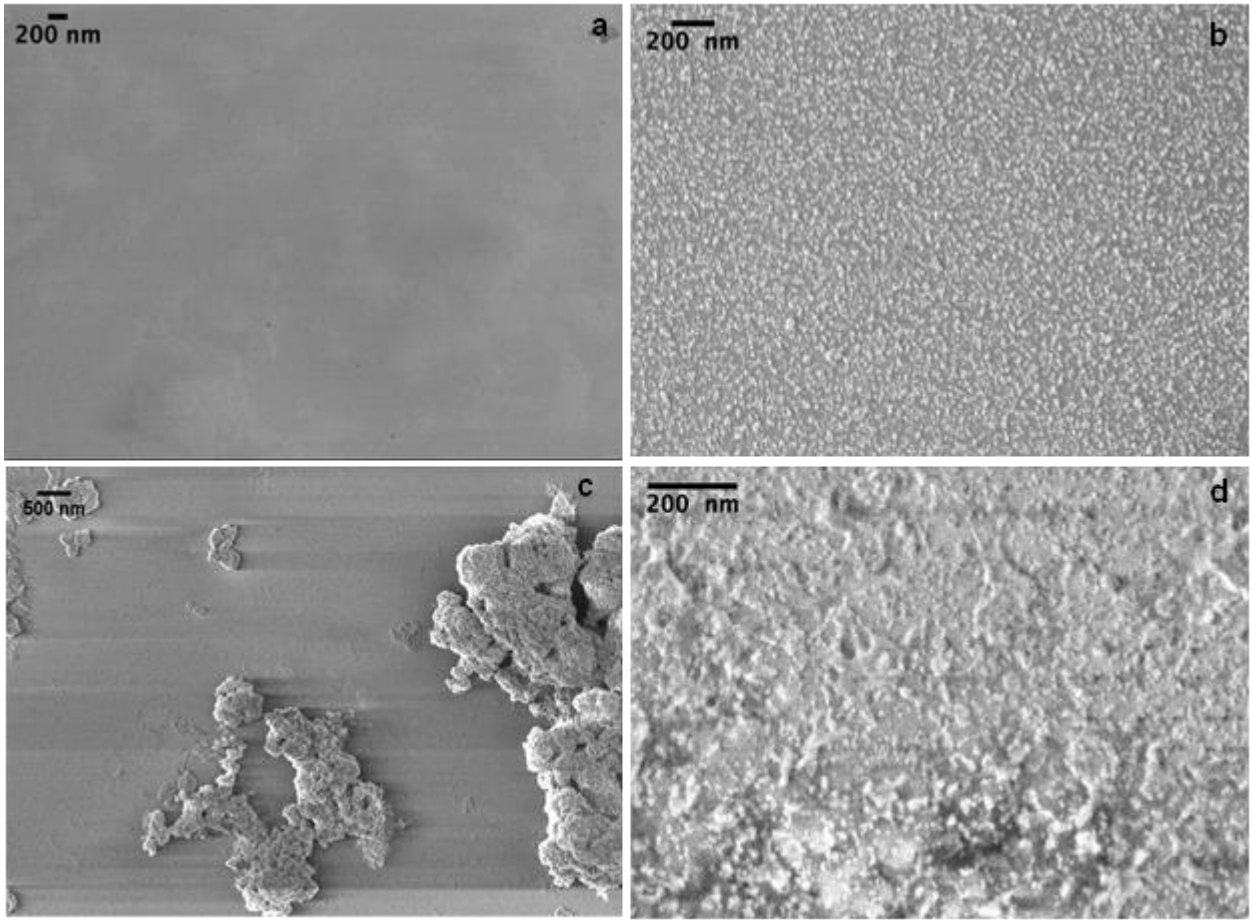

A.3 profilometry traces of Au only film (orange), CuS only film (green), bare glass (grey), and hybrid Au-CuS nanoparticle film (blue). Low positions correspond to bare glass where the nanoparticle films have been wiped away.

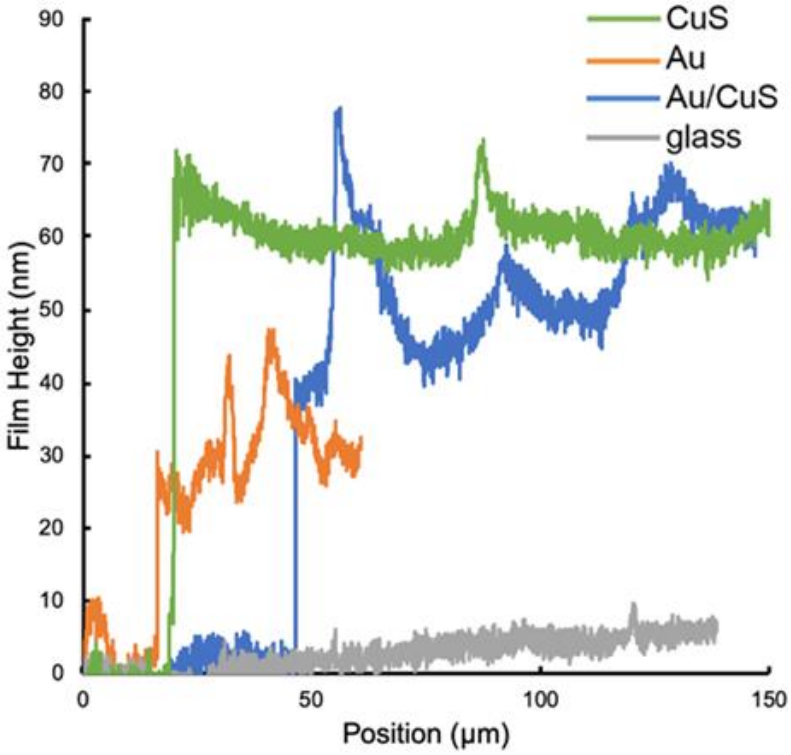

A.4 Intensity vs. wavelength spectrum acquired with an Ocean Optics USB4000 Si-CCD spectrometer of (a) laser without spectral attenuation and (b) second harmonic signal from BBO crystal with laser fundamental attenuated by filter. Dashed lines correspond to peak laser emission at 1050 nm. (c) Log-log plot of BBO upconverted intensity vs fundamental harmonic laser intensity, featuring the expected second order dependence for SHG.

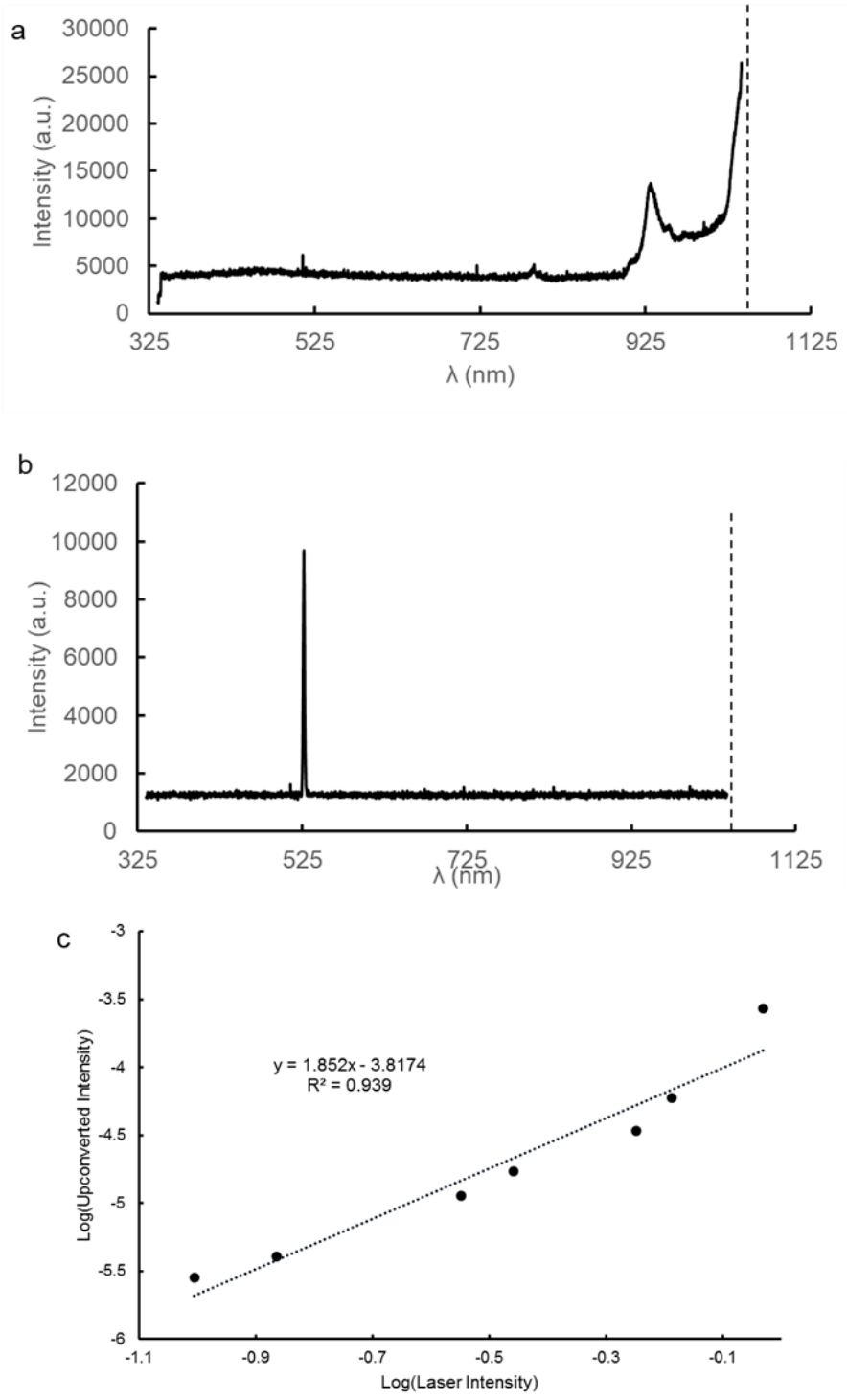

Appendix B

Supplemental Figures for Chapter 3

B.1 Scanning electron micrographs of Au-CuS nanoparticle films. (a-d) Samples with CuS in the axial orientation collected with a mixture of backscattered and SE2 electrons. (e-h) CuS in the transverse orientation collected with SE2 electrons.

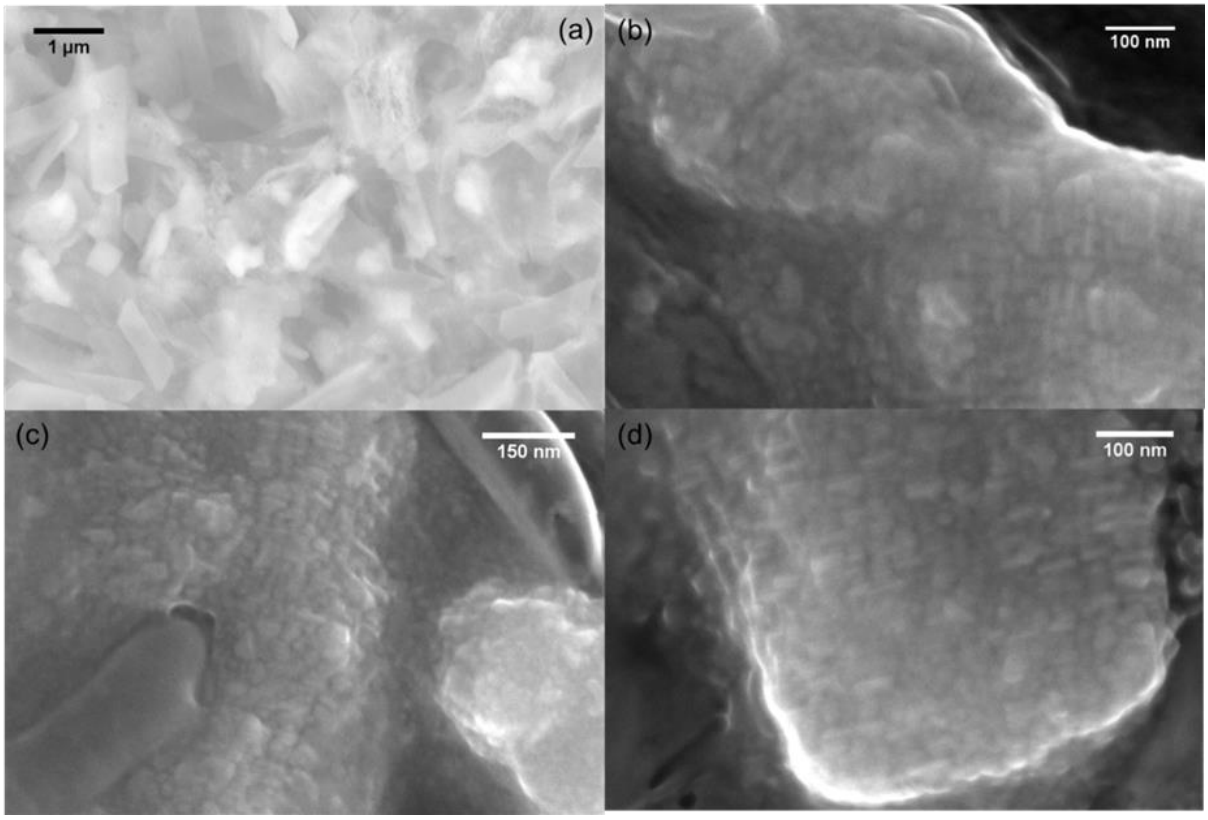

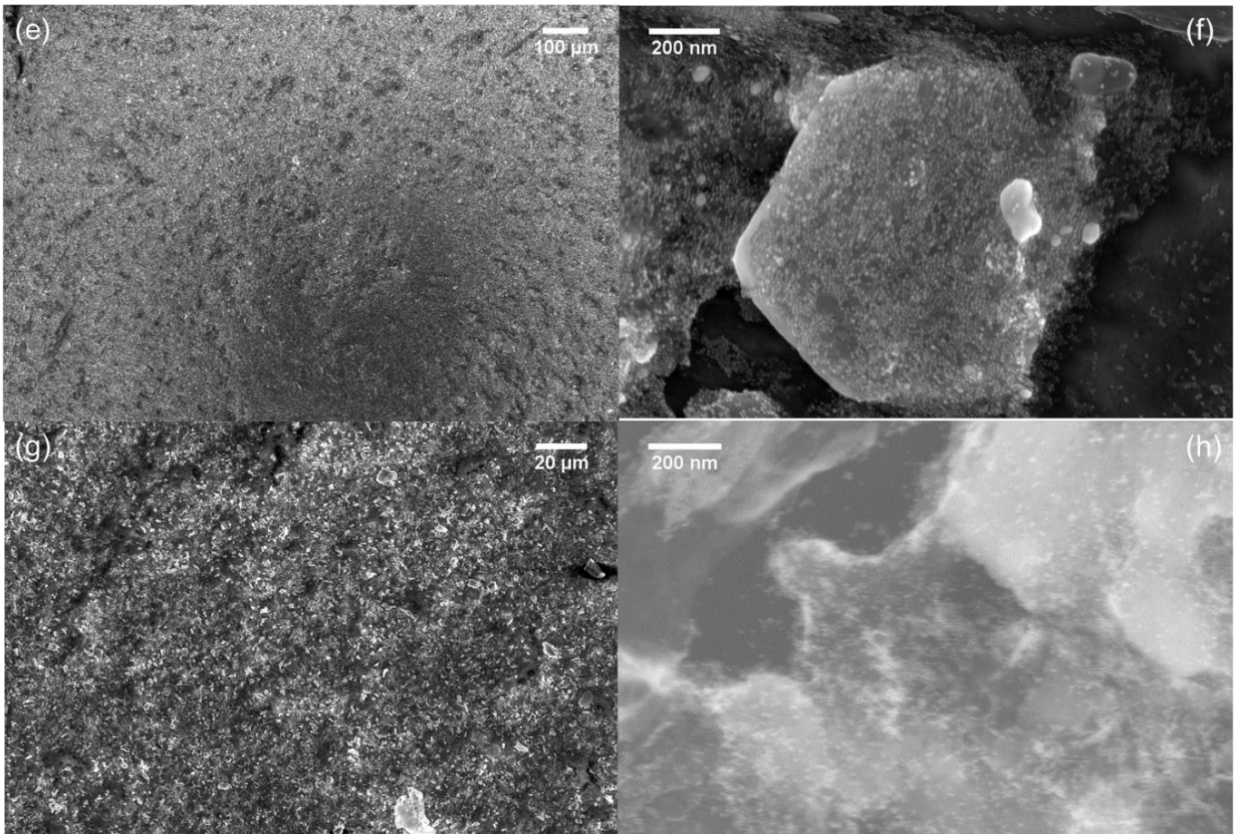

B.2 Profilometry measurement of film thickness from spin coating method. Low positions (before dotted line) correspond to bare glass where the nanoparticle films have been wiped away. Difference in average height between bare glass and film domains (film height) is 121 nm.

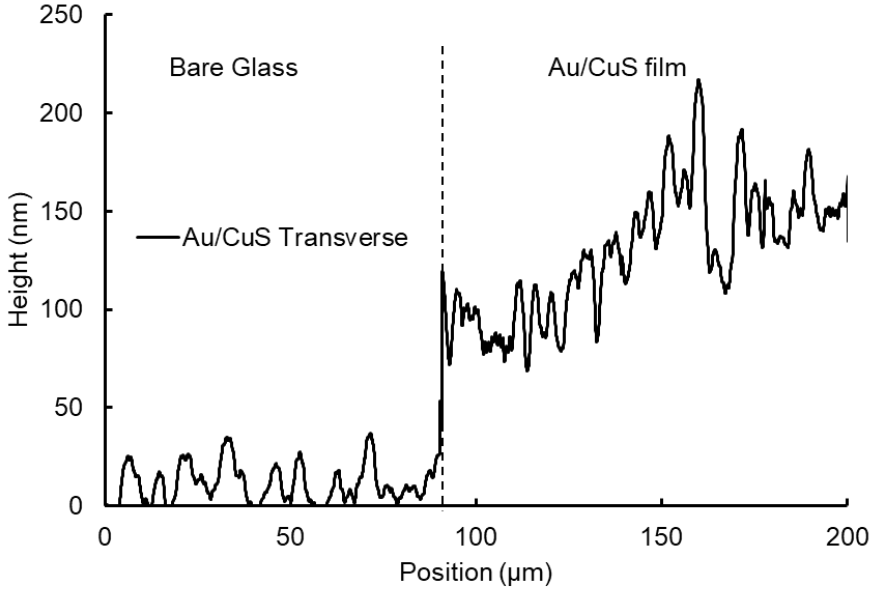

B.3 Log-log plots of data from Figures 3.2 b,c,d of bilayer (Au/CuS) films demonstrating third order dependence. Notably, the 3nm Au nanoparticles feature a sharp transition in response order from 1 to about 6. This is consistent with results from Chapter 2 from nanoparticles in which the harmonic generation and MPPL signals spectrally overlap.

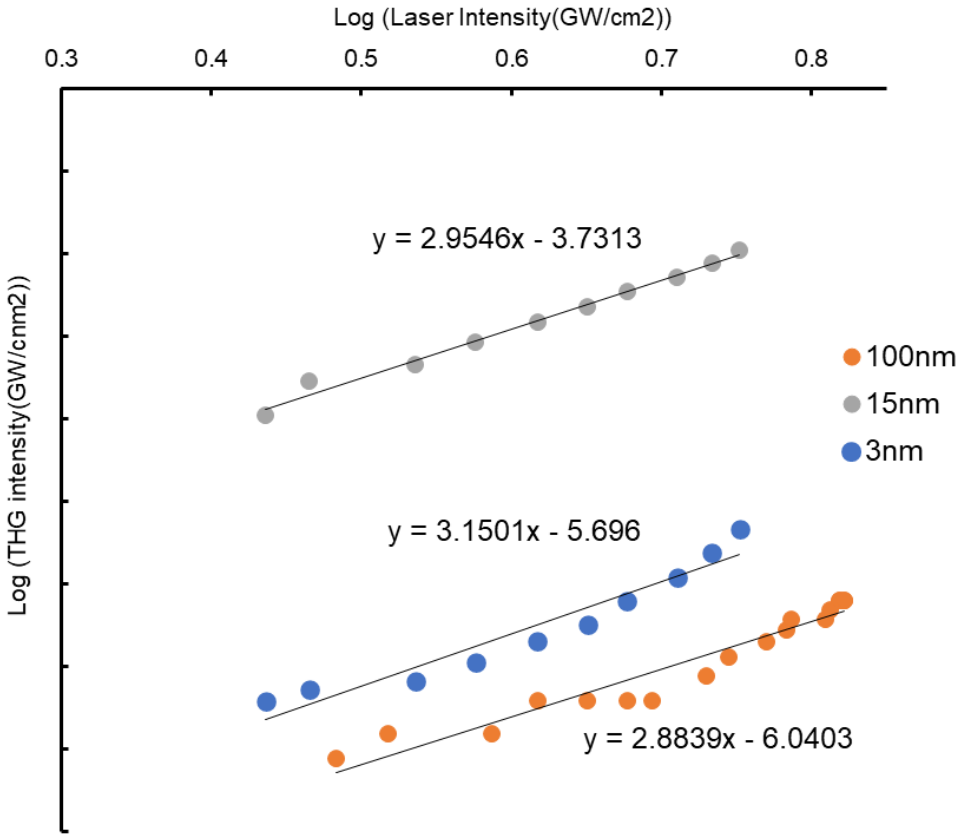

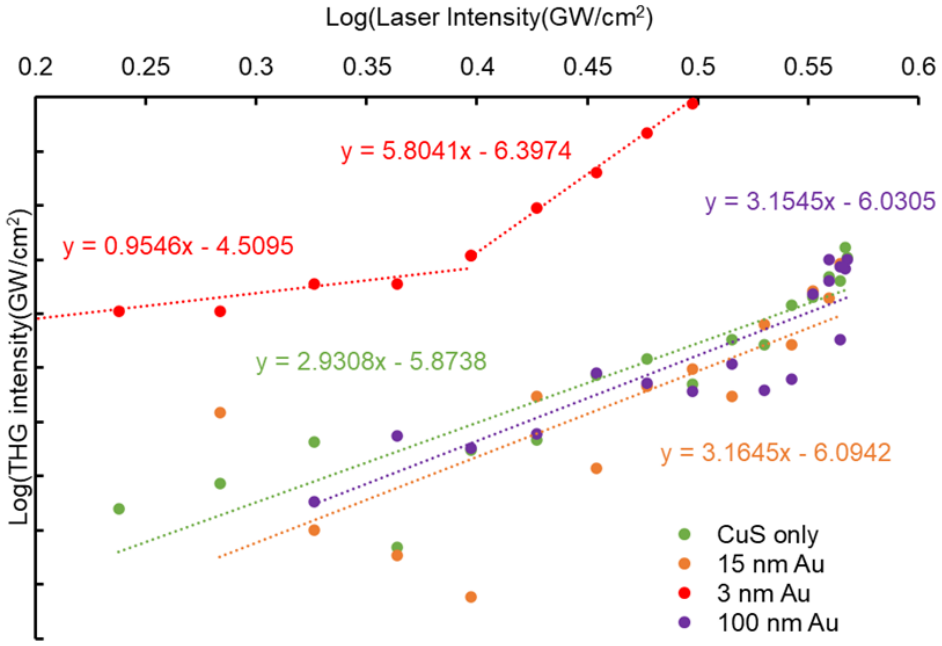

B.4 Measurement of MPPL from dual beam stimulation of Au-CuS films with 50-50 beam splitting. The quantity of MPPL is the broad band intensity of light collected by the PMT (600-300 nm) with the second harmonic (525 nm) filtered out and the THG signal (350 nm) subtracted.

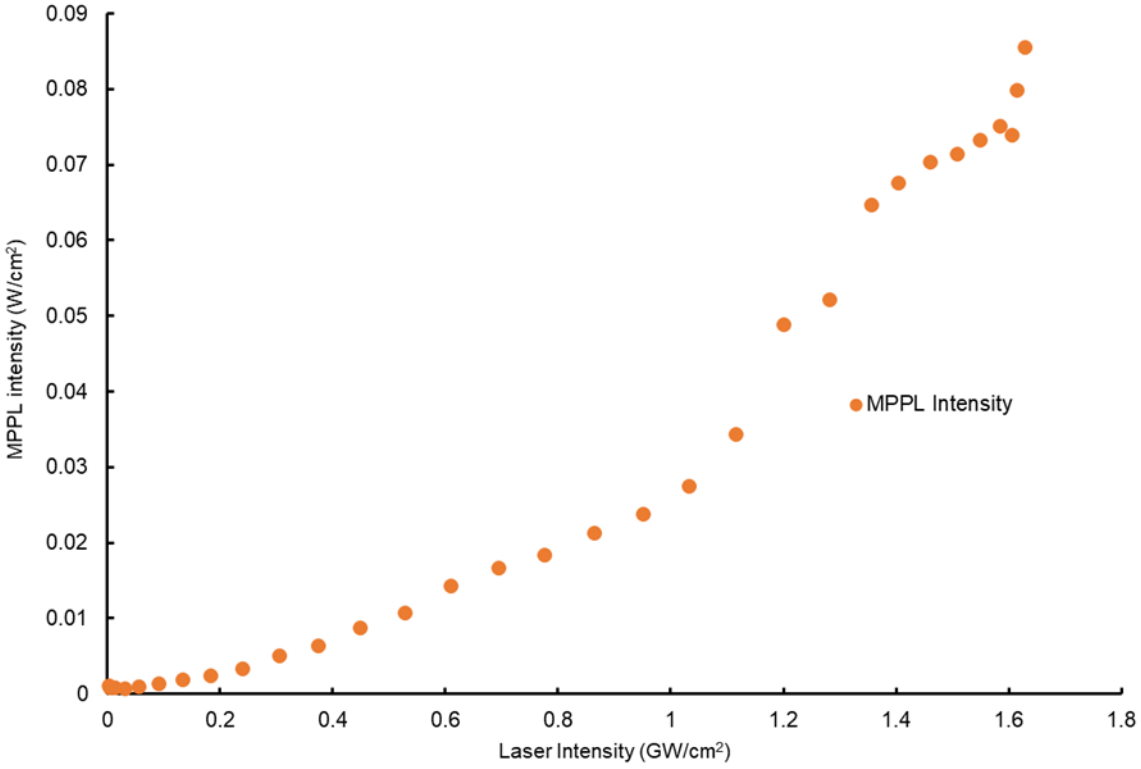

B.5 Theory of Third Harmonic Generation in Au and CuS Nanoparticle heterostructure

2.1 SPP Fields in Au and CuS nanoparticles

We consider that the metallic nanohybrid is made of an ensemble of Au nanoparticles (NPs) and CuS NPs. The nanohybrid is deposited on a substrate (i.e., background material) with dielectric constant ϵ_b. A schematic diagram of the nanohybrid is shown in Figure B.6. We know that the free electrons are present on the surface of the Au-NP. These electrons oscillate collectively and produce electron surface plasmons. When a pump field is applied to the Au-NP, photons of the pump field interact with the surface plasma and create quasiparticles called surface plasmon polaritons (SSPs).

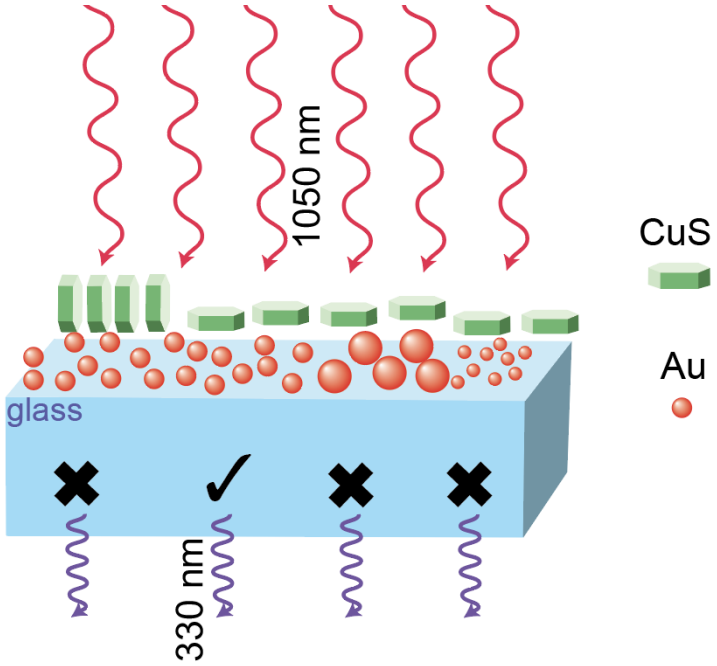

Figure B.6: Schematic diagram of a hybrid which consists of an ensemble of interacting Au-nanoparticles and CuS nanoparticles.

We know that CuS is a direct band gap semiconductor, and that CuS-NPs are heavily doped p-type semiconductors. The p-type semiconductors have positively charged holes which are free to move in materials. Hence, a CuS-NP has free holes on surface and these holes oscillate collectively and produce hole surface plasmons. When a pump field is applied on the CuS-NP, photons interact with the hole surface plasmons and create surface plasmon polaritons (SSPs).

Let us calculate the SPP electric field produced by the Au-NP and CuS-NP, considering that the Au-NPs are spherical. The dielectric constant of the Au-NP is denoted as ϵ_{au} . The radius of the Au-NP is taken as R_{Au}. We applied a pump field with amplitude E_p and frequency $\omega_p$in the nanohybrid. The pump field induces a dipole in the Au-NP, and it is denoted as p_{au}. This dipole produces the SPP field denoted as E_{spp}^{Au}. Solving the Maxwell's equations in the quasi-static approximation [102]–[106] one can find the following expression of E_{spp}^{au} as

$$E_{spp}^{Au} = \frac{p_{Au}}{4\pi\epsilon_0\epsilon_b r^3} \tag{1}$$

$$P_{au} = \epsilon_0\epsilon_b V_{Au} g_l \zeta_{Au}(E_p) \qquad V_{au} = \frac{4}{3}\pi {R_{Au}}^3 \tag{2}$$

$$\zeta_{Au} = \left[\frac{\epsilon_{Au}-\epsilon_b}{\epsilon_{Au}+2\epsilon_b}\right] \tag{3}$$

In the eqns. (2), the constant g_l is called the polarization parameter and it has values $g_l = 1$ and $g_l = -2$ for $\boldsymbol{p}_{Au} || \boldsymbol{E}_{spp}^{Au}$ and $\boldsymbol{p}_{au} \perp \boldsymbol{E}_{spp}^{Au}$, respectively. Here the ζ_{au} quantity is called the SPP polarization factor of the Au-NP.

Similarly, one can calculate the SPP field produced by the CuS-NP. We consider that the shape of CuS-NPs is rectangular whose volume is $V_{CuS} = L_x L_y L_z$. The dielectric constant of the CuS-NP is denoted as ϵ_{cus}. The pump field induces a dipole p_{CuS} in the CuS-NP. This dipole produces

the following SPP field E_{spp}^{CuS}.

$$E_{spp}^{CuS} = \frac{p_{CuS}}{4\pi\epsilon_0\epsilon_b r^3} \tag{4}$$

$$p_{CuS} = \epsilon_0\epsilon_b V_{CuS} g_l \zeta_{CuS}^i(E_p) \qquad \zeta_{CuS}^i = \frac{\epsilon_{CuS}-\epsilon_b}{3\eta_i^{CuS}(\epsilon_{CuS}-\epsilon_b)+3\epsilon_b} \qquad i = x, y, z \tag{5}$$

$$\eta_x^{CuS} = \frac{1}{2}\int_0^\infty \frac{ds}{(s+L_x^2)^{3/2}(s+L_y^2)^{1/2}(s+L_z^2)^{1/2}} \tag{6}$$

$$\eta_y^{CuS} = \frac{1}{2}\int_0^\infty \frac{ds}{(s+L_x^2)^{1/2}(s+L_y^2)^{3/2}(s+L_z^2)^{1/2}} \tag{7}$$

$$\eta_z^{CuS} = \frac{1}{2}\int_0^\infty \frac{ds}{(s+L_x^2)^{1/2}(s+L_y^2)^{1/2}(s+L_z^2)^{3/2}} \tag{8}$$

Where the ζ_{CuS}^i quantity is called the SPP polarization factor of the CuS-NP. Note that it depends on the shape of the sample. For this treatment, the condition in which CuS nanoparticles are oriented with their basal planes parallel to the substrate surface (transverse orientation) is considered. In this orientation, only the x and y shape anisotropy factors are considered, which due to the hexagonal disk shape of the nanoparticle have the same value.

The SPP fields of Au-NS and CuS-NP can be written in the compact forms as follows.

$$E_{spp}^{Au} = \Pi_{Au} E_p \quad \Pi_{Au} = \frac{V_{Au} g_l}{4\pi r^3}\xi_{Au} \tag{9}$$

$$E_{spp}^{Cus} = \Pi_{CuS} E_p \quad \Pi_{CuS} = \frac{V_{CuS} g_l}{4\pi r^3}\xi_{CuS} \tag{10}$$

Note that both electric fields depend on r^{-3}. The Π_{Au} and Π_{CuS} parameters are called the SPP coupling constants for Au-NP and CuS-NP, respectively.

Let us calculate the SPP resonance frequency of Au-NP. We consider the following form of the dielectric constant for Au-NP, which is widely used in the plasmonic literature.

$$\epsilon_{Au} = \epsilon_\infty \left(1 - \frac{\omega_{Au}^2}{\omega_p(\omega_p + i/\tau_{Au})}\right) \tag{11}$$

In the above expression, ω_{Au} is the plasmon frequency and ϵ_∞ is the dielectric constant of metal when light frequency is very large. Here τ_{Au} is the decay rate which is responsible for the heat energy loss. Note that the real part of ϵ_{Au} has a negative value when $\omega_p < \omega_{Au}$. It is interesting to find that when ϵ_{Au} has a negative value, the denominator of the polarization factor ζ_{Au} given in Equation 3 becomes zero at a certain value of the frequency. Let us call this value $\omega_p = \omega_{Au}^{res}$. This means that the polarization and SPP field have a huge value when $\omega_p = \omega_{Au}^{res}$.

2.2 THG in Au and CuS nanohybrid

We have established that the Au-NP has one SPP resonance ω_{Au}^{res}. Therefore, we treat the Au-NP as a two-level system whose ground state is denoted as |1>, and its virtual excited state as

|2>. The frequency difference between levels |1> and |2> is expressed as ω_{Au}^{res}. A schematic diagram of two-level system is shown in Figure B.7.

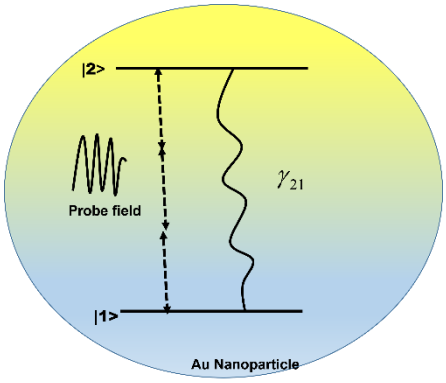

Figure B.7: A schematic diagram for a two-level Au-NP is plotted. Energy levels are denoted as |1> and |2>. To study the THG, the pump field is applied to the 1⟩ ↔ |2⟩ transition.

.

To study the nonlinear properties in the Au-NP, we calculate the third order susceptibility, $\chi_{Au}^{(3)}$ of the Au nanoparticles. We know that the third order susceptibility is responsible for the THG. Following the method of references,[2],[107] the expression of the third order polarization, $P_{Au}^{(3)}$, is given as

$$P_{Au}^{(3)} = \epsilon_0 \, \chi_{Au}^{(3)} E_p E_p E_p \tag{12}$$

Where $\chi_{Au}^{(3)}$ is the third order expressions of the susceptibility χ_{Au}. Following the method of references,[108] the polarization of the Au nanoparticles can also be expressed in terms of the quantum density matrix operator (ρ) as follows.

$$P_{Au}^{(3)} = 2\frac{p_{Au}}{V_{Au}}\left[\rho_{Au}^{(3)} + h.c.\right] \tag{13}$$

Here p_{Au} is the matrix element of the dipole moment of the Au nanoparticle and $\varrho_{Au}^{(3)} = \varrho_{21}^{(3)}$ is the third matrix element of density matrix operator ρ_{au} between transition |1⟩ ↔ |2⟩, and *h.c.* stands for the Hermitian conjugate.

Comparing Equations 12 and 13 and we found the relation between the susceptibility and the density matrix elements as follows.

$$\chi_{Au}^{(3)} = \frac{2p_{Au}\left(\rho_{Au}^{(3)}\right)+h.c.}{\epsilon_0 V_{Au} E_p E_p E_p} \tag{14}$$

We found that the third order susceptibility depends on the third order density matrix elements.

2.3 Enhancement of THG in Au-NP due to CuS-NP

We consider that the Au and CuS nanoparticles are present together to study the effect of CuS nanoparticles on the THG intensity of Au nanoparticles. Now, we calculate the third order density matrix element, $\rho_{Au}^{(3)}$ which appears in the expression of the susceptibility.

To calculate the density matrix element, we need to know what electric fields are incident on the Au nanoparticles. The pump field with amplitude E_p acts on the Au nanoparticles, while the CuS emits an electric field of the surface plasmon polariton, E_{spp}^{CuS}. Therefore, provided that the nanoparticles are spatially close, the SPP field also acts on the Au nanoparticles. Hence, there are two electric fields incident on the Au nanoparticle i.e., E_p and E_{spp}^{CuS}. The interaction of SPP field with the dipole of the Au nanoparticle is a dipole-dipole interaction.

Using the dipole and rotating wave approximations the interaction Hamiltonian is

$$H_{Au} = H_{Au-probe} + H_{DDI}^{Au} \tag{15}$$
$$H_{Au-probe} = \hbar \Lambda_{Au} \Omega_p \sigma_{21} + h.c.$$
$$H_{DDI}^{Au} = \hbar \Lambda_{Au} \Omega_{CuS} \sigma_{21} + h.c. \tag{16}$$

$$\Omega_P = \frac{\mu_{21} E_p}{\hbar} \qquad \Omega_{CuS} = \frac{\mu_{21} E_{spp}^{CuS}}{\hbar} = \Pi_{CuS} \Omega_p \qquad \Lambda_{Au} = \frac{4\pi \epsilon_0 \epsilon_b R_{Au}^3 g_l \zeta_{Au} \hbar \Omega_P}{\mu_{21}^2} \tag{17}$$

where h.c. stands for the Hermitian conjugate. Here $\sigma_{21} = |2><|1|$ is the SPP polariton creation operator. The parameter Ω_p and Ω_{CuS} are the Rabi frequencies associated with the pump and the SPP fields, respectively. The first term in the Hamiltonian is the polariton and photon interaction. The second term is the DDI between Au-NP and CuS-NP.

Density Matrix Method: Following established methods and with the Hamiltonian of Equation (15), the equations of the motion for density matrix elements are

$$\frac{d\rho_{11}}{dt} = +\gamma_{21}\rho_{22} + i\Lambda_{Au}\Omega_p(\rho_{12} - \rho_{21}) + i\Lambda_{Au}\Omega_{CuS}(\rho_{12} - \rho_{21})$$
$$\frac{d\rho_{22}}{dt} = -(\gamma_{21})\rho_{22} - i\Lambda_{Au}\Omega_p(\rho_{12} - \rho_{21}) - i\Lambda_{Au}\Omega_{CuS}(\rho_{12} - \rho_{21})$$
$$\frac{d\rho_{21}}{dt} = -d_{21}\rho_{21} + i\Lambda_{Au}\Omega_p(\rho_{22} - \rho_{11}) + i\Lambda_{Au}\Omega_{CuS}(\rho_{22} - \rho_{11}) \tag{18}$$

where

$$d_{21} = \delta_{21} + i\gamma_{21} \qquad \delta_{21} = \omega_{Au}^{res} - 3\omega_p \tag{19}$$

Here δ_{21} is called the field detuning. The physical quantity γ_{21} is the transition rate for transition $|2\rangle \leftrightarrow |1\rangle$. Note that we use notation $\rho_{21}^{(3)} = \rho_{Au}^{(3)}$.

The THG density matrix element $\rho_{Au}^{(3)} = \rho_{21}^{(3)}$ is calculated in the third order in Ω_P^3, $\Omega_P^2\Omega_{CuS}$, $\Omega_{CuS}^2\Omega_P$, and Ω_{CuS}^3, by solving Equation (18) in the steady sate. After some mathematical manipulations we obtained the following analytical expression for $\rho_{Au}^{(3)}$:

$$\rho_{Au}^{(3)} = \rho_{ppp}^{Au} + \rho_{pps}^{Au} + \rho_{pss}^{Au} + \rho_{sss}^{Au} \tag{20}$$

The density matrix elements appearing in Equation (20) are

$$\rho_{ppp}^{Au} = \left(\Lambda_{Au}\Omega_p\right)^3 F_{ppp}^{Au} = \Lambda_{Au}^3 \Omega_p^3 F_{ppp}^{Au}$$
$$\rho_{pps}^{Au} = \left(\Lambda_{Au}\Omega_p\right)^2 (\Lambda_{Au}\Omega_{CuS}).3F_{ppp}^{Au} = \Lambda_{Au}^3 \Omega_p^2 \Omega_{CuS}.3F_{ppp}^{Au}$$
$$\rho_{pss}^{Au} = \left(\Lambda_{Au}\Omega_p\right)(\Lambda_{Au}\Omega_{CuS})^2.3F_{ppp}^{Au} = \Lambda_{Au}^3 \Omega_p \Omega_{CuS}^2.3F_{ppp}^{Au}$$

$$\rho_{sss}^{au} = (\Lambda_{Au}\Omega_{CuS})^3 F_{ppp}^{Au} = \Lambda_{Au}^3\Omega_{CuS}^3 . F_{ppp}^{Au}$$

$$\rho_{ppp}^{Au} = \Omega_p^3\Lambda_{Au}^3 F_{ppp}^{Au} \qquad \rho_{pps}^{Au} = \Lambda_{Au}^3\Omega_p^2\Omega_{CuS} . 3F_{ppp}^{Au} \tag{21}$$

$$\rho_{pss}^{Au} = \Lambda_{Au}^3\Omega_p\Omega_{CuS}^2 . 3F_{ppp}^{Au}\rho_{sss}^{Au} = \Lambda_{Au}^3\Omega_{CuS}^3 F_{ppp}^{Au} \qquad F_{ppp}^{Au} = \frac{4i\,Re(d_{21})}{(\gamma_{21})d_{21}d_{21}(d_{21})^*} \tag{22}$$

We evaluate the third order susceptibility $\chi_{Au}^{(3)}$ by substituting the expression for $\varrho_{Au}^{(3)}$ from Equation (20) into Equation (14) to obtain

$$\chi_{Au}^{(3)} = \chi_{ppp}^{Au} + \chi_{pps}^{Au} + \chi_{pss}^{Au} + \chi_{sss}^{Au} \tag{23}$$

where:

$$\chi_{ppp}^{Au} = \frac{2\mu_{21}^3 p_{Au}}{V_{Au}\in_0\hbar^3}\left(\Lambda_{Au}^3 F_{ppp}^{Au}\right) \qquad \chi_{pps}^{Au} = \frac{6\mu_{21}^3 p_{Au}}{V_{Au}\in_0\hbar^3}\left(\Lambda_{Au}^3\Pi_{CuS}F_{ppp}^{Au}\right) \tag{24}$$

$$\chi_{pss}^{Au} = \frac{6\mu_{21}^3 p_{Au}}{V_{Au}\in_0\hbar^3}\left(\Lambda_{Au}^3\Pi_{CuS}^2 F_{ppp}^{Au}\right) \qquad \chi_{pps}^{Au} = \frac{2\mu_{21}^3 p_{Au}}{V_{Au}\in_0\hbar^3}\left(\Lambda_{Au}^3\Pi_{CuS}^3 F_{ppp}^{Au}\right) \tag{25}$$

The THG intensity: We calculate the THG intensity for the Au-NP as follows.

$$I_{THG}^{Au} = \frac{1}{2}\sqrt{\frac{\in_0}{\mu_0}}n_3\left|E_{THG}^{Au}\right|^2 = \frac{\in_0 c}{2}n_3\left|E_{THG}^{Au}\right|^2 \tag{26}$$

Here E_{THG}^{Au} is the THG electric field emitted by the Au nanoparticle.
The intensity of THG can be calculated by solving the nonlinear Maxwell equations. One can find the following expression of the E_{THG}^{Au} field.

$$E_{THG}^{Au} = i\frac{6\omega_3 L}{c}\begin{Bmatrix}\chi_{ppp}^{Au}E_pE_pE_p + \chi_{pps}^{Au}E_pE_pE_{CuS} \\ +\chi_{ps}^{Au}E_pE_{CuS}E_{CuS} + \chi_{sss}^{Au}E_{CuS}E_{CuS}E_{CuS}\end{Bmatrix} \tag{27}$$

Inserting Equation 27 into Equation 26 we get the expression for the THG intensity.

$$I_{THG}^{Au} = \frac{18\in_0\omega_3^2L^2n_3}{c}\begin{Bmatrix}\left|\chi_{ppp}^{Au}\right|^2\left|E_p^3\right|^2 + \left|\chi_{pps}^{Au}\right|^2\left|E_p^2E_{CuS}\right|^2 \\ +\left|\chi_{pss}^{Au}\right|^2\left|E_pE_{CuS}^2\right|^2 + \left|\chi_{pss}^{Au}\right|^2\left|E_{CuS}^3\right|^2\end{Bmatrix} \tag{28}$$

Note that the cross terms are neglected because they correspond to coherences. These were neglected due to the short dephasing time of the plasmon resonance with respect to the exciting pulse, with a dephasing time on the order of 10 fs, and pulse width of 177fs. This means that the plasmon resonances lose phase coherence due to electron-electron collisions and thermalize very quickly after the end of the pulse. Thus, coherence effects have been neglected, congruous with previous treatments of similar systems [65],[97],[105].

It is possible to include the effect of coherence in our formulation in our future works whether this effect is important or not important for the present paper. However, the inclusion of coherence will make the expression of the THG intensity very complicated and challenging. An analytical expression for the THG intensity could not be achieved. One of the aims of the present theory was to derive a simple expression of the THG intensity so that experimentalists working in the plasmonic field can compare their experiments with the current theory.

We express the E_p and E_{CuS} in terms of pump intensity I_p and SPP intensity I_{CuS} as follows

$$I_p = \frac{\epsilon_0 c}{2} n_3 \left|E_p\right|^2 \qquad I_{CuS} = \frac{\epsilon_0 c}{2} n_3 \left|E_{spp}^{CuS}\right|^2 \tag{29}$$

Now, we insert Equations 24, 25, and 29 into Equation 28 to get an expression of the THG intensity.

$$I_{THG}^{Au} = \alpha_{cst}^{Au} \Lambda_{Au}^6 \left|F_{ppp}^{Au}\right|^2 \left\{{I_p}^3 + 9{\Pi_{CuS}}^2 {I_p}^2 I_{CuS} + 9{\Pi_{CuS}}^4 {I_{CuS}}^2 I_p + {\Pi_{CuS}}^6 {I_{CuS}}^3\right\} \tag{30}$$

Where:

$$\alpha_{THG}^{Au} = \frac{144\omega_3^2 L^2 \mu_{21}^6 p_{Au}^2}{\epsilon_0^4 V_{Au}^2 c^4 \hbar^6 n_3^2} \tag{31}$$

One can see from Equation 30 that there is an enhancement in THG due to the presence of the CuS nanoparticles.

2.4 Enhancement in THG Intensity in CuS-NP due to Au-NPs

Next, we study the effect of Au nanoparticles on the THG intensity emitted by CuS-NP. We find that Au-NP emits the surface-plasmon polariton electric field, E_{spp}^{Au}. The CuS-NP is interacting with Au-NP via E_{spp}^{Au} field. This interaction is nothing but the dipole-dipole interaction. The interaction Hamiltonian for CuS nanoparticle in the dipole and rotating wave approximation can be written as follows.

$$\begin{aligned} H_{Cus} &= H_{Cus-probe} + H_{DDI}^{Cus} \\ H_{Cus-probe} &= \hbar \Lambda_{CuS} \Omega_p \sigma_{21} + h.c. \\ H_{DDI}^{CuS} &= \hbar \Lambda_{Cus} \Omega_{Au} \sigma_{21} + h.c \end{aligned} \tag{32}$$

Where the physical parameters appearing in Equation 32 are found as

$$\Omega_{Au} = \frac{\mu_{21} E_{spp}^{Au}}{\hbar} = \Pi_{Au} \Omega_P \qquad \Lambda_{CuS} = \frac{4\pi \epsilon_0 \epsilon_b V_{CuS} g_l \zeta_{CuS} \hbar \Omega_P}{\mu_{21}^2} \tag{33}$$

Note that $H_{DDI}^{CuS} = H_{DDI}^{Au}$. The first term in the interaction Hamiltonian between the SPP polariton with the pump photon. The second term the dipole-dipole interaction between CuS-NP and Au-NP.

Following the density matrix method of Au-NP, we found the third order density matrix $\varrho_{21}^{(3)} = \varrho_{CuS}^{(3)}$ for CuS-NP as

$$\rho_{CuS}^{(3)} = \rho_{ppp}^{CuS} + \rho_{pps}^{CuS} + \rho_{pss}^{CuS} + \rho_{sss}^{CuS} \tag{34}$$

The density matrix elements appearing in Equation 34 are found as

$$\rho_{ppp}^{CuS} = \Omega_p^3 \Lambda_{CuS}^3 F_{ppp}^{CuS} \qquad \rho_{pps}^{CuS} = 3\Omega_p^3 \Lambda_{CuS}^3 \Pi_{Au} F_{ppp}^{CuS} \tag{35}$$

$$\rho_{pss}^{CuS} = 3\Omega_p^3 \Lambda_{CuS}^3 \Pi_{Au}^2 F_{ppp}^{CuS} \qquad \rho_{sss}^{CuS} = \Omega_p^3 \Lambda_{CuS}^3 \Pi_{Au}^3 F_{ppp}^{CuS} \tag{36}$$

Finally, with the help of Equation 35, 36, the THG intensity emitted by the CuS-NP is calculated as follows.

$$I_{THG}^{Cus} = \alpha_{cst}^{Cus}\Lambda_{CuS}^{6}\left|F_{ppp}^{Cus}\right|^{2}\left\{{I_p}^{3} + 9{\Pi_{Au}}^{2}{I_p}^{2}I_{Au} + 9{\Pi_{Au}}^{4}{I_{Au}}^{2}I_p + {\Pi_{Au}}^{6}{I_{Au}}^{3}\right\} \quad (37)$$

where

$$\alpha_{THG}^{CuS} = \frac{144\omega_3^2 L^2 \mu_{21}^6 p_{CuS}^2}{\epsilon_0^4 V_{CuS}^2 c^4 \hbar^6 n_3^2} \quad (38)$$

We found that the THG intensity of CuS-NP is enhanced due to the presence of Au nanoparticles.

2.5 THG Intensity in Au and CuS nanohybrid

The THG intensity emitted by the Au-NP and CuS-NP hybrid can be obtained by adding the intensities of the Au and CuS nanoparticles. The THG intensity for the hybrid system is found as

$$I_{THG}^{hybrid} = I_{THG}^{Au} + I_{THG}^{CuS} \quad (39)$$

Substituting the expression for I_{THG}^{Au} and I_{THG}^{CuS} from Equations 30 and 37 into Equation 39, we get

$$I_{THG}^{hybrid} = \left[\alpha_{cst}^{Au}\Lambda_{Au}^{6}\left|F_{ppp}^{Au}\right|^{2}\left\{{I_p}^{3} + 9{\Pi_{CuS}}^{2}{I_p}^{2}I_{CuS} + 9{\Pi_{CuS}}^{4}{I_{CuS}}^{2}I_p + {\Pi_{CuS}}^{6}{I_{CuS}}^{3}\right\} + \alpha_{cst}^{Cus}\Lambda_{CuS}^{6}\left|F_{ppp}^{CuS}\right|^{2}\left\{{I_p}^{3} + 9{\Pi_{Au}}^{2}{I_p}^{2}I_{Au} + 9{\Pi_{Au}}^{4}{I_{Au}}^{2}I_p + {\Pi_{Au}}^{6}{I_{Au}}^{3}\right\}\right] \quad (40)$$

We predicted that the hybrid intensity depends on the dipoles and SPP coupling constant of the Au and CuS nanoparticles.

The expression of the THG intensity can be further written in the compact form as follows

$$I_{THG} = C_{au}\left\{{I_p}^{3} + 9{\Pi_{CuS}}^{2}{I_p}^{2}I_{CuS} + 9{\Pi_{CuS}}^{4}{I_{CuS}}^{2}I_p + {\Pi_{Cus}}^{6}{I_{CuS}}^{3}\right\} + C_{CuS}\left\{{I_p}^{3} + 9{\Pi_{Au}}^{2}{I_p}^{2}I_{Au} + 9{\Pi_{Au}}^{4}{I_{Au}}^{2}I_p + {\Pi_{Au}}^{6}{I_{Au}}^{3}\right\} \quad (41)$$

Where

$$C_{CuS} = \alpha_{cst}^{CuS}\Lambda_{CuS}^{6}\left|F_{ppp}^{CuS}\right|^{2} \quad C_{Au} = \alpha_{cst}^{Au}\Lambda_{Au}^{6}\left|F_{ppp}^{Au}\right|^{2} \quad (42)$$

Note that unit of C_{Au} and C_{CuS} is $(W/m^2)^{-2}$. The intensity parameters I_p, I_{Au} and I_{CuS} have unit (W/m^2). On the other hand, the SPP coupling parameters Π_{Au} and Π_{CuS} are unitless.

2.6 SHG intensity of Au-NP alone and CuS-NP alone

We can calculate the THG intensity emitted from Au nanoparticles alone from Equation 40 by putting $\Pi_{CuS} = 0$ and $\Lambda_{CuS} = 0$ to obtain

$$I_{THG}^{Au} = \alpha_{cst}^{Au}\Lambda_{Au}^{3}\left|F_{ppp}^{Au}\right|^{2}.I_p^3 \quad (43)$$

Similarly, the THG intensity emitted from CuS nanoparticle alone can be calculated from Equation 40 by putting $\Pi_{Au} = 0$ and $\Lambda_{Au} = 0$.

$$I_{THG}^{CuS} = \alpha_{cst}^{CuS} \Lambda_{CuS}^{3} \left| F_{ppp}^{CuS} \right|^{2} I_{p}^{3} \tag{44}$$

Comparison of Theory and Experiments

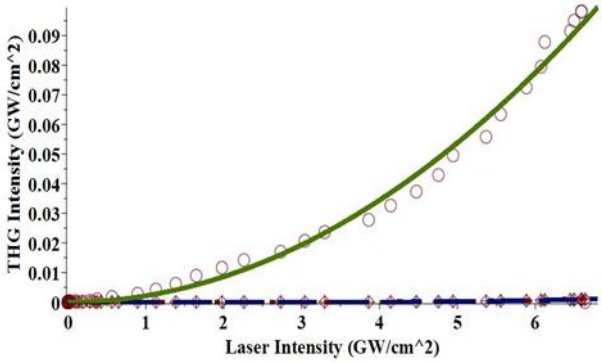

Figure B.8: A comparison between the theory and experiments for the 15 nm sample. The experimental points are shown in circles for the Au-CuS sample, crosses for the Au sample and diamonds for the CuS sample. The dashed line and dotted lines are for the Au-only and the CuS-only samples, respectively. The dash-dotted line adds the THG intensities from single layers of Au and CuS nanoparticles.

The solid line in Figure B.8 is the fit for the Au-CuS sample, derived from Equation 40. The SPP coupling parameter values that result from the fitting procedure are $\Pi_{CuS} = 3.1$ and $\Pi_{Au} = 0$, corresponding to single-beam excitation at 1050 nm as in the experiment. The theoretical value $\Pi_{CuS} = 3.1$ is used to calculate the output intensity of the third harmonic as shown in Figure B.9.

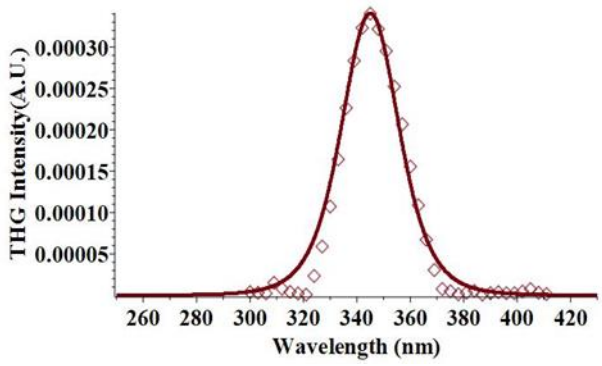

Figure B.9: Output intensity of the THG signal with 1050 nm fundamental input. Experimentally measured points are shown in diamonds. The solid line is theoretical calculation from input beam properties.

By substituting the following physical constants into Equations 5, 6 and 10,

ε_{CuS} = 5.76, ε_b = 1.69, $L_x = L_y$ = 15 nm, $\frac{V_{CuS}}{4\pi r^3} = 2.1$

where the ratio $\frac{V_{CuS}}{4\pi r^3} = 2.1$ is based on the estimated packing fraction of the nanoparticles on the surface in Figure 3.1d, we calculate the value of Π_{CuS} to be 1.7; within the limits of accuracy with which we can estimate the physical parameters, this is reasonably close to the value derived from fitting the experimental data.

B.10 SEM of Au/CuS bilayer films at (a-c) the site of laser exposure and (e-f) sites without laser exposure

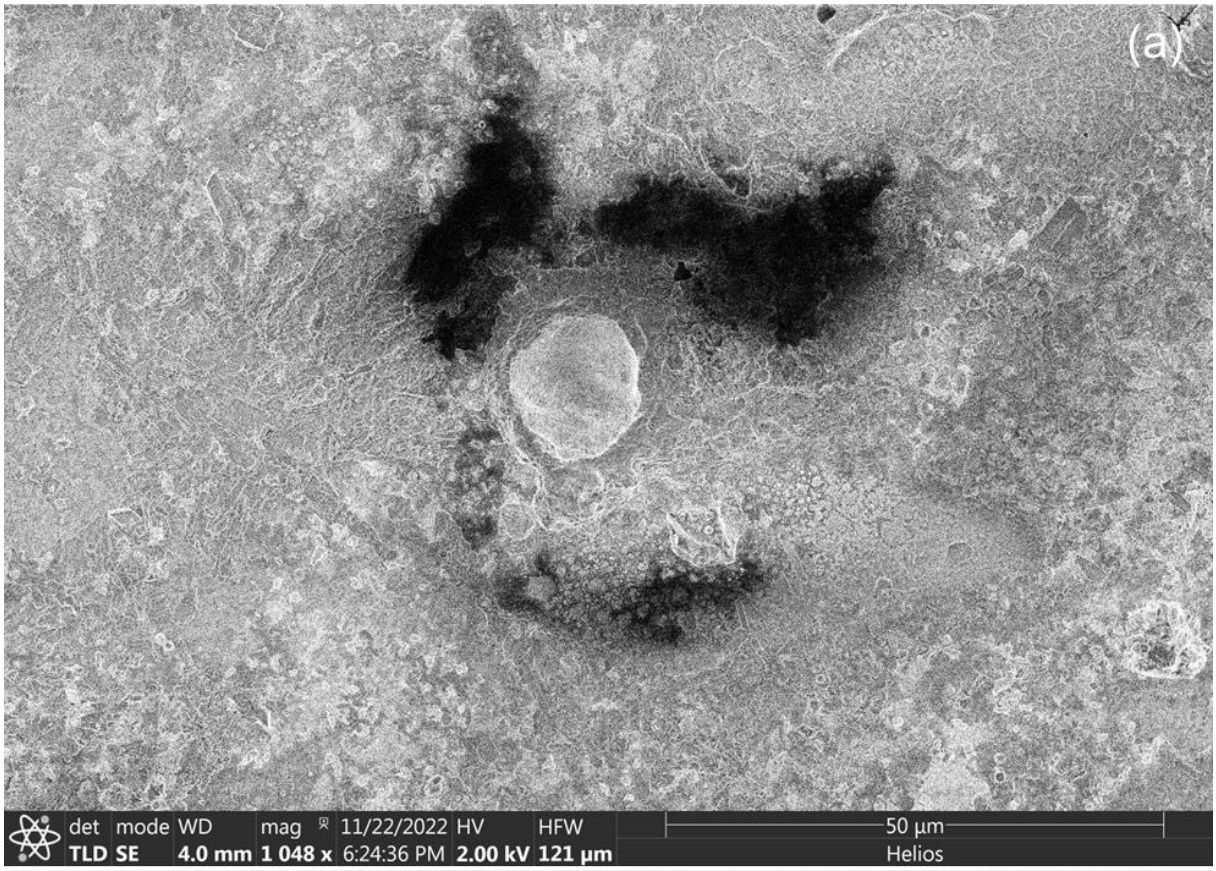

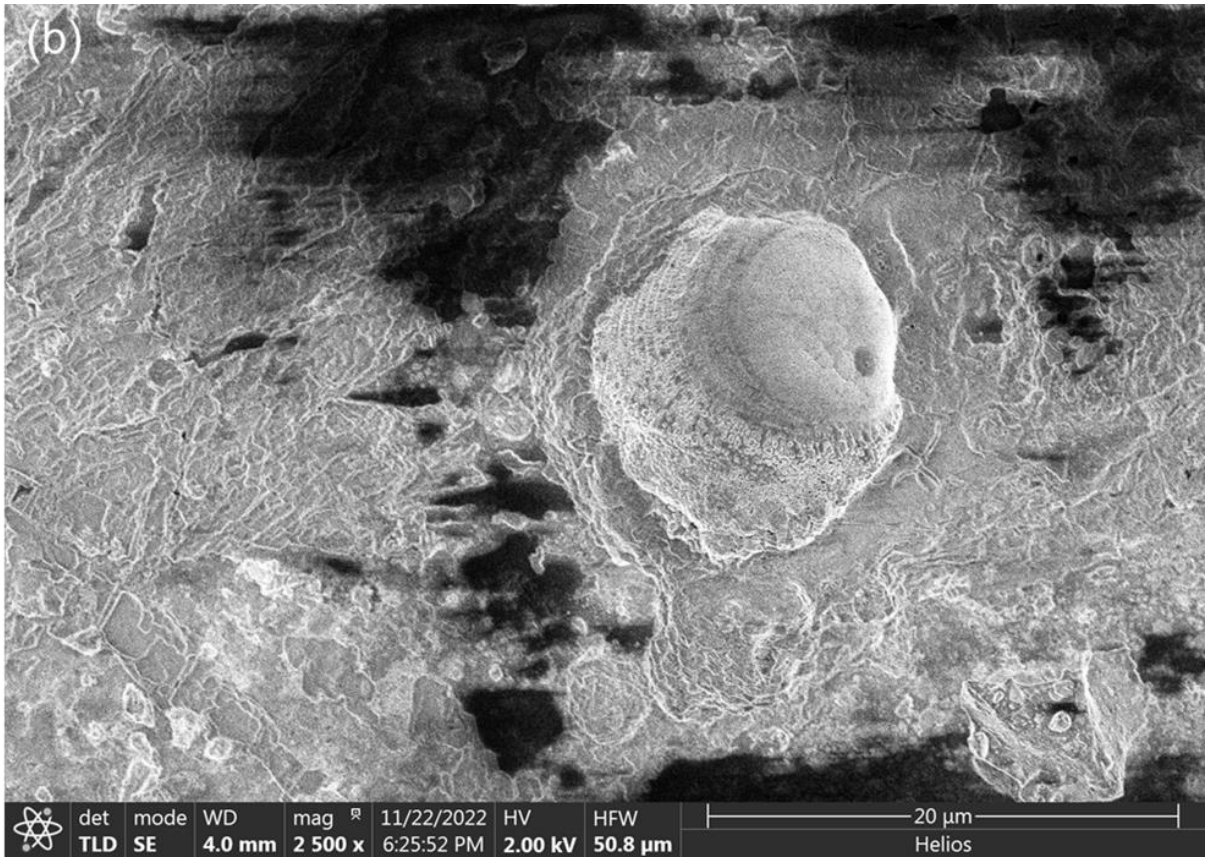
(b)
det mode WD mag 11/22/2022 HV HFW
TLD SE 4.0 mm 2 500 x 6:25:52 PM 2.00 kV 50.8 µm
20 µm
Helios

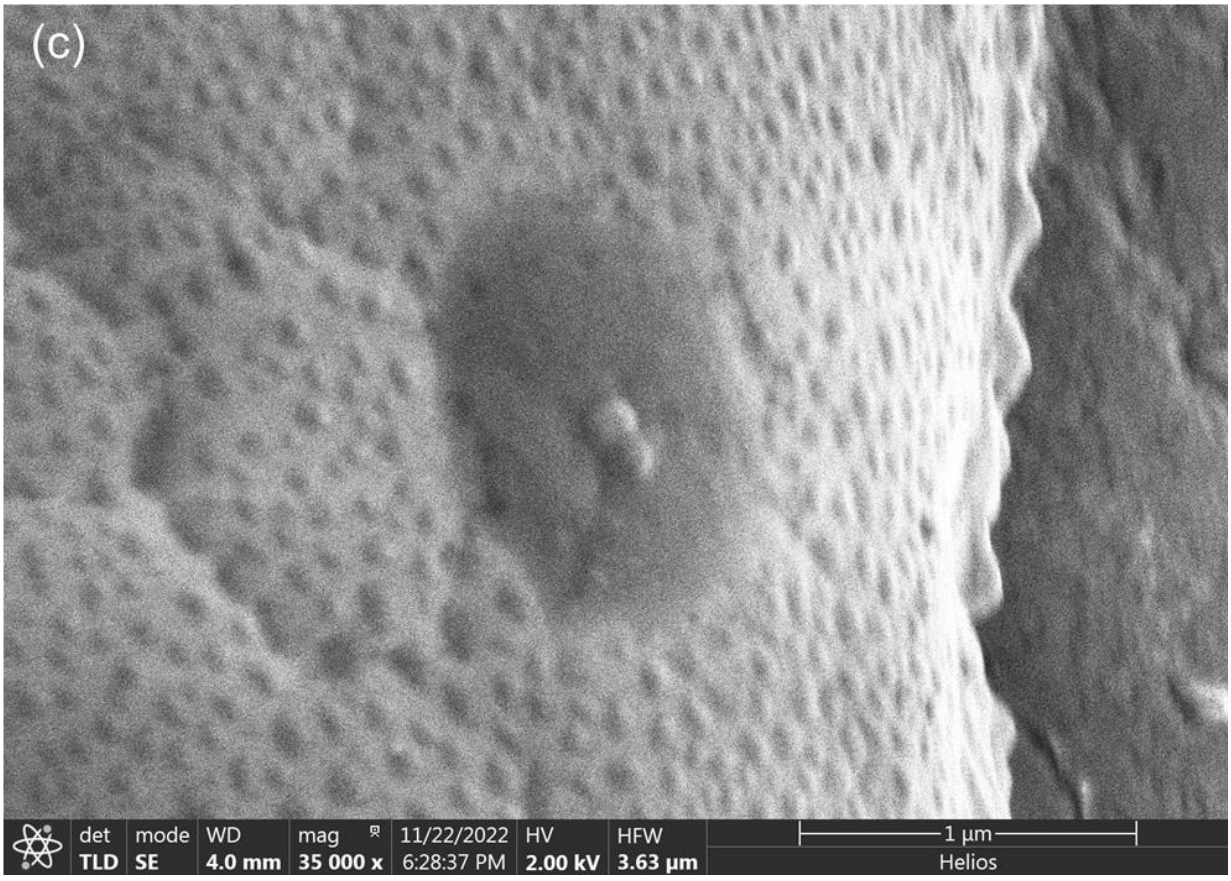
(c)
det mode WD mag 11/22/2022 HV HFW
TLD SE 4.0 mm 35 000 x 6:28:37 PM 2.00 kV 3.63 µm
1 µm
Helios

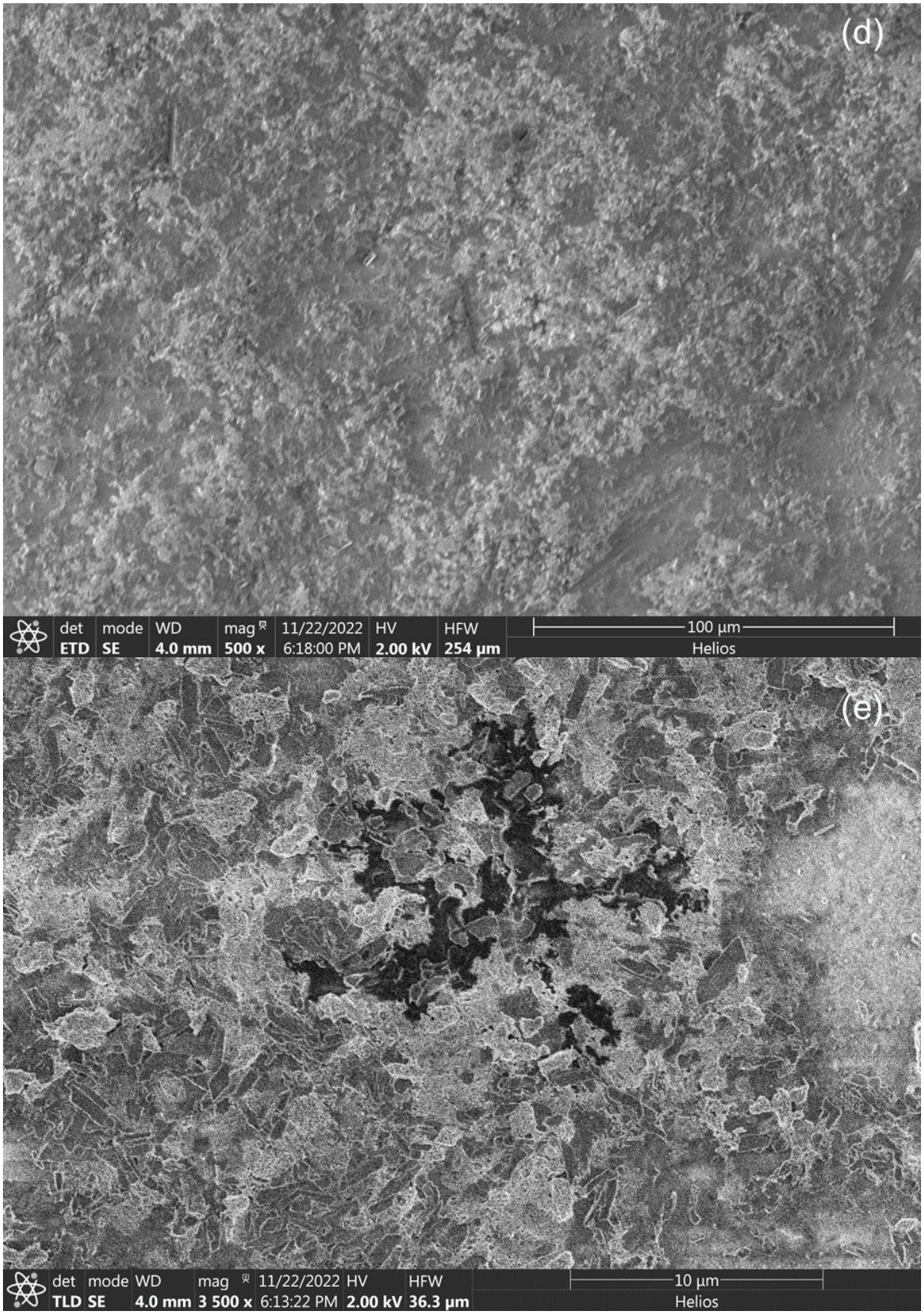
(d)
det mode WD mag 11/22/2022 HV HFW
ETD SE 4.0 mm 500 x 6:18:00 PM 2.00 kV 254 µm
100 µm
Helios
(e)
det mode WD mag 11/22/2022 HV HFW
TLD SE 4.0 mm 3 500 x 6:13:22 PM 2.00 kV 36.3 µm
10 µm
Helios

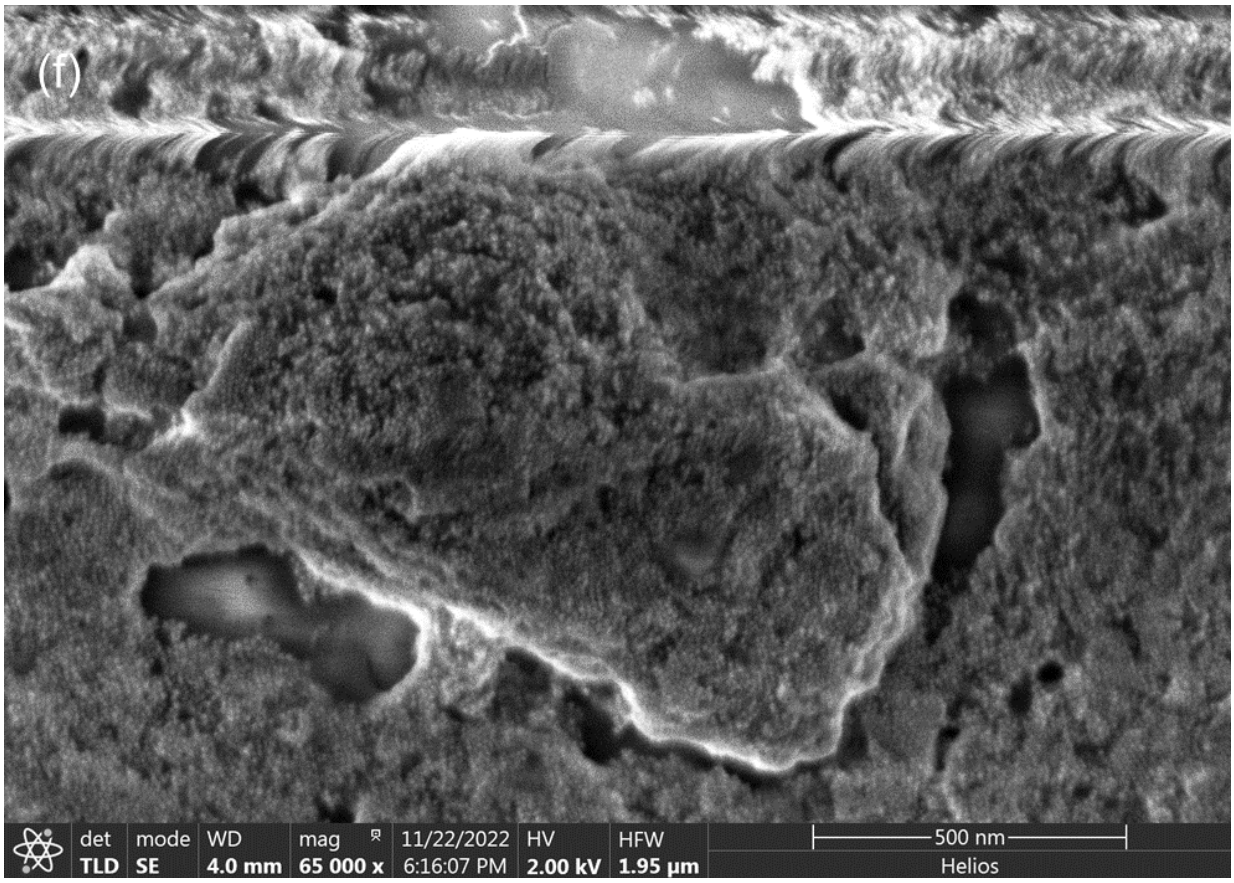
(f)
det
TLD
mode
SE
WD
4.0 mm
mag
65 000 x
11/22/2022
6:16:07 PM
HV
2.00 kV
HFW
1.95 µm
500 nm
Helios

References

[1] M. Fox. "Optical Properties of Solids", 2nd ed.; Oxford University Press.

[2] R. Boyd. "Nonlinear Optics", Third Edit.; Academic Press: Burlington, MA.

[3] M. Celebrano, A. Locatelli, L. Ghirardini, G. Pellegrini, et al. "Evidence of Cascaded Third-Harmonic Generation in Noncentrosymmetric Gold Nanoantennas," *Nano Lett.*, vol. 19, no. 10, pp. 7013–7020, 2019. https://doi.org/10.1021/acs.nanolett.9b02427.

[4] M. Haase, H. Schäfer. "Upconverting Nanoparticles," *Angew. Chemie - Int. Ed.*, vol. 50, no. 26, pp. 5808–5829, 2011. https://doi.org/10.1002/anie.201005159.

[5] W. Park, D. Lu, S. Ahn. "Plasmon Enhancement of Luminescence Upconversion," *Chem. Soc. Rev.*, vol. 44, no. 10, pp. 2940–2962, 2015. https://doi.org/10.1039/c5cs00050e.

[6] J. Liu, H. He, D. Xiao, S. Yin, et al. "Recent Advances of Plasmonic Nanoparticles and Their Applications," *Materials (Basel).*, vol. 11, no. 10, 2018. https://doi.org/10.3390/ma11101833.

[7] M. D. McMahon, R. Lopez, R. F. Haglund, E. A. Ray, et al. "Second-Harmonic Generation from Arrays of Symmetric Gold Nanoparticles," *Phys. Rev. B - Condens. Matter Mater. Phys.*, vol. 73, no. 4, pp. 1–4, 2006. https://doi.org/10.1103/PhysRevB.73.041401.

[8] T. Y. Jeon, D. J. Kim, S. G. Park, S. H. Kim, et al. "Nanostructured Plasmonic Substrates for Use as SERS Sensors," *Nano Converg.*, vol. 3, no. 1, 2016. https://doi.org/10.1186/s40580-016-0078-6.

[9] J. Butet, P.-F. Brevet, O. J. F. Martin. "Optical Second Harmonic Generation in Plasmonic Nanostructures: From Fundamental Principles to Advanced Applications," *ACS Nano*, vol. 9, no. 11, pp. 10545–10562, 2015. https://doi.org/10.1021/acsnano.5b04373.

[10] B. Lamprecht, J. R. Krenn, A. Leitner, E. R. Aussenegg. "Resonant and Off-Resonant Light-Driven Plasmons in Metal Nanoparticles Studied by Femtosecond-Resolution Third-Harmonic Generation," *Phys. Rev. Lett.*, vol. 83, no. 21, pp. 4421–4424, 1999. https://doi.org/10.1103/PhysRevLett.83.4421.

[11] R. B. Davidson, J. I. Ziegler, G. Vargas, S. M. Avanesyan, et al. "Eflcient Forward Second-Harmonic Generation from Planar Archimedean Nanospirals," *Nanophotonics*, vol. 4, no. 1, pp. 108–113, 2015. https://doi.org/10.1515/nanoph-2015-0002.

[12] G. Bachelier, I. Russier-Antoine, E. Benichou, C. Jonin, et al. "Multipolar Second-Harmonic Generation in Noble Metal Nanoparticles," *J. Opt. Soc. Am. B*, vol. 25, no. 6, pp. 955, 2008. https://doi.org/10.1364/josab.25.000955.

[13] Y. Zhang, X. Zhu, Y. Zhang. "Exploring Heterostructured Upconversion Nanoparticles: From Rational Engineering to Diverse Applications," *ACS Nano*, vol. 15, no. 3, pp. 3709–3735, 2021. https://doi.org/10.1021/acsnano.0c09231.

[14] D. Ratchford, F. Shafiei, S. Kim, S. K. Gray, et al. "Manipulating Coupling between a Single Semiconductor Quantum Dot and Single Gold Nanoparticle," *Nano Lett.*, vol. 11, no. 3, pp. 1049–1054, 2011. https://doi.org/10.1021/nl103906f.

[15] S. I. Shopova, C. W. Blackledge, A. T. Rosenberger. "Enhanced Evanescent Coupling to Whispering-Gallery Modes Due to Gold Nanorods Grown on the Microresonator Surface," *Appl. Phys. B Lasers Opt.*, vol. 93, no. 1, pp. 183–187, 2008. https://doi.org/10.1007/s00340-008-3180-6.

[16] H. Lange, B. H. Juárez, A. Carl, M. Richter, et al. "Tunable Plasmon Coupling in

Distance-Controlled Gold Nanoparticles," *Langmuir*, vol. 28, no. 24, pp. 8862–8866, 2012. https://doi.org/10.1021/la3001575.
[17] J. Olesiak-Banska, M. Waszkielewicz, P. Obstarczyk, M. Samoc. "Two-Photon Absorption and Photoluminescence of Colloidal Gold Nanoparticles and Nanoclusters," *Chem. Soc. Rev.*, vol. 48, no. 15, pp. 4087–4117, 2019. https://doi.org/10.1039/c8cs00849c.
[18] V. Knittel, M. P. Fischer, T. De Roo, S. Mecking, et al. "Nonlinear Photoluminescence Spectrum of Single Gold Nanostructures," *ACS Nano*, vol. 9, no. 1, pp. 894–900, 2015. https://doi.org/10.1021/nn5066233.
[19] M. W. Knight, N. S. King, L. Liu, H. O. Everitt, et al. "Aluminum for Plasmonics," *ACS Nano*, vol. 8, no. 1, pp. 834–840, 2014. https://doi.org/10.1021/nn405495q.
[20] M. J. McClain, A. E. Schlather, E. Ringe, N. S. King, et al. "Aluminum Nanocrystals," *Nano Lett.*, vol. 15, no. 4, pp. 2751–2755, 2015. https://doi.org/10.1021/acs.nanolett.5b00614.
[21] H. Yin, Y. Kuwahara, K. Mori, C. Louis, et al. "Properties, Fabrication and Applications of Plasmonic Semiconductor Nanocrystals," *Catal. Sci. Technol.*, vol. 10, no. 13, pp. 4141–4163, 2020. https://doi.org/10.1039/c9cy02511a.
[22] Y. Wang, B. Liu, Y. Wang, H. Yuan, et al. "Plasmonic Semiconductor: A Tunable Non-Metal Photocatalyst," *Int. J. Hydrogen Energy*, vol. 46, no. 58, pp. 29858–29888, 2021. https://doi.org/10.1016/j.ijhydene.2021.06.142.
[23] J. Kim, A. Agrawal, F. Krieg, A. Bergerud, et al. "The Interplay of Shape and Crystalline Anisotropies in Plasmonic Semiconductor Nanocrystals," *Nano Lett.*, vol. 16, no. 6, pp. 3879–3884, 2016. https://doi.org/10.1021/acs.nanolett.6b01390.
[24] Z. Wang, C. Yang, T. Lin, H. Yin, et al. "H-Doped Black Titania with Very High Solar Absorption and Excellent Photocatalysis Enhanced by Localized Surface Plasmon Resonance," *Adv. Funct. Mater.*, vol. 23, no. 43, pp. 5444–5450, 2013. https://doi.org/10.1002/adfm.201300486.
[25] M. Kanehara, H. Koike, T. Yoshinaga, T. Teranishi. "Indium Tin Oxide Nanoparticles with Compositionally Tunable Surface Plasmon Resonance Frequencies in the Near-IR Region," *J. Am. Chem. Soc.*, vol. 131, no. 49, pp. 17736–17737, 2009. https://doi.org/10.1021/ja9064415.
[26] R. J. Mendelsberg, S. H. N. Lim, Y. K. Zhu, J. Wallig, et al. "Achieving High Mobility ZnO: Al at Very High Growth Rates by Dc Filtered Cathodic Arc Deposition," *J. Phys. D. Appl. Phys.*, vol. 44, no. 23, 2011. https://doi.org/10.1088/0022-3727/44/23/232003.
[27] Y. Xie, L. Carbone, C. Nobile, V. Grillo, et al. "Metallic-like Stoichiometric Copper Sulfide Nanocrystals: Phase- and Shape-Selective Synthesis, near-Infrared Surface Plasmon Resonance Properties, and Their Modeling," *ACS Nano*, vol. 7, no. 8, pp. 7352–7369, 2013. https://doi.org/10.1021/nn403035s.
[28] B. C. Marin, S. W. Hsu, L. Chen, A. Lo, et al. "Plasmon-Enhanced Two-Photon Absorption in Photoluminescent Semiconductor Nanocrystals," *ACS Photonics*, vol. 3, no. 4, pp. 526–531, 2016. https://doi.org/10.1021/acsphotonics.6b00037.
[29] J. Li, S. K. Cushing, F. Meng, T. R. Senty, et al. "Plasmon-Induced Resonance Energy Transfer for Solar Energy Conversion," *Nat. Photonics*, vol. 9, no. 9, pp. 601–607, 2015. https://doi.org/10.1038/nphoton.2015.142.
[30] M. You, J. Zhong, Y. Hong, Z. Duan, et al. "Inkjet Printing of Upconversion Nanoparticles for Anti-Counterfeit Applications," *Nanoscale*, vol. 7, no. 10, pp. 4423–4431, 2015. https://doi.org/10.1039/c4nr06944g.
[31] G. Grinblat, M. Rahmani, E. Cortés, M. Caldarola, et al. "High-Efficiency Second

Harmonic Generation from a Single Hybrid Zno Nanowire/Au Plasmonic Nano-Oligomer," *Nano Lett.*, vol. 14, no. 11, pp. 6660–6665, 2014. https://doi.org/10.1021/nl503332f.

[32] Y. Zhang, A. Manjavacas, N. J. Hogan, L. Zhou, et al. "Toward Surface Plasmon-Enhanced Optical Parametric Amplification (SPOPA) with Engineered Nanoparticles: A Nanoscale Tunable Infrared Source," *Nano Lett.*, vol. 16, no. 5, pp. 3373–3378, 2016. https://doi.org/10.1021/acs.nanolett.6b01095.

[33] Y. Zhang, N. K. Grady, C. Ayala-Orozco, N. J. Halas. "Three-Dimensional Nanostructures as Highly Efficient Generators of Second Harmonic Light," *Nano Lett.*, vol. 11, no. 12, pp. 5519–5523, 2011. https://doi.org/10.1021/nl2033602.

[34] F. B. P. Niesler, N. Feth, S. Linden, M. Wegener. "Second-Harmonic Optical Spectroscopy on Split-Ring-Resonator Arrays," vol. 36, no. 9, pp. 1533–1535, 2011.

[35] O. J. F. Martin. "Augmenting Second Harmonic Generation Using Fano Resonances in Plasmonic Systems," 2013. https://doi.org/10.1021/nl400636z.

[36] Q. Ai, L. Gui, D. Paone, B. Metzger, et al. "Ultranarrow Second-Harmonic Resonances in Hybrid Plasmon-Fiber Cavities," *Nano Lett.*, vol. 18, no. 9, pp. 5576–5582, 2018. https://doi.org/10.1021/acs.nanolett.8b02005.

[37] M. Celebrano, X. Wu, M. Baselli, S. Großmann, et al. "Mode Matching in Multiresonant Plasmonic Nanoantennas for Enhanced Second Harmonic Generation," *Nat. Nanotechnol.*, vol. 10, no. 5, pp. 412–417, 2015. https://doi.org/10.1038/nnano.2015.69.

[38] R. Czaplicki, H. Husu, R. Siikanen, J. Mäkitalo, et al. "Enhancement of Second-Harmonic Generation from Metal Nanoparticles by Passive Elements," *Phys. Rev. Lett.*, vol. 110, no. 9, pp. 1–5, 2013. https://doi.org/10.1103/PhysRevLett.110.093902.

[39] Z. Q. Cheng, Z. L. Li, X. Luo, H. Q. Shi, et al. "Enhanced Second Harmonic Generation by Double Plasmon Resonances in Mesoscale Flower-like Silver Particles," *Appl. Phys. Lett.*, vol. 114, no. 1, 2019. https://doi.org/10.1063/1.5079241.

[40] K. Y. Yang, J. Butet, C. Yan, G. D. Bernasconi, et al. "Enhancement Mechanisms of the Second Harmonic Generation from Double Resonant Aluminum Nanostructures," *ACS Photonics*, vol. 4, no. 6, pp. 1522–1530, 2017. https://doi.org/10.1021/acsphotonics.7b00288.

[41] S. Ding, D. Yang, X. Liu, F. Nan, et al. "Asymmetric Growth of Au-Core/Ag-Shell Nanorods with a Strong Octupolar Plasmon Resonance and an Efficient Second-Harmonic Generation," *Nano Res.*, vol. 11, no. 2, pp. 686–695, 2018. https://doi.org/10.1007/s12274-017-1678-0.

[42] N. E. Motl, A. F. Smith, C. J. Desantis, S. E. Skrabalak. "Engineering Plasmonic Metal Colloids through Composition and Structural Design," *Chem. Soc. Rev.*, vol. 43, no. 11, pp. 3823–3834, 2014. https://doi.org/10.1039/c3cs60347d.

[43] P. M. Jais, C. Von Bilderling, A. V. Bragas. "Plasmon-Enhanced Second Harmonic Generation in Semiconductor Quantum Dots Close to Metal Nanoparticles," *Pap. Phys.*, vol. 3, no. 0, pp. 1–5, 2011. https://doi.org/10.4279/pip.030002.

[44] H. Linnenbank, Y. Grynko, J. Förstner, S. Linden. "Second Harmonic Generation Spectroscopy on Hybrid Plasmonic/Dielectric Nanoantennas," *Light Sci. Appl.*, vol. 5, no. 1, pp. e16013–e16013, 2016. https://doi.org/10.1038/lsa.2016.13.

[45] M. R. Singh. "Enhancement of the Second-Harmonic Generation in a Quantum Dot-Metallic Nanoparticle Hybrid System," *Nanotechnology*, vol. 24, no. 12, 2013. https://doi.org/10.1088/0957-4484/24/12/125701.

[46] E. Shaviv, U. Banin. "Synergistic Effects on Second Harmonic Generation of Hybrid CdSe-Au Nanoparticles," *ACS Nano*, vol. 4, no. 3, pp. 1529–1538, 2010.

https://doi.org/10.1021/nn901778k.
[47] D. Dorfs, T. Härtling, K. Miszta, N. C. Bigall, et al. "Reversible Tunability of the Near-Infrared Valence Band Plasmon Resonance in Cu2- XSe Nanocrystals," *J. Am. Chem. Soc.*, vol. 133, no. 29, pp. 11175–11180, 2011. https://doi.org/10.1021/ja2016284.
[48] A. Agrawal, S. H. Cho, O. Zandi, S. Ghosh, et al. "Localized Surface Plasmon Resonance in Semiconductor Nanocrystals," *Chem. Rev.*, vol. 118, no. 6, pp. 3121–3207, 2018. https://doi.org/10.1021/acs.chemrev.7b00613.
[49] J. B. Brzoska, N. Shahidzadeh, F. Rondelez. "Evidence of a Transition Temperature for the Optimum Deposition of Grafted Monolayer Coatings," *Nature*, vol. 360, no. 6406, pp. 719–721, 1992. https://doi.org/10.1038/360719a0.
[50] C. A. Goss, C. H. Deborah, M. Majda. "Applicaiton of (3-Mercaptopropyl)Trimethoxysilane as a Molecular Adhesive in the Fabrication of Vapor-Deposited Gold Electrodes on Glass Substrates," *Anal. Chem.*, No. 63, pp. 85–88, 1990.
[51] N. E. Motl, E. Ewusi-annan, I. T. Sines, L. Jensen, et al. "Au-Cu Alloy Nanoparticles with Tunable Composition and Plasmonic Properties: Experimental Determination of Composition and Correlation with Theory," *J. Phys. Chem. C*, pp. 19263–19269, 2010.
[52] B. Metzger, M. Hentschel, T. Schumacher, M. Lippitz, et al. "Doubling the Efficiency of Third Harmonic Generation by Positioning ITO Nanocrystals into the Hot-Spot of Plasmonic Gap-Antennas," *Nano Lett.*, vol. 14, no. 5, pp. 2867–2872, 2014. https://doi.org/10.1021/nl500913t.
[53] J. Wang, J. Butet, A. L. Baudrion, A. Horrer, et al. "Direct Comparison of Second Harmonic Generation and Two-Photon Photoluminescence from Single Connected Gold Nanodimers," *J. Phys. Chem. C*, vol. 120, no. 31, pp. 17699–17710, 2016. https://doi.org/10.1021/acs.jpcc.6b04850.
[54] S. Palomba, M. Danckwerts, L. Novotny. "Nonlinear Plasmonics with Gold Nanoparticle Antennas," *J. Opt. A Pure Appl. Opt.*, vol. 11, no. 11, 2009. https://doi.org/10.1088/1464-4258/11/11/114030.
[55] J. Ludwig, L. An, B. Pattengale, Q. Kong, et al. "Ultrafast Hole Trapping and Relaxation Dynamics in p - Type CuS Nanodisks," 2015. https://doi.org/10.1021/acs.jpclett.5b01078.
[56] A. Kheirandish, N. S. Javan, H. Mohammadzadeh. "Second Harmonic Generation from Metal Nanoparticle Dimer: An Analytical Approach in Dipole Approximation," *Phys. Scr.*, vol. 96, no. 2, pp. 0–10, 2020. https://doi.org/10.1088/1402-4896/abd27d.
[57] J. Butet, J. Duboisset, G. Bachelier, I. Russier-Antoine, et al. "Optical Second Harmonic Generation of Single Metallic Nanoparticles Embedded in a Homogeneous Medium," *Nano Lett.*, vol. 10, no. 5, pp. 1717–1721, 2010. https://doi.org/10.1021/nl1000949.
[58] M. Lippitz, M. A. Van Dijk, M. Orrit. "Third-Harmonic Generation from Single Gold Nanoparticles," *Nano Lett.*, vol. 5, no. 4, pp. 799–802, 2005. https://doi.org/10.1021/nl0502571.
[59] M. Hentschel, T. Utikal, H. Giessen, M. Lippitz. "Quantitative Modeling of the Third Harmonic Emission Spectrum of Plasmonic Nanoantennas," *Nano Lett.*, vol. 12, no. 7, pp. 3778–3782, 2012. https://doi.org/10.1021/nl301686x.
[60] M. Castro-Lopez, D. Brinks, R. Sapienza, N. van Hulst. "Aluminum for Nonlinear Plasmonics: Resonance-Driven Polarized Luminescence of Al, Ag, and Au Nanoantennas," *Opt. InfoBase Conf. Pap.*, pp. 4674–4678, 2012. https://doi.org/10.1364/qels.2012.qtu1f.3.
[61] K. L. Kelly, E. Coronado, L. L. Zhao, G. C. Schatz. "The Optical Properties of Metal Nanoparticles: The Influence of Size, Shape, and Dielectric Environment," *J. Phys.*

Chem. B, vol. 107, no. 3, pp. 668–677, 2003. https://doi.org/10.1021/jp026731y.
[62] A. Bouhelier, R. Bachelot, G. Lerondel, S. Kostcheev, et al. "Surface Plasmon Characteristics of Tunable Photoluminescence in Single Gold Nanorods," *Phys. Rev. Lett.*, vol. 95, no. 26, pp. 4–7, 2005. https://doi.org/10.1103/PhysRevLett.95.267405.
[63] S. Thota, Y. Wang, J. Zhao. "Colloidal Au-Cu Alloy Nanoparticles: Synthesis, Optical Properties and Applications," *Mater. Chem. Front.*, vol. 2, no. 6, pp. 1074–1089, 2018. https://doi.org/10.1039/C7QM00538E.
[64] P. Bhatia, S. S. Verma, M. M. Sinha. "Tunable Plasmonic Properties of Elongated Bimetallic Alloys Nanoparticles towards Deep UV-NIR Absorbance and Sensing," *J. Quant. Spectrosc. Radiat. Transf.*, vol. 241, pp. 106751, 2020. https://doi.org/10.1016/j.jqsrt.2019.106751.
[65] X. Han, K. Wang, P. D. Persaud, X. Xing, et al. "Harmonic Resonance Enhanced Second-Harmonic Generation in the Monolayer WS2-Ag Nanocavity," *ACS Photonics*, vol. 7, no. 3, pp. 562–568, 2020. https://doi.org/10.1021/acsphotonics.9b01499.
[66] M.-L. Ren, S.-Y. Liu, B.-L. Wang, B.-Q. Chen, et al. "Giant Enhancement of Second Harmonic Generation by Engineering Double Plasmonic Resonances at Nanoscale," *Opt. Express*, vol. 22, no. 23, pp. 28653, 2014. https://doi.org/10.1364/oe.22.028653.
[67] J. Shi, X. He, W. Chen, Y. Li, et al. "Remote Dual-Cavity Enhanced Second Harmonic Generation in a Hybrid Plasmonic Waveguide," *Nano Lett.*, vol. 22, no. 2, pp. 688–694, 2022. https://doi.org/10.1021/acs.nanolett.1c03824.
[68] G. M. Pan, D. J. Yang, L. Zhou, Z. H. Hao, et al. "Enhanced Second Harmonic Generation by Mode Matching in Gain-Assisted Double-Plasmonic Resonance Nanostructure," *Sci. Rep.*, vol. 7, no. 1, pp. 1–10, 2017. https://doi.org/10.1038/s41598-017-10243-y.
[69] J. W. You, N. C. Panoiu. "Tunable and Dual-Broadband Giant Enhancement of Second-Harmonic and Third-Harmonic Generation in an Optimized Graphene-Insulator-Graphene Metasurface," *Phys. Rev. B*, vol. 102, no. 12, pp. 121403, 2020. https://doi.org/10.1103/PhysRevB.102.121403.
[70] N. Weber, M. Protte, F. Walter, P. Georgi, et al. "Double Resonant Plasmonic Nanoantennas for Efficient Second Harmonic Generation in Zinc Oxide," *Phys. Rev. B*, vol. 95, no. 20, pp. 1–6, 2017. https://doi.org/10.1103/PhysRevB.95.205307.
[71] G. Govindasamy, K. Pal, M. Abd Elkodous, G. S. El-Sayyad, et al. "Growth Dynamics of CBD-Assisted CuS Nanostructured Thin-Film: Optical, Dielectric and Novel Switchable Device Applications," *J. Mater. Sci. Mater. Electron.*, vol. 30, no. 17, pp. 16463–16477, 2019. https://doi.org/10.1007/s10854-019-02022-4.
[72] S. S. Kalanur, H. Seo. "Tuning Plasmonic Properties of CuS Thin Films via Valence Band Filling," *RSC Adv.*, vol. 7, no. 18, pp. 11118–11122, 2017. https://doi.org/10.1039/c6ra27076j.
[73] I. Saadon Najm, S. Mahmood Kadhim, A. Abdulkhaleq Alwahib. "Investigation the CuS Thin Film Prepared by Pulsed Laser Deposition," *Mater. Today Proc.*, vol. 42, pp. 2609–2615, 2021. https://doi.org/10.1016/j.matpr.2020.12.589.
[74] L. Gonzalez-García, J. Parra-Barranco, J. R. Sanchez-Valencia, J. Ferrer, et al. "Tuning Dichroic Plasmon Resonance Modes of Gold Nanoparticles in Optical Thin Films," *Adv. Funct. Mater.*, vol. 23, no. 13, pp. 1655–1663, 2013. https://doi.org/10.1002/adfm.201201900.
[75] A. Wolf, T. Kodanek, D. Dorfs. "Tuning the LSPR in Copper Chalcogenide Nanoparticles by Cation Intercalation, Cation Exchange and Metal Growth," *Nanoscale*, vol. 7, no. 46, pp. 19519–19527, 2015. https://doi.org/10.1039/c5nr05425g.

[76] M. N. An, H. Song, K. S. Jeong. "Intraband Transition and Localized Surface Plasmon Resonance of Metal Chalcogenide Nanocrystals and Their Dependence on Crystal Structure," *CrystEngComm*, vol. 24, no. 21, pp. 3828–3840, 2022. https://doi.org/10.1039/d2ce00312k.
[77] S. W. Hsu, K. On, A. R. Tao. "Localized Surface Plasmon Resonances of Anisotropic Semiconductor Nanocrystals," *J. Am. Chem. Soc.*, vol. 133, no. 47, pp. 19072–19075, 2011. https://doi.org/10.1021/ja2089876.
[78] I. Kriegel, J. Rodríguez-Fernández, A. Wisnet, H. Zhang, et al. "Shedding Light on Vacancy-Doped Copper Chalcogenides: Shape-Controlled Synthesis, Optical Properties, and Modeling of Copper Telluride Nanocrystals with near-Infrared Plasmon Resonances," *ACS Nano*, vol. 7, no. 5, pp. 4367–4377, 2013. https://doi.org/10.1021/nn400894d.
[79] N. E. Motl, A. F. Smith, C. J. Desantis, S. E. Skrabalak. "Engineering Plasmonic Metal Colloids through Composition and Structural Design," *Chem. Soc. Rev.*, vol. 43, no. 11, pp. 3823–3834, 2014. https://doi.org/10.1039/c3cs60347d.
[80] P. Patoka, M. Giersig. "Self-Assembly of Latex Particles for the Creation of Nanostructures with Tunable Plasmonic Properties," *J. Mater. Chem.*, vol. 21, no. 42, pp. 16783–16796, 2011. https://doi.org/10.1039/c1jm11936b.
[81] C. L. Nehl, H. Liao, J. H. Hafner. "Optical Properties of Star-Shaped Gold Nanoparticles," *Nano Lett.*, vol. 6, no. 4, pp. 683–688, 2006. https://doi.org/10.1021/nl052409y.
[82] S. Link, M. A. El-Sayed. "Size and Temperature Dependence of the Plasmon Absorption of Colloidal Gold Nanoparticles," *J. Phys. Chem. B*, vol. 103, no. 21, pp. 4212–4217, 1999. https://doi.org/10.1021/jp984796o.
[83] B. Lamprecht, A. Leitner, F. R. Aussenegg. "SHG Studies of Plasmon Dephasing in Nanoparticles," *Appl. Phys. B Lasers Opt.*, vol. 68, no. 2–3, pp. 419–423, 1999. https://doi.org/10.1007/s003400050643.
[84] C. Hubert, L. Billot, P. M. Adam, R. Bachelot, et al. "Role of Surface Plasmon in Second Harmonic Generation from Gold Nanorods," *Appl. Phys. Lett.*, vol. 90, no. 18, pp. 88–91, 2007. https://doi.org/10.1063/1.2734503.
[85] T. Hanke, G. Krauss, D. Träutlein, B. Wild, et al. "Efficient Nonlinear Light Emission of Single Gold Optical Antennas Driven by Few-Cycle near-Infrared Pulses," *Phys. Rev. Lett.*, vol. 103, no. 25, pp. 1–4, 2009. https://doi.org/10.1103/PhysRevLett.103.257404.
[86] A. Slablab, L. Le Xuan, M. Zielinski, Y. de Wilde, et al. "Second-Harmonic Generation from Coupled Plasmon Modes in a Single Dimer of Gold Nanospheres," *Opt. Express*, vol. 20, no. 1, pp. 220, 2012. https://doi.org/10.1364/oe.20.000220.
[87] Q. Ai, F. Sterl, H. Zhang, J. Wang, et al. "Giant Second Harmonic Generation Enhancement in a High- Q Doubly Resonant Hybrid Plasmon-Fiber Cavity System," *ACS Nano*, vol. 15, no. 12, pp. 19409–19417, 2021. https://doi.org/10.1021/acsnano.1c05970.
[88] N. J. Spear, K. A. Hallman, E. A. Hernández-Pagán, R. B. Davidson, et al. "Enhanced Broadband and Harmonic Upconversion from Coupled Semiconductor and Metal Nanoparticle Films," *ACS Appl. Nano Mater.*, vol. 3, no. 4, pp. 3144–3150, 2020. https://doi.org/10.1021/acsanm.0c00064.
[89] A. Zilli, D. Rocco, M. Finazzi, A. Di Francescantonio, et al. "Frequency Tripling via Sum-Frequency Generation at the Nanoscale," *ACS Photonics*, vol. 8, no. 4, pp. 1175–1182, 2021. https://doi.org/10.1021/acsphotonics.1c00112.
[90] A. Zilli, A. Locatelli, A. Di Francescantonio, X. Wu, et al. "Coherent Modulation of the

Nonlinear Emission of a Plasmonic Nanoantenna by Dual-Beam Pumping,". In *Nanophotonics IX*; Andrews, D. L., Nunzi, J.-M., Bain, A. J., Eds.; SPIE: Strasbourg, France; p 10. https://doi.org/10.1117/12.2621333.

[91] N. R. Jana, L. Gearheart, C. J. Murphy. "Seeding Growth for Size Control of 5-40 Nm Diameter Gold Nanoparticles," *Langmuir*, vol. 17, no. 22, pp. 6782–6786, 2001. https://doi.org/10.1021/la0104323.

[92] S. D. Perrault, W. C. W. Chan. "Synthesis and Surface Modification of Highly Monodispersed, Spherical Gold Nanoparticles of 50-200 Nm," *J. Am. Chem. Soc.*, vol. 131, no. 47, pp. 17042–17043, 2009. https://doi.org/10.1021/ja907069u.

[93] M. Karg, N. Schelero, C. Oppel, M. Gradzielski, et al. "Versatile Phase Transfer of Gold Nanoparticles from Aqueous Media to Different Organic Media," *Chem. - A Eur. J.*, vol. 17, no. 16, pp. 4648–4654, 2011. https://doi.org/10.1002/chem.201003340.

[94] S. L. Arrowood. "Synthetic Routes to Hybrid Nanoparticles of Gold and Copper Sulfides,", Vanderbilt University.

[95] W. W. Weare, S. M. Reed, M. G. Warner, J. E. Hutchison. "Improved Synthesis of Small (d CORE ≈ 1 . 5 Nm)," *J. Am. Chem. Soc.*, vol. 122, no. 51, pp. 12890–12891, 2000.

[96] V. Amendola, R. Pilot, M. Frasconi, O. M. Maragò, et al. "Surface Plasmon Resonance in Gold Nanoparticles: A Review," *J. Phys. Condens. Matter*, vol. 29, no. 20, 2017. https://doi.org/10.1088/1361-648X/aa60f3.

[97] M. R. Singh, G. Brassem, S. Yastrebov. "Optical Quantum Yield in Plasmonic Nanowaveguide," *Nanotechnology*, vol. 32, no. 13, 2021. https://doi.org/10.1088/1361-6528/abd05d.

[98] D. Russell. *Superposition of Waves*Acoustics and Vibration Animationshttps://www.acs.psu.edu/drussell/Demos/superposition/superposition.html#:~:text=The principle of superposition may be applied to,simply the sum of the individual wave displacements. (accessed 2022-11-08).

[99] L. Novotny. "Strong Coupling, Energy Splitting, and Level Crossings: A Classical Perspective," *Am. J. Phys.*, vol. 78, no. 11, pp. 1199–1202, 2010. https://doi.org/10.1119/1.3471177.

[100] C. R. Jacobson, D. Solti, D. Renard, L. Yuan, et al. "Shining Light on Aluminum Nanoparticle Synthesis," *Acc. Chem. Res.*, vol. 53, no. 9, pp. 2020–2030, 2020. https://doi.org/10.1021/acs.accounts.0c00419.

[101] P. Bessel, A. Niebur, D. Kranz, J. Lauth, et al. "Probing Bidirectional Plasmon-Plasmon Coupling-Induced Hot Charge Carriers in Dual Plasmonic Au/CuS Nanocrystals," *Small*, 2023. https://doi.org/10.1002/smll.202206379.

[102] B. Novotny, Lukas, Hecht. "Principles of Nano-Optics"; Cambridge University Press: Cambridge. https://doi.org/https://doi.org/10.1017/CBO9780511813535.

[103] W. Sarid, Dror; A. Challener. "Modern Introduction to Surface Plasmons"; Cambridge University Press: Cambridge, UK. https://doi.org/https://doi.org/10.1017/CBO9781139194846.

[104] M. Singh. "Electronic, Photonic, Polaritonic, and Plasmonic Materials"; Wiley Custom: Toronto.

[105] M. R. Singh, S. Yastrebov. "Switching and Sensing Using Kerr Nonlinearity in Quantum Dots Doped in Metallic Nanoshells," *J. Phys. Chem. C*, vol. 124, no. 22, pp. 12065–12074, 2020. https://doi.org/10.1021/acs.jpcc.0c02122.

[106] M. R. Singh. "Theory of All-Optical Switching Based on the Kerr Nonlinearity in Metallic Nanohybrids," *Phys. Rev. A*, vol. 102, no. 1, pp. 1–10, 2020.

https://doi.org/10.1103/PhysRevA.102.013708.
[107] A. Hanamura, Eiichi; Kawabe, Yutaka; Yamanaka. "Quantum Nonlinear Optics"; Springer US.
[108] M. O. Scully, M. S. Zubairy. "Quantum Optics"; Cambridge University Press: Cambridge, UK. https://doi.org/10.1017/CBO9780511813993.